Realistic Chipless RFID: Protocol, Encoding and System Latency

Der Fakultät für Ingenieurwissenschaften,
Abteilung Elektrotechnik und Informationstechnik
der Universität Duisburg-Essen

zur Erlangung des akademischen Grades

Doktor der Ingenieurwissenschaften (Dr.-Ing.)

genehmigte Dissertation

von

Ahmed Elawamry

aus

Kalyobiya, Egypt

Gutachter:

Prof. Dr.-Ing. Thomas Kaiser

Prof. Dr. ir. AJ Han Vinck

Tag der mündlichen Prüfung: 13.12.2016

Fachgebiet Digitale Signalverarbeitung (DSV)
Universität Duisburg-Essen
Bismarckstrasse 81
47057 Duisburg
Germany
Tel.: +49 (203) 3 79-32 87
Fax : +49 (203) 3 78-34 98

Referent: Prof. Dr.-Ing. Thomas Kaiser
Co-Referent: Prof. Dr. ir. AJ Han Vinck
Vorsitzende: Prof. Dr. Andreas Stöhr
Tag der Promotion: 13.12.2016

Mit Unterstützung des Deutschen
Akademischen Austauschdienstes

Acknowledgements

Foremost, I thank Allah (God) for his endless bestowal in making me live these fabulous moments. Without his conferral, I could never have completed this work.

This thesis was written while the author was with the Institute of Digital Signal Processing (DSV), in the Faculty of Engineering at the University of Duisburg-Essen in Germany.

I would like to express my gratitude to my supervisor Prof. Dr.-Ing. Thomas Kaiser for his continuous support, encouragement, motivations, and understanding. He taught me how to think, how to be creative, and how to be in the right side of research. He usually give us the smile even in the critical times. It was honor for me to work with such a positive supervisor. I am deeply indebted to him, not only for his great support, but also for the spirit and the research liberty he gave me during my work in this thesis. I am really proud to be one of his students.

I would like to offer my special thanks to Prof. Dr. ir. AJ Han Vinck – Duisburg-Essen University for his interest in my work and for being my second supervisor.

I would like to show my greatest appreciation to the wonderful team (Abdelfattah Fawky and Maher Khaliel). With this team, I did research with fun. We had a common dream and we did our best to successfully achieve it. Over the years, we set an example of how the teamwork should look like.

I also would like to express my deepest thanks to Prof. Hadia Elhennawy – Ain Shams University, Egypt for her usual support and encouragement.

I would like to acknowledge Dr.-Ing. Mohamed El-Hadidy for his appreciated support and cooperation. Thanks also go to Marc Hoffmann for his usual support and assistance.

I would like to thank Frau Sabine Jankowski for her continuous cooperation and support.

I would like to express my sincere love and special thanks to my wife Bassma. Without her understanding and genuine support, this thesis would have remained a dream. She usually give me the smile at hard times. I cannot forget my little kids, princess, Mariam and Rokaia, they are the light of my eyes. This work would not come true without mentioning the moral support

and prayers of my mother Samia, brothers Amr and Ali, father in law Yahya, and mother in law Layla. Also, I cannot forget my idol and the source of my power, my father Abdelhamid. I would like to give all my success to his memory because I am living with his guidelines and teaches.

Finally, I would like to thank the university of Duisburg-Essen, the institute of Digital Signal Processing (DSV) and my friends their for providing the required support, tools, and labs. Additionally, I would also thank the German Academic Exchange Service - Deutscher Akademischer Austauschdienst Dienst (DAAD) for their financial support.

Ahmed Elawamry
Duisburg, Germany
November, 2017

Abstract

Chipless Radio Frequency IDentification (RFID) is a promising technology predicted to replace the optical barcode in the near future. This is due to several problematic issues **i)** the barcode cannot read Non-Line-Of-Sight (NLOS) tags; **ii)** each barcode needs human assistance to be read; **iii)** it is impossible to identify multiple tags at the same time; and **iv)** the considerable time delay in case of massive queues because different types of objects need to be serially scanned.

The contributions included in this dissertation concentrate on three main aspects of the Frequency Coded (FC) chipless RFID system. The first one is the multi-tag identification, which deals with the existence of multiple tags in the reader's interrogation region. The second aspect is the system latency that describes the time the reader needs to identify the tags. Finally, there is the coding capacity that is responsible for designing a chipless tag with larger information bits. The aim of these aspects is to realize a chipless RFID system.

Since the chipless tags are memoryless as they do not include Integrated Circuits (ICs), the number of bits to be stored in the chipless tag is limited. Consequently, the current RFID standards and protocols designed for the chipped RFID systems are not applicable to the chipless systems. The main objective of the first contribution is to introduce novel multi-tag anti-collision protocols based on Notch Position Modulation (NPM) and Look-Up-Table (LUT) schemes determining the network and MAC layers of the chipless RFID systems. The first generation of the proposed protocol (Gen-1) relies on dividing the spectrum into two parts; the first one is the preamble bandwidth that includes a unique frequency shift for each tag. The second part is the frame bandwidth which represents the tag ID. The tag ID is obtained based on the predefined frequency positions, making use of the unique frequency shift. Consequently, the interference is avoided as there will not be any overlap between the tags' responses. The second generation of the protocol (Gen-2) introduces an improvement in the spectrum utilization and coding capacity. This is realized by transferring the tag-ID to be stored in a table in the main memory of the reader (look-up-table). The unique shift of each tag represents the address of the tag's ID. Therefore,

the complexity of the tag structure will be significantly reduced with an enhanced probability of detection. Furthermore, the key performance indicators for the chipless RFID system are explored to validate the protocol's performance. Both protocols are modeled and simulated to identify 10-chipless tags in order to set the regulations of the tag and reader design. Moreover, a novel real-world testbed for a multi-tag Ultra Wideband (UWB) chipless RFID system based on Software Defined Radio (SDR) is introduced. In this testbed, all the signaling schemes related to the transmitted signal, the detection techniques, the empty room calibration for the clutter removal process, and the identification protocols are applied.

The aim of the second aspect is to introduce novel techniques that reduce the time required by the reader to identify the FC chipless RFID tags existent in the reader's interrogation region. This time delay is called *system latency*. The main parameters that significantly affect the overall system latency are the frequency scanning methodology, the number of spectrum scanning iterations for the clutter removal process, and the hop duration. Therefore, the Adaptive Frequency Hopping (AFH) and the Adaptive Sliding Window (ASW) methodologies are proposed to meet the requirements of the FC chipless RFID tags. Regarding the ASW technique, it is suitable to identify the tags using the Gen-1 protocol which utilizes a sliding window (for detecting the notch) with an adaptive size to extract the tag's-ID. The second adaptive methodology, AFH, can identify the tags with the Gen-2 protocol by using a variable frequency step that fits the corresponding notch patterns. These techniques are proven to be efficient for the chipless RFID systems with regard to latency and accuracy. Likewise, the designed AFH and ASW technique's performance is compared to the classical Fixed Frequency Hopping (FFH) methodology with a fine frequency step to validate the accuracy of the proposed techniques. A real-world SDR based testbed is designed and the proposed adaptive algorithms as well as the classical FFH methodology are implemented. The experiments show that the proposed AFH combined with the ASW algorithms significantly reduce the system latency by 58%.

The goal of the third aspect is to introduce a novel technique that increases the coding capacity of the FC chipless RFID system. The proposed Notch Width Modulation (NWM) scheme encodes 4 bits (16-combinations) per single resonator exploiting the notch bandwidth and its corresponding frequency position. Furthermore, each notch can reserve a window with a bandwidth of 150 MHz and inside this window the notch can obtain a certain bandwidth with a specific resonant frequency constructing the coding pairs C_j (f_k,B_l). Hence, 80-bits could be achieved at the operating frequency 2–5 GHz, preserving the operating frequency bandwidth. Also, a Smart Singular Value Decomposition (SSVD) technique is designed to estimate the

notch bandwidth and to ensure a low probability of error. In addition, the utilization of a linear block code as an error correcting code is explored to make the best use of the obtained coding gain. Consequently, a high encoding efficiency and an accurate detection can be achieved in addition to a simplified reader design. Moreover, a novel 4×5 cm^2 tag structure is designed to meet the requirements of the NWM coding technique achieving a coding density of 4 bits/cm^2. Different tag configurations are manufactured and validated by measurements using the SDR platform. The introduced coding methodology is conclusively validated using Electromagnetic (EM) simulations and real-world testbed measurements.

The considered achievements for the proposed aspects offer a robust chipless RFID system that can be considered in real scenarios. Furthermore, all the proposed contributions are validated using analytical modeling, simulation and measurements in order to list their difficulties and limitations.

Abstrakt

Chiplose Identifikation über Funkfrequenzen, RFID (engl., Radio Frequency IDentification) ist eine vielversprechende Technology, der man die Fähigkeit zuschreibt, in naher Zukunft den optischen Barcode zu ersetzen. Letztgenannter hat Einschränkungen durch **i)** RFID Tags sind bei nicht vorhandener Sichtverbindung (engl. Non-Line-Of-Sight, NLOS) auch nicht lesbar; **ii)** das Scannen der Barcodes benötigt in den meisten Fällen manuelles Eingreifen; **iii)** es ist unmöglich mehrere Barcodes gleichzeitig auszulesen; **iv)** und als Folge davon entsprechende Verzögerungen beim Auslesen größerer Mengen von Barcodes, da alle einzeln gescannt werden müssen.

Die Beiträge der vorliegenden Dissertation konzentrieren sich auf drei Schwerpunkte von frequenzcodierten (engl. frequency coded, FC) chiplosen RFID Systemen. Der erste Schwerpunkt ist die gleichzeitige Identifikation von mehreren RFID Tags und kümmert sich um den Fall, dass sich mehrere RFID Tags in der Lesezone des RFID Lesegerätes befinden. Der zweite Aspekt betrifft die Verzögerung des Systems, die Zeit, das Lesegerät zum Identifizieren der RFID Tags benötigt. Und drittens die Coding Kapazität des Systems, sie ist verantwortlich für die zu erreichende Bittiefe des RFID Systems. Ein real umsetzbares RFID System erfordert Lösungen in allen drei Aspekten.

Da chiplose RFID Tags keine integrierten Schaltungen (ICs) und somit auch keine Speicherbausteine besitzen, ist die Anzahl der auf dem RFID Tag speicherbaren Bits begrenzt. Und als Folge davon sind die Standards und Protokolle, die für die herkömmlichen chipbehafteten RFID Systeme entwickelt worden, nicht auf chiplose RFID Systeme übertragbar. Das wesentliche Ziel des ersten Beitrages ist die Einführung eines neuen Multi-Tag Antikollisionsprotokolls, das auf der Modulation der Notchposition (engl. Notch Position Modulation, NPM) und Tabellen (engl. Look-Up-Table, LUT) zur Bestimmung der Netzwerk- und MAC- Layer des chiplosen RFID Systems basiert. Die erste Generation der vorgeschlagenen Protokolls (Gen-1) baut auf einer Zweiteilung des zur Verfügung stehenden Spektrums auf. Im unteren

Frequenzbereich, als Präambel Bandbreite bezeichnet, wird jedem RFID Tag seine individuelle Frequenzverschiebung übermittelt und im zweiten Bereich, der sogenannten Frame Bandbreite, ist die Identifikationsnummer (ID) des RFID Tags hinterlegt. Mit dieser Anordnung lässt sich jegliche Interferenz zwischen den verschiedenen RFID Tags unterbinden, da sich die Antworten der RFID Tags nicht gegenseitig überlagern. Die zweite Generation dieses Protokolls bringt eine Verbesserung sowohl bei der Coding Kapazität als auch bei der Nutzung des zur Verfügung stehenden Frequenzspektrums. Dies wird dadurch erreicht, dass die ID des RFID in einer Tabelle im Lesegerät gespeichert wird. Die individuelle Frequenzverschiebung dient dabei als Adresse für die gespeicherten IDs. Dieser Schritt vereinfacht die Komplexität der Struktur des RFID Tags signifikant, während gleichzeitig die Erkennungswahrscheinlichkeit erhöht wird. Des Weiteren werden die Key Performance Indikatoren untersucht um die Leistungsfähigkeit der Protokolle zu beweisen. Beide Protokollversionen werden modelliert und in einer Umgebung mit 10 chiplosen RFID Tags simuliert, um die Randbedingungen für die Entwicklung der RFID Tags und des RFID Lesegerätes zu ermitteln. Außerdem wird eine neuartige Testumgebung für ein Multi-Tag Ultra Breitband (engl. ultra wideband UWB) RFID System unter realen Testbedingungen basierend auf einem Software Defined Radio (SDR) Ansatz entwickelt. In dieser Testumgebung werden sowohl die gesendeten Signal als auch Detektierungstechniken, Leerraum Kalibrierung zur Reduzierung der Streustrahlung und die Identifikationsprotokolle untersucht.

Als zweiter Schwerpunkt dieser Arbeit werden neue Techniken zur Reduzierung der Systemlaufzeit (engl. System Latency) eingeführt. Das Ziel dabei ist, die Zeit, die das RFID Lesegerät zum Erkennen aller in Lesereichweite befindlichen chiplosen FC RFID Tags braucht, zu verkürzen. Der Großteil der Systemlaufzeit wird durch das gewählte Frequenzscanverfahren, durch die Anzahl der Mittelungen zur Eliminierung der umgebenden Streustrahlung und durch die Dauer eines Frequenzsprungs bestimmt. In dieser werden dazu ein adaptives Frequenzsprungverfahren (engl. adaptive frequency hopping, AFH) sowie ein Verfahren Mittels adaptiver gleitender Fensterung (engl. adaptive sliding window, ASW) eingeführt. Das ASW Verfahren ist dabei im Hinblick auf die Identifizierung der RFID Tags nach dem Gen-1 Protokoll entwickelt, da es ein gleitendes Fenster zur Detektierung der Notches mit einer variablen Breite zum Auslesen der ID erfordert. Im Gegensatz dazu wird das Auffinden der im Gen-2 Protokoll verwendeten Notchpattern durch das AFH Verfahren verbessert. Dies wird über variable Frequenzsprünge, die auf die jeweiligen Notchpattern optimiert werden, erreicht. Beide Verfahren haben sich als effektiv sowohl im Hinblick auf die Systemlaufzeit als auch auf die Genauigkeit erwiesen. Das ASW und das AFH Verfahren wurden dazu in der oben erwähnten Testumgebung implementiert und

mit dem klassischen Frequenzsprungverfahren, feste feingraduierte Frequenzschritte, verglichen. Die Experimente haben gezeigt, dass das vorgeschlagene AFH Verfahren in Kombination mit ASW zu einer beachtlichen Reduzierung der Systemlaufzeit von 58% führen.

Das Ziel des dritten Schwerpunkts dieser Arbeit ist die Einführung einer neuartigen Technik zur Erhöhung der Informationsdichte (engl. Coding capacity) in einem chiplosen FC RFID Systems. Die hierfür vorgeschlagene Modulation der Notchbreite (engl. notch width modulation, NWM) ermöglicht die Kodierung von 4 Bits (16 Zuständen) pro Resonator in dem die Notchbreite und die dazugehörige Frequenzlage ausgenutzt werden. Für jeden Notch werden 150MHz Bandbreite reserviert, innerhalb derer das Codebit durch eine bestimmte Bandbreiten an unterschiedlichen Frequenzen bestimmt wird C_j (f_k,B_l). Das bedeutet, bei einer Arbeitsfrequenz im Bereich von 2–5 GHz können so 80 Bits realisiert werden. Des Weiteren wurde eine smarte Singulärwertzerlegung (engl. smart singular value decomposition, SSVD) Technik entwickelt, um die Notchbreite zu ermitteln und eine geringe Fehlerwahrscheinlichkeit zu garantieren. Die Nutzung von Blockcodes zur Behebung von Fehlern wurde untersucht, um den größtmöglichen Nutzen aus der so gewonnene Bittiefe zu erzielen. Als Folge konnte eine große Bittiefe mit einer hohen Lesegenauigkeit bei vereinfachtem Aufbau des Lesegeräts erzielt werden. Außerdem wurde eine neuartige RFID Tag Struktur entworfen, die bei einer Größe von 4×5 cm^2 eine Codedichte von 4 Bits/cm^2 erreicht. Verschiedene RFID Tag Konfigurationen wurden erstellt und das neu eingeführte Codierungsverfahren mit Hilfe von elektromagnetischen (EM) Simulation und der bereits erwähnten Testplattform überprüft.

Die erzielten Ergebnisse ermöglichen ein widerstandsfähiges RFID System in einer realen Umgebung. Alle vorgeschlagenen Beiträge sind durch analytische Modelle, Simulationen und Messungen auf mögliche Probleme und die Grenzen einer Realisierung unter realistischen Bedingungen geprüft worden.

Contents

List of Figures

List of Acronyms

AFH	Adaptive Frequency Hopping
ASW	Adaptive Sliding Window
ECC	Error Correcting Code
EIRP	Effective Isotropic Radiated Power
EPC	Electronic Product Code
FC	Frequency Coded
FFH	Fixed Frequency Hopping
FMCW	Frequency Modulated Continuous Wave
ID	Identification number
KPIs	Key Performance Indicators
LFM	Linear Frequency Modulation
LUT	Look-Up-Table
MAC	Media Access Control
NPM	Notch Position Modulation
NWM	Notch Width Modulation
RCS	Radar Cross Section
RFID	Radio Frequency Identification
SAW	Surface Acoustic Wave

SDR	Software Defined Radio
SSR	Signal Space Representation
SVD	Singular Value Decomposition
SSVD	Smart Singular Value Decomposition
USRP	Universal Software Radio Peripheral
VCO	Voltage Controlled Oscillator
VNA	Vector Network Analyzer

1 Introduction

With the increasing demand for identification and tracking applications when it comes to the Internet-of-Things (IoT), or Internet-of-Objects [1–4], RFID technology has sparked considerable interest due to its remarkable advantages such as automated communication and remote reading. The use of conventional Integrated Circuit (IC) chip-based RFID tags, however, has lead to enormous challenges to their use in the supply chain for item-level tracking and the identification of consumer goods, mainly because of the high price. Auspiciously, chipless RFID tags, combine some of the benefits of the chipped RFID systems (non-line-of-sight requirement, unique identification of each tag, can include sensors and good reading range) and barcode benefits (low cost, printable working even under high environmental temperature). Thus, they have a better chance of entering the era of penny-cost tags and item-level identification demands. The dissertation summarizes the author's endeavors towards the realization of extremely inexpensive chipless RFID tags [5].

1.1 Chipless RFID: Challenges, Motivation and Scope

Chipless RFID is a promising technology intended to replace the barcode by 2020 as it exhibits some of the same advantages as the barcode such as low manufacturing costs in addition to some advantages of the RFID with chip system. However, here are some of the challenges of implementing the chipless system, as follows:

1. The chipless tags are chip-less (without any registers, memory or, IC). Thus, they have a very limited number of bits compared to the chipped RFID.

2. Low backscattered power, such that the reflected power from the tag is very weak.

3. Reading range, which determines how far the tags can be placed from the reader, is another problem. This could be enhanced by using high gain directive antennas at the reader side. The tag should also have high radar-cross-section values.

4. Environmental clutter significantly affects the accuracy of the detection and tag identification.

5. The collision between the multi-tag responses because the tags share the same spectrum. So, if several tags are located within the same interrogation region, the backscattered signal from each tag may interfere with another tag.

6. Coding capacity, which is the number of bits to be assigned to each tag, also needs to be considered.

Therefore, the existing RFID standards and protocols designed for the chipped RFID systems are not applicable to the chipless systems.
In this dissertation, novel techniques for obtaining a robust chipless RFID system are proposed. Fig. 1.1 summarizes the main topics explored throughout the dissertation such as:

1. **Multi-tag identification:** There are very few studies dealing with the multi-tag identification for the Frequency Coded (FC) chipless RFID. There are only simulation results for two-chipless tag scenarios. However in this dissertation, a clear (easy-to-use) medium access control algorithm that prevents the collision between multi-chipless tags is proposed. Furthermore, the key performance indicators for evaluating the proposed MAC protocol are explored.

2. **Chipless RFID system latency:** The system latency could be defined as the time required to identify the tags existent in the reader's interrogation region. There is no prior research that considers the system latency for the FC chipless RFID. The latency is improved by designing adaptive techniques for sweeping the operating frequencies conserving the detection accuracy of the tag.

3. **Coding capacity:** The number of bits that could be assigned to the chipless tags is a critical issue as they do not include memories or storage elements. Furthermore, the coding technique should be easily decoded and resistant against environmental effects. Consequently, a novel technique that significantly increases the number of bits that are

coded on the chipless tag depending on the notch bandwidth and frequency location is developed..

As can be seen from the aspects mentioned above, the topics covered by this dissertation are highly attractive since they include the critical issues of the utilized FC chipless RFID systems considering the real-world implementation as well as practical issues. Consequently, the aim of the designed system is to create an in-hand product in order to serve the commercial market.

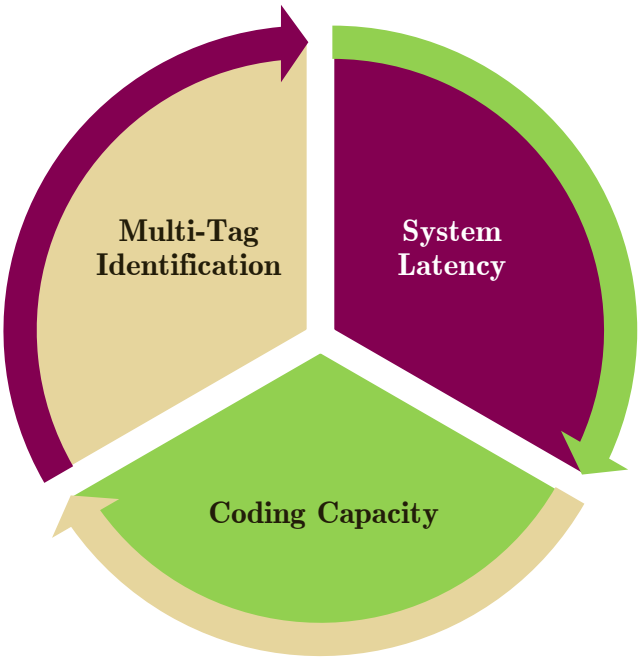

Figure 1.1: The main topics included in the thesis.

1.2 Dissertation Contributions and Organization

In this dissertation, we design novel techniques and algorithms in order to improve the overall performance of the FC chipless RFID system. The main contributions and structure of this dissertation can be summarized as follows.

- **Chapter 2: Basic Concepts and State of the Art**
  This chapter introduces the RFID systems and lists the main groups of the chipped RFID. Furthermore, the factors that have an effect on the reading range are illustrated. Also, the difficulties of obtaining a low-cost RFID tag with chip are discussed. Afterwards, the core functions of the FC chipless RFID system are explained while also mentioning the different

types of existing chipless tags. The proposed reader based on a software-defined-radio, that can be used to identify chipless tags, is then described. Finally, a comprehensive study that compares the chipped RFID, the barcode, and the chipless RFID is included.

- **Chapter 3: Multi-Tag Identification and Protocol Evaluation Framework**
  Chapter 3 describes novel techniques that identify several chipless tags existent in the reader's interrogation region. This chapter introduces two generations of the MAC protocols that serve to prevent the collision between the chipless tags' responses. The first generation of the MAC algorithm, Gen-1, is based on notch position modulation. With this technique, the spectrum is divided into two main parts. The first part is called the preamble region, and is responsible for obtaining the unique tag frequency shift. The second part represents the tag-ID. A certain process is utilized to identify the tag and to extract its ID. The second generation of the MAC protocol, Gen-2, is based on a look-up-table stored in the reader's main memory that contains the tags' ID. Consequently, at Gen-2, the design of the tag is much simpler as it only includes the unique frequency shift which is used as a reference for the look-up-table. Furthermore, a complete mathematical framework is presented for both techniques. Additionally, the key performance indicators (spectrum utilization efficiency, the probability of error and overhead) are defined in order to estimate the performance of the two proposed protocols. Finally, measurements are presented based on the proposed software-defined-radio based reader.
  The contributions to this chapter are listed below:

  - A. El-Awamry, M. Khaliel, A. Fawky and T. Kaiser, "A Novel Multi-Tag Identification Technique for Frequency Coded Chipless RFID Systems based on Look-Up-Table Approach," 2017 11th European Conference on Antennas and Propagation (EuCAP), Paris, 2017, pp. 1-5.
  - M. El-Hadidy, A. El-Awamry, A. Fawky, M. Khaliel and T. Kaiser, "A novel collision avoidance MAC protocol for multi-tag UWB chipless RFID systems based on Notch Position Modulation," 2015 9th European Conference on Antennas and Propagation (EuCAP), Lisbon, 2015, pp. 1-5.
  - El-Hadidy, M., El-Awamry, A., Fawky, A., Khaliel, M., and Kaiser, T. (2016) Real-world testbed for multi-tag UWB chipless RFID system based on a novel collision avoidance MAC protocol. Trans. Emerging Tel. Tech., doi: 10.1002/ett.3124.

- **Chapter 4: Adaptive Frequency Sweeping Techniques to Reduce System Latency**
  After identification of multiple chipless tags existent in the same interrogation region of the reader, the identification process should be performed in a short time. Consequently, Chapter 4 introduces those factors that directly influence the overall system latency. Furthermore, novel adaptations that reduce system latency are proposed. The first one is applicable to the Gen-1 protocol, which utilizes an adaptive sliding window technique in order to identify and extract the tag-IDs. The window size can be adjusted to capture the signal backscattered from the tag. Another novel technique based on the adaptive frequency hopping method is introduced. It is suitable for the Gen-2 MAC protocol and all the FC chipless tags existent. With this technique, the reader transmits a signal with several hopping rates in order to fit the physical properties of the chipless tags. This technique is practically proven to be efficient for the FC chipless RFID systems as it offers a high detection accuracy (by utilizing the simple energy detection)

  - A. El-Awamry, M. Khaliel, A. Fawky and T. Kaiser, "Adaptive Frequency Sweeping Techniques for Enhancing the Chipless RFID System Latency," Transactions on Emerging Telecommunications Technologies (Weily), 2016, pp. 1-16.
  - A. El-Awamry, A. Fawky, M. Khaliel,and T. Kaiser, "A Novel Adaptive Spectrum Scanning Technique for Reducing the Identification Time of the UWB Chipless RFID System," 14th IEEE International Conference on Networking, Sensing and Control, Calabria, Italy, 2017, pp. 1-6.
  - A. El-Awamry, M. Khaliel, A. Fawky, M. El-Hadidy and T. Kaiser, "Novel adaptive sliding window algorithm reducing latency for multi-tag chipless RFID systems," Radio Science Meeting (Joint with AP-S Symposium), 2015 USNC-URSI, Vancouver, BC, Canada, 2015, pp. 206-206.
  - A. El-Awamry, A. Fawky, M. El-Hadidy and T. Kaiser, "Smart notch detection techniques for robust frequency coded chipless RFID systems," 2015 9th European Conference on Antennas and Propagation (EuCAP), Lisbon, 2015, pp. 1-5.
  - A. Fawky, M. Khaliel, A. El-Awamry, M. El-Hadidy and T. Kaiser, "Novel Pseudo-Noise coded chipless RFID system for clutter removal and tag detection," 2015 IEEE International Conference on RFID (RFID), San Diego, CA, 2015, pp. 100-104.

- **Chapter 5: Coding Capacity**
  In this chapter, a novel technique that increases the maximum number of bits that can be

coded on the chipless tag is introduced. The proposed technique is based on the notch bandwidth and frequency location. 16-combinations are achieved per single resonator, which denotes to 4-bits per resonator (the maximum number of bits per single resonator in the literature is 2-bits/resonator). Each notch obtains a specific bandwidth (one of three predefined values, $BW1$, $BW2$, and $BW3$) and a particular frequency position, constructing a 2D constellation diagram with 16 possible combinations. A novel tag structure is presented to obtain the predefined bandwidths and frequency locations. Furthermore, a complete mathematical framework relates the tag's ID to the proposed coding pairs C_j (f_k,B_l). An intelligent singular value decomposition technique is designed to decode the backscattered signal from the tag and to then retrieve the tag's ID. The probability of error is estimated for the detection of three designed tags based on the proposed coding technique. Additionally, the utilization of a linear block code as an error correcting code for the chipless RFID system is shown. Finally, the robustness of the proposed coding technique is verified by applying the decoding technique to the software defined radio based reader.

- A. El-Awamry, M. Khaliel, A. Fawky, M. El-Hadidy and T. Kaiser, "Novel notch modulation algorithm for enhancing the chipless RFID tags coding capacity," 2015 IEEE International Conference on RFID (RFID), San Diego, CA, 2015, pp. 25-31.
- A. Fawky, M. Khaliel, A. El-Awamry and T. Kaiser, "'Novel Notch Detection and Identification Techniques for Frequency Coded Chipless RFID Readers," *submitted in* IET Communications, 2016, pp. 1-20.
- M. Khaliel, A. El-Awamry, A. Fawky, M. El-Hadidy and T. Kaiser, "A novel co/cross-polarizing chipless RFID tags for high coding capacity and robust detection," 2015 IEEE International Symposium on Antennas and Propagation and USNC/URSI National Radio Science Meeting, Vancouver, BC, 2015, pp. 159-160.

- **Chapter 6: Conclusions and Future Work**

  This chapter summarizes the main research challenges and highlights the results achieved. Moreover, it offers effective guidelines and recommendations for future extensions of this work.

Fig. 1.2 shows a diagram of the dissertation outline and the contribution used for each chapter. Furthermore, the relation between the proposed contributions constructing a complete system for the FC chipless RFID is illustrated.

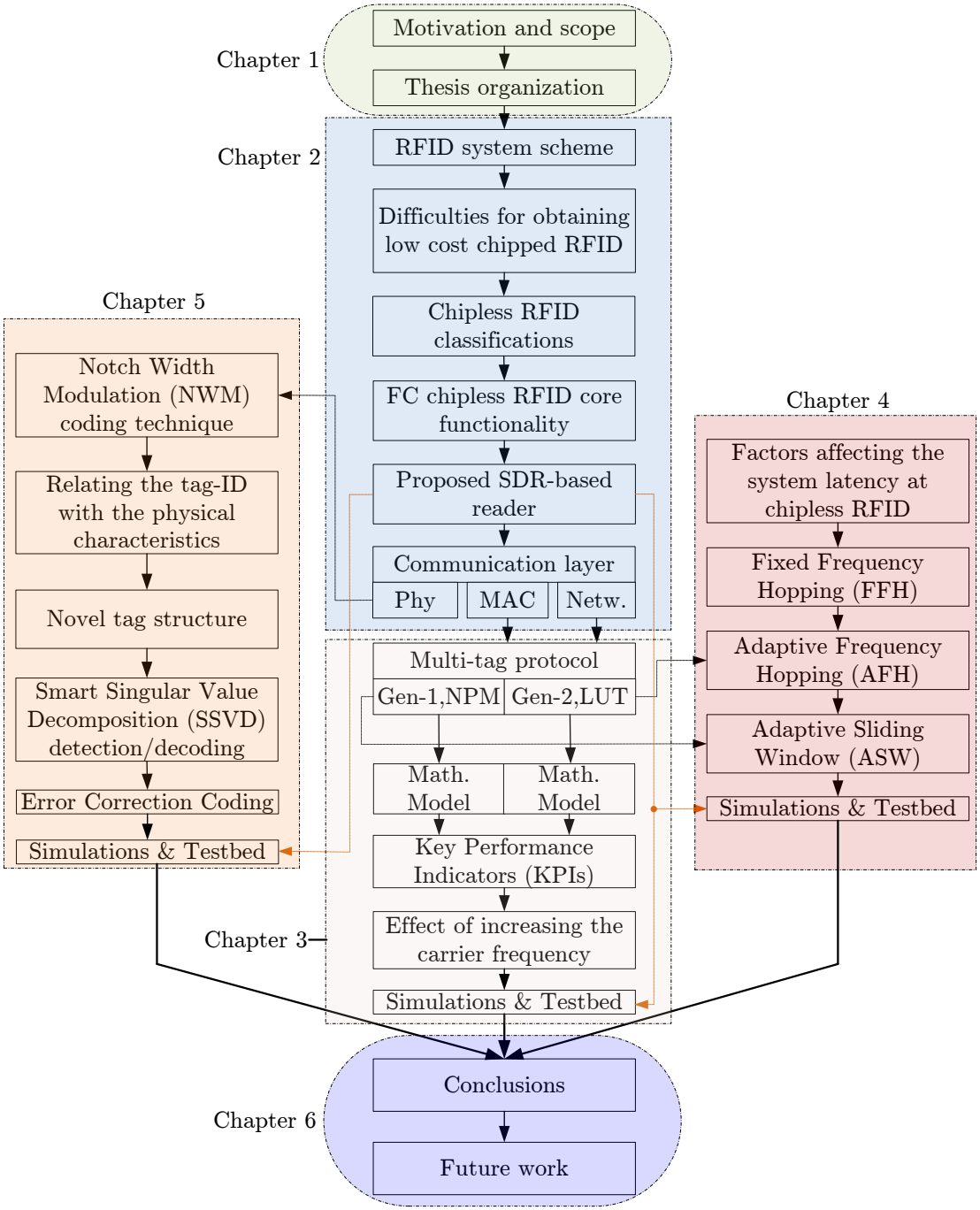

Figure 1.2: Schematic representation of the contributions and the chapters.

2 Basic Concepts and State of the Art

In this chapter, the fundamental principles and the background of the chipless RFID system will be introduced. Additionally, the main procedures of the automatic-ID are analyzed. Moreover, the two main families of the chipped RFID (near-field and far-field) are illustrated. The difficulties of realizing a low-cost RFID tag with a chip will be discussed. Furthermore, the different types of existing chipless tags and the corresponding reader requirements are introduced. An overview of the proposed software-defined-radio based reader will be presented. Afterwards, the communication layers (physical, data-link, and network) are defined for the proposed chipless RFID system. Finally, a comprehensive study is performed focusing on the chipped RFID, the barcode, and the chipless RFID.

2.1 Introduction

Radio Frequency Identification (RFID) is a wireless technique for capturing data. It uses Radio Frequency (RF) waves to automatically identify objects [6]. Fig. 2.1 illustrates the well-known existing procedures for automatic identification. The goal of this automatic identification (or Auto-ID) is the creation of an "Internet of Objects". In such a highly connected network, devices linked within an enterprise can communicate with one another, providing real-time information about the location, contents, destination, and ambient conditions of goods. This communication allows much-sought-after machine-to-machine communication and decision-making, rendering human assistance unnecessary and significantly reducing the number of errors [7]. Ideally, the data should be stored in a silicon chip. The most common form of electronic data-carrying devices in use in everyday life is a smart card which uses a contact field (telephone smart card, bank cards). However, the mechanical contact employed by the smart card has often been

impractical. A contactless transfer of data between the data-carrying device and its reader is far more flexible. Ideally, the power required to operate the electronic data-carrying device would also be transferred from the reader using contactless technology. Because of the procedures used for the transfer of power and data, contactless ID systems are called RFID systems (radio frequency identification) [8].

RFID relies on RF waves for data transmission between the data-carrying device, called the RFID tag, and the interrogator. The generic configuration of an RFID system consists of:

1. The ID data-carrying tag that contains the identification code.
2. A reader, which sends the interrogation signal to the tags in range.
3. The middleware, which maintains the interface and the software protocol to encode and decode the identification data from the reader and to transfer it into a mainframe or personal computer. It establishes a link using an enterprise application.

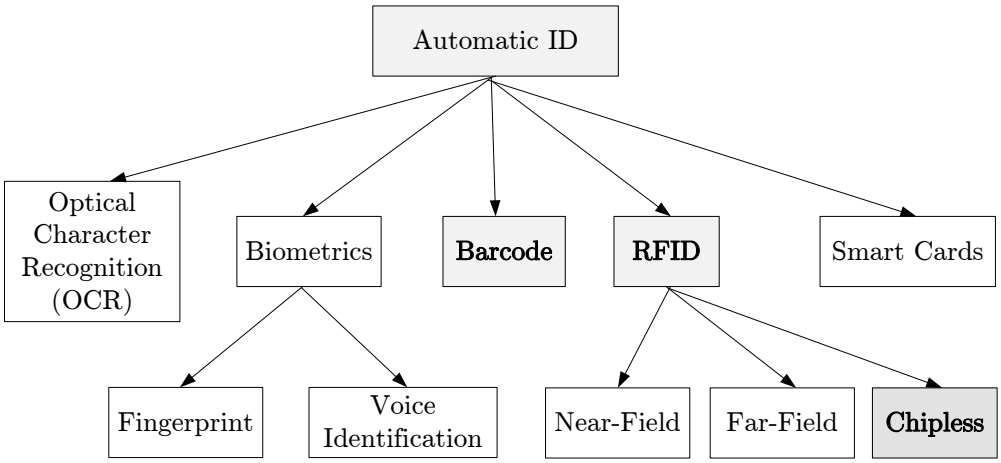

Figure 2.1: Overview of automatic identification procedures.

2.2 RFID: System Description and Difficulties

The operations of the main groups of the RFID are illustrated in this section. Furthermore, the factors affecting the reading range are discussed. Finally, the difficulties of obtaining low-cost RFID tags are described.

2.2.1 RFID System Scheme

Fig. 2.2 shows the two main groups of the RFID-with-chip system: near-field RFID as shown in Fig. 2.2a and far-field RFID as illustrated in Fig. 2.2b. Regarding the near-field RFID, its operation depends on Faraday's principle of magnetic induction to establish near-field coupling between reader and tag. A reader passes a large alternating current through a reading coil, resulting in an alternating magnetic field in its locality. If a tag incorporated by a smaller coil is placed in this field, an alternating voltage (electromotive force, emf) will be generated across the tag's coil. Then this alternating voltage is rectified and passed to a capacitor to power the tag's chip. Afterwards, the in-field tags send back their data to the reader using load modulation [9]. ISO 15693 and 14443 standards set frequencies below 14 MHz (most of the near-field readers usually operate at 13.56 MHz), which results in a range of a few centimeters. Near-field RFID is widely used for cards and access control, but not for the management of goods due to its limited range.

As shown in Fig. 2.2b, RFID tags based on far-field emission capture electromagnetic (EM) waves propagating from a dipole antenna attached to the reader [9]. A smaller dipole antenna in the tag receives this energy as an alternating potential difference that appears across the dipole's terminals. A diode rectifies this potential and delivers it to a capacitor, which will result in a storage of energy in order to power its electronics. The operation of the far-field tags is based on a backscattering technique which is presented in [9–11]. There are several types of far-field based RFID systems: active, passive, and semi-passive [12–14]. Unlike the near-field RFID, the reading range of the far-field RFID systems is determined by the amount of power required for energizing the tag's circuit. Consequently, the reading range depends on [15]:

- The Effective Isotropic Radiated Power (EIRP) from the reader which is the reader's transmitted power.
- The reader sensitivity, which defines the minimum level of the tag's signal which the reader can detect and resolve.
- The tag-chip sensitivity, that is the minimum RF power received that is necessary to power RFID chip. The lower it is, the longer is the distance at which the tag can be detected.
- The reader's antenna gain, the tag range is greatest in the direction of the maximum gain which is significantly limited by the frequency of operation and the tag size.

- The tag's antenna polarization, the tag should match the reader's antenna polarization.

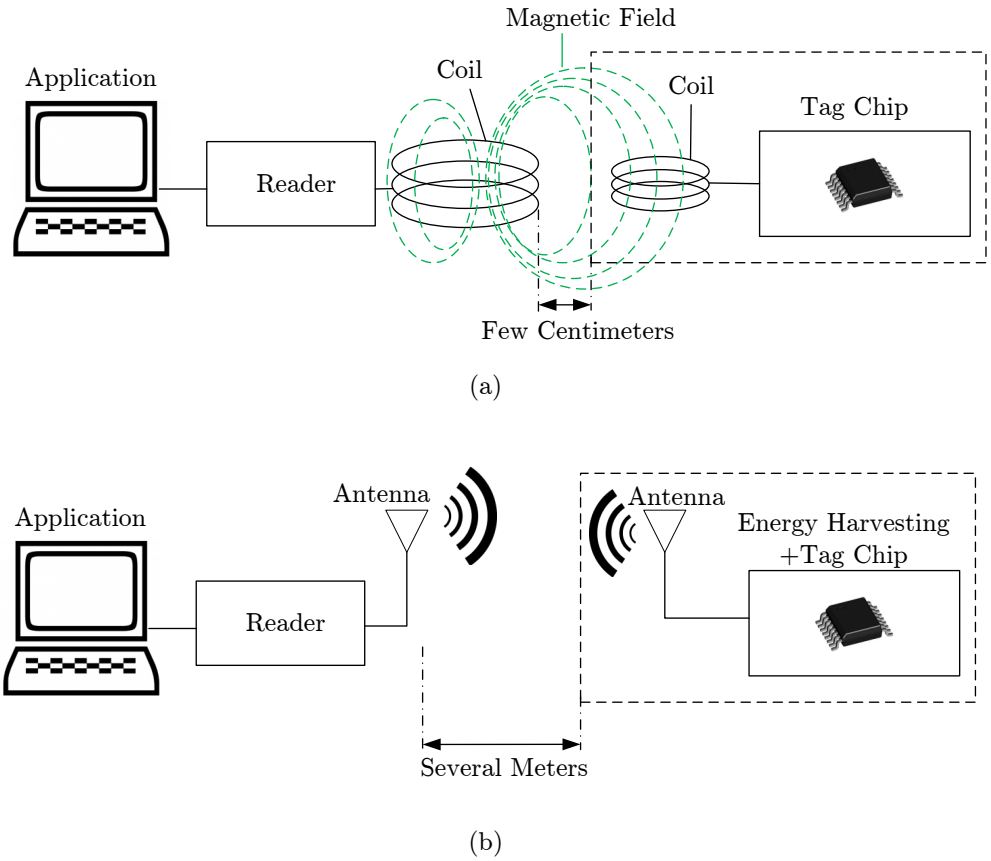

Figure 2.2: RFID system schemes: (a) Near-Field Communication RFID principle. (b) Far-Field Communication RFID principle.

2.2.2 Restrictions of Realizing Low Cost RFID

In order to manufacture an RFID tag, the process illustrated in Fig. 2.3 is performed. The limitations for not having a cheap RFID tag are presented in [16]. Much of the cost of an RFID tag does not only result from the integrated electronic chip, but, more importantly, from the manufacturing complexity of the entire tag. This involves handling the tiny electronic chip and assembling the whole electronic label including the tag's antenna, silicon chip, and harvesting circuit. Furthermore, the cost of the silicon wafer is independent of the IC's design, the cost of the RFID chip is estimated based on the silicon area used for the RFID chip. Significant achievements have been made in reducing the size of the transistors allowing more transistors per wafer area [17].

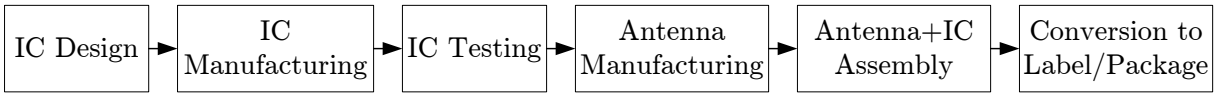

Figure 2.3: The basic process for manufacturing an RFID label.

2.3 Chipless RFID: Towards a Low Cost Identification System

The chipless tags can be considered as a specific type of passive RFID tags. In these tags, instead of storing the ID in a digital IC, it is encoded in physical permanent modifications when the tag is manufactured. These modifications are unique for each tag.

2.3.1 Core Functionality

Chipless tags are a promising low-cost alternative to RFID systems, since they do not require an IC to work [18, 19]. In chipless tags, the ID is stored in physical permanent modifications in a scattering antenna. The modifications are unique for each tag and change its RF backscattered response. This represents the tag's signature.

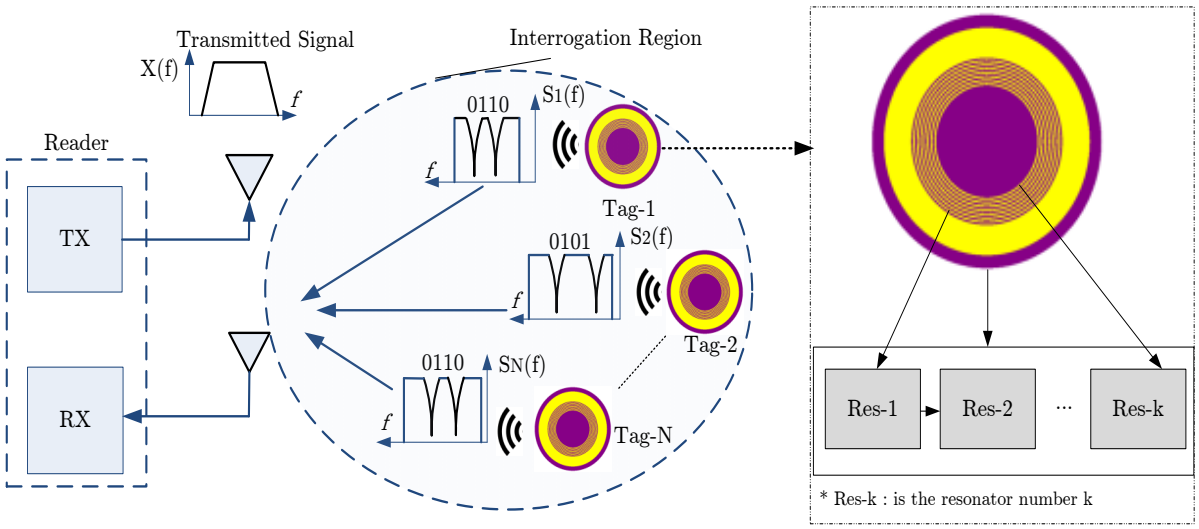

Figure 2.4: Overview of frequency coded chipless RFID.

Fig. 2.4 illustrates a layout of the chipless RFID system. It is worth noting that the information stored in the chipless tags cannot be changed once they have been manufactured, since their physical characteristics are permanent. Still, chipless RFID can provide a low-cost

alternative, which could increase the capabilities of automatic identification. Unlike the RFID with chip-based tags, there is no standard for the chipless RFID; there are several approaches that attempt to create chipless RFID tags. Fig. 2.5 shows a classification of chipless RFID tags given in [18, 20–22].

2.3.2 Chipless RFID Tags' Classifications

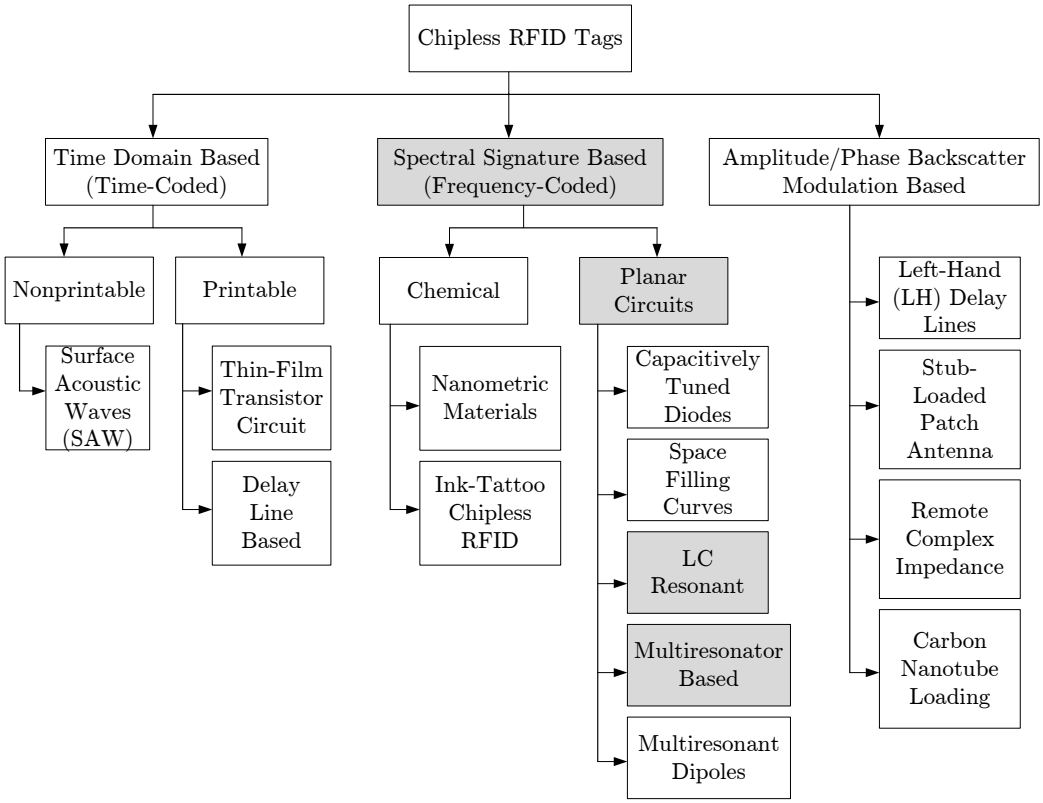

Figure 2.5: Classifications of chipless RFID tags.

The functionality of time domain based chipless RFID tags is evaluated by transmitting a pulse signal from the reader and listening to the reflected signal from the tag. The data is encoded by sending adjacent pulses at different time slots [23, 24]. The Surface Acoustic Wave (SAW), described in [25, 26], is an example of the time domain chipless RFID tags that are successfully commercialized. However, the tag contains a low number of bits despite its large size.

The printable time domain-based chipless tags can be realized either as a thin-film-transistor circuit (TFTC) or as microstrip-based tags with discontinuities. The TFTC tags are printed at high speed on low-cost plastic film [27]. TFTC tags provide advantages over active and

passive chip-based tags due to their small size and low power requirements. Still, they require more power than other chipless tags but also offer a greater functionality. However, low-cost manufacturing processes for TFTC tags have not yet been developed. Organic TFTC could provide a cost-efficient solution [18]. One of the places that develop organic TFTC is the National Institute of Advanced Industrial Science and Technology (AIST) in Japan. An organic TFTC printed on flexible plastic film is illustrated in [28,29]. Another issue is the low electron mobility, which limits the frequency of operation up to several MHz.

The operation of the delay-line-based chipless tags is based on the utilization of microstrip discontinuity after a section of delay-line, as reported in [30–32]. The reader excites the tag by a short pulse (usually 1 ns). The interrogation pulse is received by the tag and reflected at various points along the microstrip line, creating multiple echoes of the interrogation pulse. The delay between the echoes is determined by the length of the delay-line between the microstrip discontinuities. Nevertheless, the initial trials on this chipless technology have shown that only 4 bits of data can be successfully encoded, which shows the limited potential of this technology.

Spectral signature based chipless tags, also called Frequency Coded (FC), encode data into the spectrum using a resonant design. This means that each data bit is commonly associated with the presence or absence of a resonant peak at a predetermined frequency position in the spectrum. The advantages of these types of tags are that they are fully printable, robust, have greater data capacity capabilities than the other chipless tags, and can be manufactured at low cost. The disadvantages of these tags are a large spectrum utilization for data encoding, greater sensitivity to chipless tag orientation requirements, tag-size, and wideband dedicated RFID reader RF components.

Chemical tags are designed from a deposition of resonating fibers or special electronic ink. These tags consist of tiny particles of chemicals, which exhibit varying degrees of magnetism. When EM waves impinge on them, they resonate with certain frequencies, which are analyzed by the reader [18]. These tags are very cheap and can easily be used inside banknotes. They are potentially low cost and can work on low-grade paper and plastic packaging material. Unfortunately, they only operate at frequencies up to a few kilohertz, although this gives them a very high tolerance to metal and water.

Ink-tattoo chipless tags use electronic ink patterns embedded in the surface of the object tagged; no actual substrate is required [20]. The corresponding reader interrogates the ink-tattoo tagged objects with an operating frequency in the microwave range (>10 GHz). The tag creates a unique pattern which can be detected by the reader. Depending on the limited information

available for this technology (which is still in the experimental phase) the author assumes that it is spectral signature based.

Planar circuit chipless RFID tags are designed using standard planar microstrip resonant structures, such as antennas, filters, and fractals. They are printed on thick, thin, and flexible laminates and polymer substrates. Capacitively tuned dipoles were first utilized by Jalaly [33] to design an RF barcode. The tags consist of an array of microstrip dipole-like structures that act as resonant bandpass or bandstop filters tuned to predetermined frequencies. They are successfully identified using a vector network analyzer. A frequency-coded tag based on space-filling curves at 900 MHz is presented in [34]. Space-filling curves are able to create resonances with very small footprints. The advantage of the tag is its compact size due to the properties of the space-filling curves. However, the disadvantage of the tag is that it requires significant layout modifications to encode data [18]. The LC resonant chipless tags consist of a magnetic resonant coil at a distinct frequency. Instead of working at a predetermined frequency, as with NFC standards, the reader sweeps a frequency band searching for a peak resonant frequency, which corresponds to the tag's unique frequency (ID). Commercial LC resonant chipless tags are widely used for surveillance portals and anti-theft purposes in supermarkets as explained in [16].

The multiresonator based FC chipless tags consist of several resonators that provide a peak resonance at predefined frequencies representing the tag's ID. There are two commonly used multiresonator based tags, the retransmission based tag and the backscattering based tag. The former relies on two antennas (cross-polarized, for transmission and reception) and a transmission line with surrounding resonators as in [35]. The other type is illustrated in Fig. 2.4. Here the signal is backscattered from the tag due to the resonators. The reader is able to detect these tags using a sweeping method as discussed in [36]. Furthermore, another approach for utilizing a structure of dipole multiresonator based tags is presented in [37]. In this case, the design is based on several dipoles which backscatter the incoming wave in its orthogonal polarization. Each dipole is tuned to a predetermined frequency, and its presence or absence codes the corresponding bit state. The benefit of depolarization is to mitigate the environmental clutter effects and the coupling between the reader's antennas, providing a better detection of the tags. Moreover, a novel tag structure will be presented in this thesis (Chapter 5). It consists of a dipole, a rectangular ring, and a rectangular patch which increase the coding capacity.

Amplitude-phase backscatter modulation-based chipless RFID tags operate at narrower bandwidths compared to time or frequency-coded tags. This type of tags encodes the ID by varying the amplitude or phase of the backscattered signal based on the loading impedance of

the chipless tag as described in [38]. The variation of the impedance is realized by varying the reactive loading of the tag's antenna [39] which will affect the tag's radar cross section [18]. The advantages of this type of chipless tag are that the range of the operating frequency bandwidth is narrow, and that it has a simple structure. The disadvantages are that the data are encoded using lumped elements that will increase the cost of the tag. The left-hand (LH) delay line based tags consist of a narrow-band antenna connected to a series of cascaded LH delay lines [40]. Each LH section produces a discontinuity in the phase of the incident wave. The reader analyzes the LH-based tag using a modulated signal, such as the quadrature phase shift keying (QPSK) scheme. Each tag produces a unique phase variation in the carrier signal. The remote complex impedance-based chipless tags [41] are implemented by a printable scattering antenna (a patch antenna, for the moment) equipped with a lossless reactance. Each tag has a unique reactance that generates a particular inductive loading. The backscattered signal, then, exhibits a different phase for each tag. Stub-loaded-patch antenna based tags [42] are similar to the remote complex impedance based tags, but with increased robustness. In this case, an open circuit with high impedance stub loads a patch antenna. The ID is coded in the cross-polarized phase difference between electric (E) and magnetic (H) planes. In summary, carbon nanotube-loaded chipless tags consist of RFID antennas loaded by carbon nanotubes (CNTs), which modify the scattering signature depending on their state. In [43] a conformal UHF RFID antenna is loaded with single-walled CNTs to realize a chipless RFID gas sensor. The CNL chipless RFID tag operates by varying the amplitude of the backscattered signal, depending on the concentration of NH3. Consequently, the amplitude variation of the backscattered power from the tag can be detected at the reader end and decoded to estimate the level of NH3. The coding of the amplitude will be inhibited by the channel environmental effects because the amplitude is sensitive to noise and clutter. Additionally, the phase coding will require a technique for phase error compensation due to its sensitivity to the multipath and clutter effects.

2.3.3 Reader Design for FC Chipless Tag Identification

The Software Defined Radio (SDR) [44] provides flexibility in the design and implementation of different radio systems. One of the popular tools for implementing the SDR is an open source software called GNU Radio [45]. Its corresponding hardware counterpart is Ettus' USRP (Universal Software Radio Peripheral). The proposed SDR based reader to identify the FC chipless tags is shown in Fig. 2.6. The USRP consists of an RF daughter-board and a fixed function FPGA which is connected to the PC via a 1 Gigabit Ethernet interface. The transmission

and reception paths of the USRP are separated such that:

- The utilized N210 USRP is connected to a host PC that serves as a software-defined radio. Incoming signals are mixed down using a Direct-Conversion Receiver (DCR) [46], also called a homodyne receiver, to baseband I/Q components, which are sampled by a 2-channel, 100 MS/s, 14-bit Analog-to-Digital Converter (ADC). The digitalized I/Q data follow parallel paths through a Digital-Down-Conversion (DDC) process that mixes, filters, and decimates the incoming 100 MS/s signal to a user-specified rate. The down-converted samples, when represented as 32-bit numbers (16 bits each for I and Q), are passed to the host computer at up to 20 MS/s via a standard Gigabit Ethernet connection.

- For the signal's transmission path, baseband I/Q signal samples are synthesized by the host computer and fed to the USRP at up to 20 MS/s over a Gigabit Ethernet when represented with 32-bits (16-bits each for the I and Q components). The USRP hardware interpolates the incoming signal to 400 MS/s using a Digital-Up-Conversion (DUC) process and then converts the signal to analog with a dual-channel, 16-bit Digital-to-Analog converter (DAC). The resulting analog signal is then mixed up to the specified carrier frequency (controlled by the user).

Regarding the processing executed on the PC, there are two tasks performed simultaneously:

- A linear frequency sweeping mechanism is used as the transmitted signal to interrogate the achievable chipless tags. The details of the utilized frequency sweeping mechanism will be discussed in detail in the following chapters.

- The reader continuously monitors the backscattered signals reflected by the tags. Afterwards, an FFT process is performed on the received signal as the USRP is a time domain device. Then, the designed protocol for multi-tag identification is applied (as will be described in Chapter 3) using a technique that employs fast identification (as will be described in Chapter 4). Finally, the signal is decoded to obtain the corresponding tag-ID (as illustrated in Chapter 5).

2.4 Proposed Communication Layers

Unlike for the chipped RFID system, there is no standard for the chipless RFID systems. Consequently, the thesis proposes the communication layers for the reader for its communication

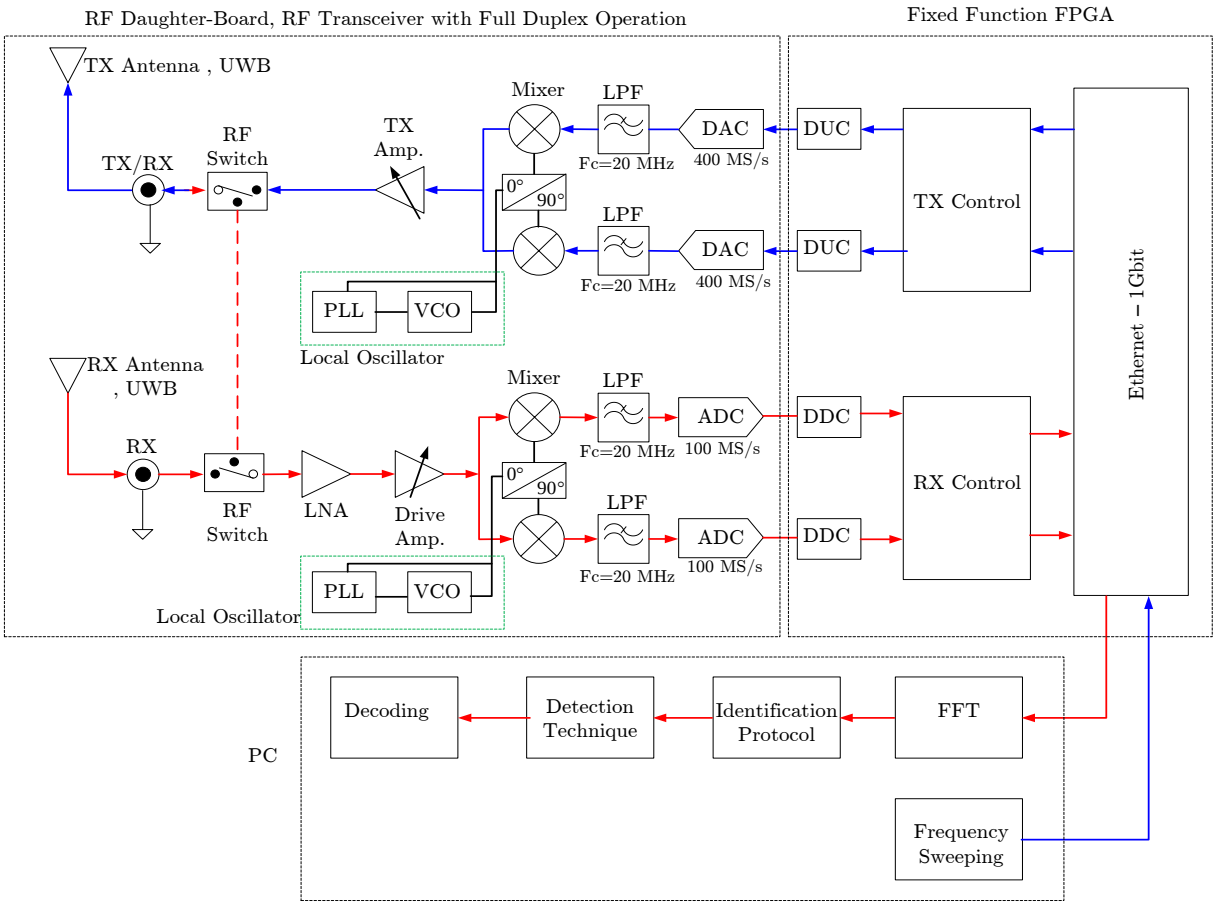

* DUC : Digital-Up-Conversion
DDC : Digital-Down-Conversion
LPF : Low Pass Filter
Fc : low pass filter cutoff frequency
LNA : Low Noise Amplifier

Figure 2.6: Block diagram of the proposed reader to identify the FC chipless tags.

with the chipless tags as follows:

- a physical layer which includes the detection and decoding process.
- a data link layer that constitutes the Medium Access Control (MAC) technique which prevents the collision of multiple identified tags existent in the same interrogation region.
- a network layer which is responsible for defining a rule for the identification of multiple tags (distinguishing one tag from the other).

Regarding the security issues, the chipless tags are hard-coded (the code is printed on the chipless tag, as will be described in the following chapters). Thus, the risk of hacking the tag's code is slim.

2.5 Conclusion

Chipless RFID is an upcoming technology predicted to replace the optical barcode within the next five years. This is due to the constraints of the latter in **i)** the barcode cannot read non-line-of-sight (NLOS) tagged items; **ii)** each barcode needs human assistance to be read; **iii)** the limited information-carrying ability of the barcode [47] **iv)** it is impossible to identify multiple tags at the same time; and **v)** a considerable time delay in case of large queues because each different type of objects needs to be scanned serially.

The prospective passive chipless RFID systems can provide both identification and high-definition localization [48–50] of objects with improved reliability and accuracy while maintaining low power requirements [51, 52] and reduced production costs (unlike conventional RFID systems that are defined by a high cost per tag unit and low robustness [53]). Since the chipless RFID tags are memoryless, capture very low backscattered power and have a short reading range, the classical modulation and encoding schemes are not applicable [54]. Table 2.1 illustrates the comparison between the chipped RFID, the barcode, and the chipless RFID.

Table 2.1: Comparison between the chipped RFID, the barcode, and the chipless RFID.

Attribute	Chipped RFID	**Barcode**	**Chipless RFID**
Line-of-Sight	Not Required	Required	Not Required
Cost	0.22 Euro	Less than 1 cent	Less than 1 cent
Identification	Uniquely Identify Each Tagged Object	Only Identify the Type pf Object	Uniquely Identify Each Tagged Object
Printability	No	Yes	Yes
Operating Temperature	-25°to 65°C	-40°to 80°C	-20°to 80°C
Reading Range	for Passive tags up to 10 m, at TX = 30 dBm but about 5 cm, at TX = 0 dBm .	Some modern scanning techniques can provide up to 6 m with perfect orientation	Currently it can reach about 1 m and some researches aim to enhance the reading range
Multi-Object Collection	200 tags per second [55]	only one object at a time	50 tags in 9 seconds
Standard	EPCglobal and ISO 18000-V1-7 for Air interface	ISO/IEC 15426-1/2 and GS1 Global Code	Not Existent
Interference	Little known interference (with tuning)	Anything blocking/warping the label will interfere (dirt, packaging, paint, coating and etc.)	Little known interference some new techniques are designed to completely mitigate the interference

3 Multi-Tag Identification and Protocol Evaluation Framework

Chipless RFID tags are dummies, memoryless, with a limited number of bits, very low backscattered power, and a short reading range. Therefore, the existing RFID standards and protocols designed for the chipped RFID systems are not applicable to the chipless systems. The main objective of this contribution is to introduce novel multi-tag anti-collision protocols based on Notch Position Modulation (NPM) and Look-Up-Table (LUT) schemes defining the network and MAC layers for the chipless RFID systems. The first generation of the proposed protocol relies on coding the chipless tags according to predefined notch frequency positions that avoid interference between the tags' responses. Furthermore, the tag-ID is encoded with a unique frequency shift for each tag. The second generation of the protocol improves the spectrum utilization and coding capacity. This is accomplished by transferring the tag-ID to be stored in a table in the main memory of the reader (look-up-table). The unique shift of each tag represents the address of the tag's ID. The key performance indicators for the chipless RFID system are explored to validate the protocol's performance. Both protocols are modeled and simulated to identify 10-chipless tags in order to set the regulations for the tag and reader design. Moreover, a novel real-world testbed for the multi-tag UWB chipless RFID system based on a software defined radio is introduced. In this testbed, all the signaling schemes related to the transmitted signal, the detection techniques, an empty room calibration for the clutter removal process, and the identification protocols are applied. The contents of this chapter have been partially published in reference [54, 56].

3.1 Introduction

The identification of multiple tags is one of the most important challenges in order to realize the chipless RFID systems. Since the chipless tags share the same operating frequency, there needs to be a Media Access Control (MAC) technique that is responsible for preventing the collision between the shared tags and that ensures a successful identification of the chipless tags. Thereafter, a protocol needs to be designed to define a rule to identify the tags.

Tag-tag collision occurs when multiple tags respond to the same reader simultaneously, the response of one tag interferes with the response of the other tags. Collisions reduce the throughput of data collection, increase the identification delay, and lower the system's efficiency and reliability [57]. In chipped RFID systems many anti-collision algorithms are proposed to identify multiple tags, illustrated in [58]. Popular solutions such as the Tree Walking Algorithm (TWA) [59] and the Slotted Termination Adaptive Collection (STAC) [60] protocol have been introduced for UHF/HF respectively. However, these protocols are used in chipped RFID standards like EPC [61] and IEC [62], they can therefore not be used in chipless RFID systems, since chipless tags are memoryless and lack the ability to perform complex operations. They also do not have a reconfigurable signature ID to suit any conventional multi-access algorithm.

Few prior contributions have addressed the chipless multi-tag collision problem using signal processing techniques. An algorithm based on transmitting Linear Frequency Modulated (LFM) signals and using Fractional Fourier Transform (FrFT) for multi-chipless-tag detection was used in [63]. This algorithm requires high post-processing computational power and the increase in the overlap region will lead to faulty detection. In [64, 65] the Time Difference Of Arrival (TDOA) of the backscattered signal has been utilized to detect signals from various distances. Additionally, a spread spectrum signature was used in [66] for the coding of the Time Domain Refractometry (TDR) chipless tags to avoid collisions. Furthermore, an algorithm based on the Short-Time-Matrix-Pencil Method (STMPM) has been presented in [67, 68] in order to separate the IDs of chipless tags from one another. Some of the aforementioned algorithms are collected and listed in [69]. However, all these contributions have high-performance computing needs, which will slow down the reading process in real-time systems and will significantly increase the reader's price. In addition, these contributions discuss the identification of tags without considering the tags' ID representation. Moreover, some contributions depend on the time of arrival which can lead to faulty identifications in a multipath fading channel [70]. A logical solution is spatial multiplexing which uses a narrow steerable reader antenna [71]. However, in

problematic scenarios several tags might be in close proximity to each other in the main lobe of the antenna.

To enable the reader to decode the IDs of multiple tags correctly, an approach for collision-free tag communication must be developed. Unlike chipped RFID, chipless RFID tags pose a number of problems that arise from the nonexistence of a MAC protocol and lack of a chipless RFID standard. The MAC anti-collision protocols provide identification of the various tags in the interrogation region to enable conflict free communication. The MAC protocol also provides a high quality-of-service and fair medium access to all contending devices [72].

In this contribution, the MAC and protocol (network) layers are proposed to be used for frequency coded multi-tag communication which will lead to the development of a global chipless RFID standard to control both the tag and the reader design. Consequently, two anti-collision MAC protocols are introduced. The first generation (Gen-1) is based on NPM in which the tag's ID is modulated according to a predefined frequency position of notches. The second generation (Gen-2) is an enhancement of the Gen-1 algorithm so that the tag's ID is stored in the main memory of the reader side while the tag's signature represents an address for the stored ID. This methodology is called LUT as the reader looks for the tags' ID in the table stored in the main memory.

The Radar Cross Sections (RCSs) of the chipless RFID tags have been designed and simulated based on the requirements of a multi-tag scenario. The mathematical framework of both NPM-Gen-1 and LUT-Gen-2 techniques is introduced, followed by the simulation results and performance analyses of the proposed MAC protocols. Finally, a real-world testbed for a multi-tag scenario is developed in an indoor environment illustrating the MAC protocol and the clutter removal technique based on Software Defined Radio (SDR) platforms.

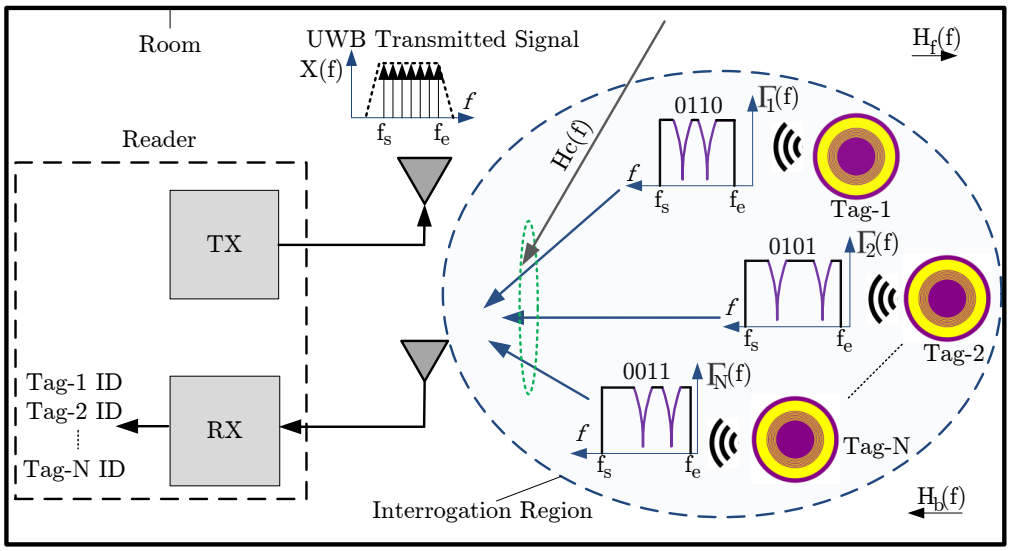

Figure 3.1: Frequency coded chipless RFID system for multi-tag scenario considering clutter effects.

3.2 Frequency Coded Chipless RFID System

In a chipless RFID system, a tag reflects the UWB signal sent from the reader's transmitter. The ID information of the RF tag depends on the resonance frequencies of the tag. In a multi-tag scenario, as shown in Fig. 3.1, all tags in the interrogation zone will modulate the signal transmitted from the reader-transmitter ($X(f)$) by its signature (ID) generating the modulated signal $\Gamma_n(f)$ which is reflected back to the reader-receiver. The total received signal $Y(f)$ is the summation of all backscattered signals from the tags and the influence of the channel and environmental clutter. This will be presented in detail in Section 3.4.

$$Y(f) = X(f).[\sum_{n=1}^{N} H_{fn}(f).\Gamma_n(f).H_{bn}(f) + H_c(f)] \tag{3.1}$$

where $H_{fn}(f)$ is the forward channel towards tag-n, H_{bn} is the backward channel for tag-n, and $H_c(f)$ is the environmental clutter.

Furthermore, all the FC chipless tags share the same operating frequency. Consequently, if several tags have the same ID, a collision will occur.

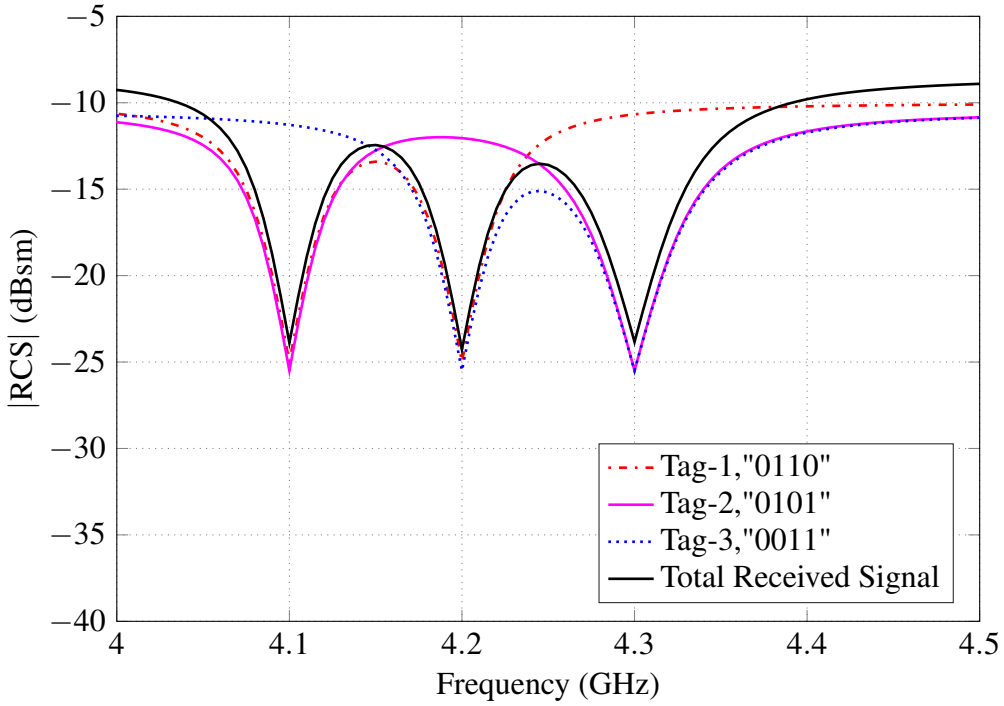

Figure 3.2: Illustration of a collision between 3-chipless tags.

Fig. 3.2 illustrates the collision between three chipless tags. Here, Tag-1, Tag-2, and Tag-3 IDs are "0110", "0101" and "0011", respectively. Thus, there should be a criterion (rule) that prevents a collision between the chipless tags existent within the same interrogation zone. This rule is the proposed anti-collision protocol.

3.3 Protocol Description

In this section, the two generations of MAC protocols (NPM-Gen-1 and LUT-Gen-2) will be thoroughly analyzed. The analysis is divided into two parts. The first section deals with the layout and design of the chipless tag's ID signature. The second part is concerned with the reader's design and with the decoding process.

3.3.1 Gen-1: Notch Position Modulation

The first generation of the proposed MAC protocol is based on the NPM scheme. There are some guidelines for notch positions that allow the identification of different chipless tags at the same time even if they have the same ID.

A. Chipless Tag

The requirement for chipless tags based on the Gen-1 protocol is adapted to match the tags' signature illustrated in Fig. 3.3 according to the following rules.

1. All the resonator based tags need to contain a fixed resonance of the preamble frequency (F_{pr}), this will represent the first bit. The preamble frequency will give an indication to the reader as to whether or not a tag is present in the interrogation region. It will also prevent the reader from scanning the whole spectrum looking for a tag, saving power and time.

2. The second resonator will be unique for each tag and it will generate a notch at a frequency position ε, which is part of the preamble frequency. It will denote the value of the frequency shift for the rest of the tag ID from the bit reference frequency ($Fstart_i$). This bit will allow the reader to differentiate between multiple tags since every tag must have a different frequency shift value. Therefore, no collision can occur. The rest of the resonators will contain the actual tag ID taking into consideration the frequency shift in every bit based on the second resonator.

3. The space between the notch positions should prevent inter-symbol-interference assuming there is a suitable guard band ζ between the notches, which can be estimated by:

$$\zeta = \frac{\text{Resonant frequency of the last notch} - \text{Resonant frequency of first notch}}{2 \times \text{Resonator quality factor}} \tag{3.2}$$

The block diagram of the chipless tag structure considering the Gen-1 protocol requirements is shown in Fig. 3.4.

The maximum number of tags N that could be supported by a reader is represented in Equation (3.3). Moreover, the maximum number of bits per tag K is a function of the frame bandwidth (Δf) and the whole UWB transmitted signal bandwidth excluding the reserved band of the preamble as illustrated in Equation (3.4).

$$N_{\text{Gen-1}} = \left\lfloor \frac{\text{Preamble BW}}{\text{Notch BW}} \right\rfloor - 1 \tag{3.3}$$

$$K_{\text{Gen-1}} = \left\lfloor \frac{\text{UWB Txed Signal BW} - \text{Preamble BW}}{\text{Frame BW}} \right\rfloor - 1 \tag{3.4}$$

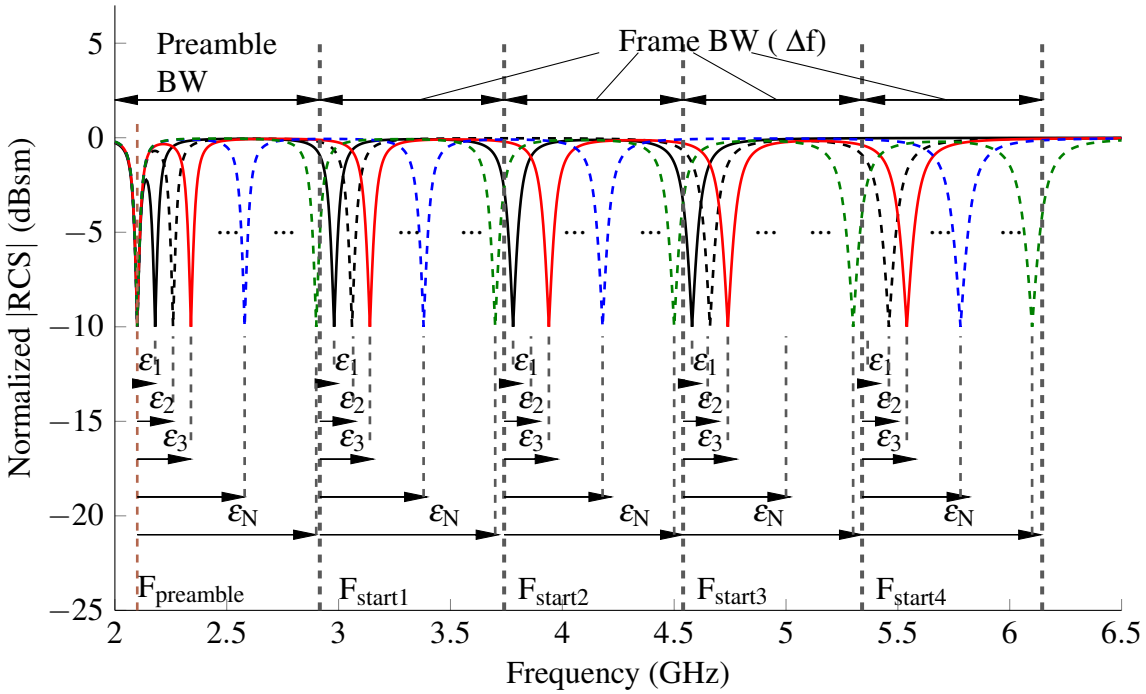

Figure 3.3: The TAG-ID frequency response of n chipless RFID tags based on the novel multi-tag MAC protocol.

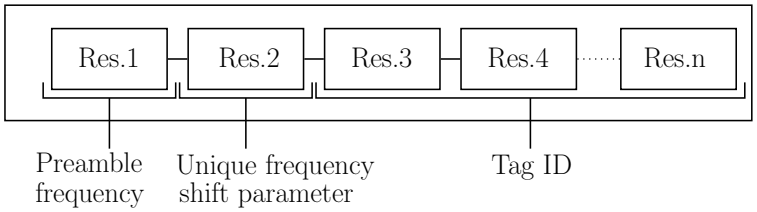

Figure 3.4: Conceptual physical design of the MAC protocol on the chipless RFID tag.

B. Reader

The reader receives signals from multiple tags that are located in the interrogation region as shown in Fig. 3.1. The reader has two main functions. First, it sweeps the operating frequency (using the method described in Chapter 4). Second, it identifies the tags. Algorithm 3.1 describes the processing required by the Gen-1 protocol. The reader starts scanning the preamble bandwidth with a fine frequency hopping methodology in order to:

- Obtain the number of tags,
- Estimate the corresponding frequency shift for each tag (ε_i), such that $\varepsilon_i = [\varepsilon_1, \varepsilon_2, ..., \varepsilon_N]_{1\times N}$, where N is the number of tags.

Algorithm 3.1 Gen-1 MAC algorithm for chipless multi-tag identification

```
1: //BW_pr is the preamble bandwidth
2: //F_pr is the preamble frequency
3: //Bit_res is the bit resolution
4: //Bit_BW is the bit bandwidth
5: //ε_i is the i^th tag shift parameter
6: //Fstart_i is the reference frequency for the i^th bit bandwidth
7: //Ftag_m is the unique absorption frequency for tag m
8: //Bit_position is the position of the bit
9: //ζ is the guard band between notches
10: for all BW_pr do
11:    if F_pr is existent then
12:       ε_i ← Ftag_m − F_pr − ζ
13:       Calculate the number of tags;
14:       Switch to the k^th bit bandwidth;
15:    else
16:       Go to the idle state (at F_pr position);
17:    end if
18: end for
19: for all Bit_BW do
20:    Formulate the tag's ID;
21:    Bit_position ← Fstart_i + ε_i
22:    if Bit_position resonance is existent then
23:       This bit represents one of the i^th order;
24:    else
25:       This bit represents zero of the i^th order;
26:    end if
27: end for
28: Arrange the tag's ID in a matrix;
```

Depending on the value of $\varepsilon_i s$, the interrogator will effectively jump to different frequencies that correspond to the shifts starting at the most significant bit for each tag. This will save power and reduce complexity by avoiding searching for resonances in the unused bands. The advantage of the proposed algorithm is that it is only frequency dependent (it does not depend on time and avoids synchronization problems).

3.3.2 Gen-2: Look-Up-Table Based

The second generation of the chipless RFID protocol is based on the LUT methodology to store the tag's ID. The reader will look for the tag's ID in a table stored in the main memory of the reader based on the unique address extracted from the tag's response.

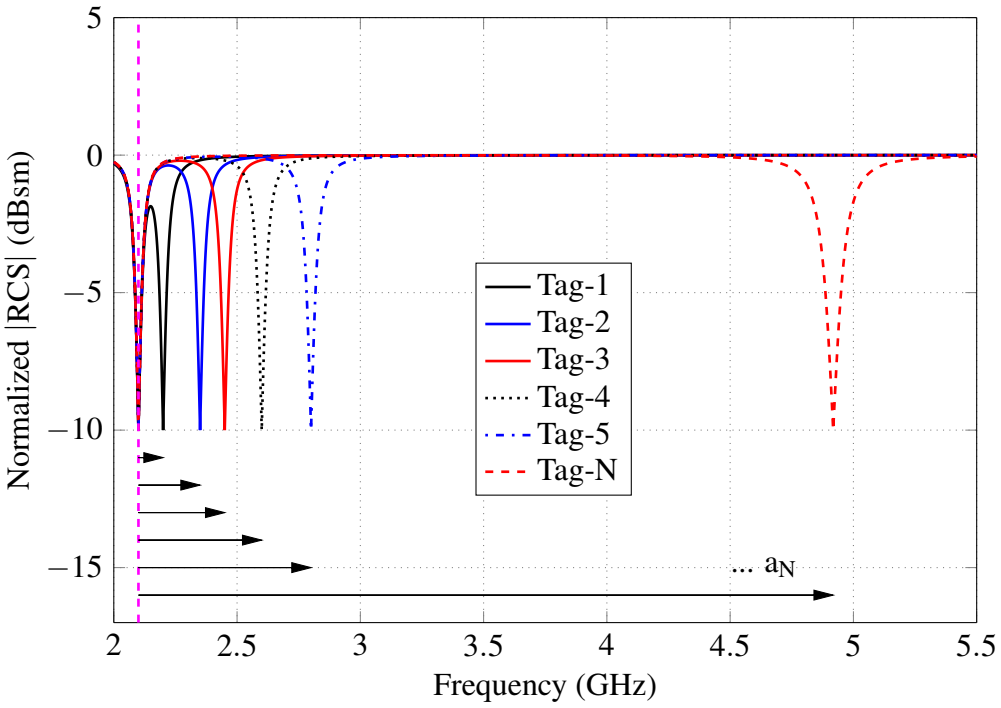

Figure 3.5: Proposed multi-tag identification methodology.

A. Chipless Tag

Each tag includes only two notches, the first one is the same for all tags and the second one is unique for each tag. Fig. 3.5 shows the required tag response to meet the requirements of the Gen-2 protocol. The block diagram of the tag's structure looks like Fig. 3.4 but without the tag ID.

Therefore, the number of tags that can be identified by the reader using the LUT-Gen-2 protocol is expressed by Equation (3.5). It has been observed that a larger number of tags can be represented at a much lower operating frequency, as will be illustrated in Section 3.5.

$$N = \left\lfloor \frac{f_{\text{end}} - f_{\text{start}}}{BW_{\text{Notch}}} \right\rfloor - 1 \tag{3.5}$$

where f_{end} is the end of the operating frequency, f_{start} is the start of the operating frequency, and BW_{Notch} is the notch bandwidth.

The number of bits is not restricted by the physical structure of the tag since they are stored digitally in the LUT.

B. Reader

The table that contains the tags' IDs is stored in the main memory of the reader. This table will be stored once with all the possibilities that the chipless tag's ID could obtain as shown in Table 3.1. The addresses in this table represent the unique frequency shift between the tag's unique notch and the preamble frequency position.

Table 3.1: Look Up Table (LUT) for the chipless tags' IDs.

Unique Address	Tag ID				
	bk	...	b2	b1	b0
$a1$	1	...	0	1	1
$a2$	0	...	0	1	1
...	X	...	X	X	X
...	X	...	X	X	X
a_{N-1}	X	...	X	X	X
a_N	0	...	1	0	0

Algorithm 3.2 describes the functionality of the enhanced Gen-2 protocol. It ensures a much lower complexity, a greater accuracy, and greater spectrum utilization efficiency than the previously mentioned Gen-1 technique.

Algorithm 3.2 Gen-2 MAC algorithm for chipless multi-tag identification

```
1: //UWB_BW is the preamble bandwidth
2: //F_pr is the preamble frequency
3: //ε_N is the N^th tag shift parameter
4: //Ftag_N is the unique absorption frequency for tag N
5: //ζ is the guard band between notches
6: for all UWB_BW do
7:    if F_pr is existent then
8:       ε_N ← Ftag_N − F_pr − ζ
9:       Obtain the tag's ID from the look-up-table;
10:   else
11:      Go to the idle state (at F_pr position);
12:   end if
13: end for
```

The size of the LUT is determined by the number of tags that could be identified at operating frequency. However, the hardware used for the reader's implementation limits the operating frequency and, accordingly, the number of tags (for both Gen-1 and Gen-2).

3.3.3 Key Performance Indicators for the Chipless RFID Protocols

The performance of the designed protocols can be evaluated by means of Key Performance Indicators (KPIs). The most well-known KPIs in networking societies are:

1. Probability of Error; this parameter indicates the robustness of the designed protocols with the variation of a signal-to-noise ratio. Moreover, it represents the probability that the decoded tag-ID is not equal to the real tag-ID.

2. Overhead; it represents the number of bits used by the protocol in the RFID network to identify the tags. It is called overhead because these bits do not represent data, but they are only used for identification purposes. This indicator can be expressed as seen in Equation (3.6).

3. Spectrum utilization; it indicates the number of tags that can be represented at operating frequency.

$$V = \left\lfloor \frac{\text{Preamble Bits}}{\text{Total No. of Bits}} \right\rfloor \times 100 \tag{3.6}$$

3.4 Mathematical Framework and Signalling Schemes

In this section, the mathematical framework of both the NPM-Gen-1 and the LUT-Gen-2 protocol for the FC chipless RFID system is introduced. The chipless tags consist of notches with predefined frequency locations as described in the anti-collision protocols. Therefore, the notch can be modelled like a 2^{nd} order notch filter, as will be discussed in Chapter 5.

$$S(\omega) = \frac{\omega_r^2 - \omega^2}{(\omega_r^2 - \omega^2) + (\frac{\omega_r}{Q}\omega)i} \tag{3.7}$$

$$S(f) = \frac{f_r^2 - f^2}{(f_r^2 - f^2) + (\frac{f_r}{Q}f)i} \tag{3.8}$$

where ω_r equals $2\pi f_r$ and represents the notch angular resonance frequency. Q is the quality factor of the notch filter (resonator used in the chipless tag design). Moreover, the quality factor for the designed protocol-based chipless tag is a constant.

3.4.1 Mathematical Framework of the Gen-1 Protocol

First, the tag's ID frequency response $\Gamma(f)$ based on the NPM-Gen-1 will be presented, followed by the complete RFID signaling scheme of the proposed protocol.

A. Tag Frequency Response

The overall frequency response for a chipless RFID tag n based on the Gen-1 anti-collision protocol is expressed by Equation (3.9). The tag's response consists of a common notch for all tags at the preamble frequency f_{pre}, a unique notch for each tag at frequency position f_{n}, and the tag's ID.

$$Tag_{\text{overall response}} = Tag_{\text{preamble freq}} + Tag_{\text{unique freq}} + Tag_{\text{ID}} \tag{3.9a}$$

$$\Gamma_n^{\text{Gen-1}}(f) = S(f)|_{f_{\text{r}}=f_{\text{pre}}} + S(f)|_{f_{\text{r}}=f_n-f_{\text{pre}}} + \sum_{k=1}^{K} c_{n,k}.S(f-k\Delta f-\varepsilon_n) \tag{3.9b}$$

where $S(f)$ is the notch shape in the frequency domain as described in Equation (3.8), n is the tag index, k is the index of the digital bit representation in the frequency domain that represents the tag's ID, Δf is the frame bandwidth, ε_n is the unique frequency shift for the tag n that has the value of $f_n - f_{pre}$, and $c_{n,k}$ is the binary code of the n^{th} tag at the k^{th} index which has a value of either 1 or 0. Thus, Equation (3.9) yields the shape and spectral position of every resonance in the proposed notch position modulation scheme.

B. RFID Signalling Schemes

In a typical chipless RFID system, the tags are identified by using an UWB impulse signal. This offers a fast detection, but with the disadvantage of a short reading range due to the low transmitted signal power to meet the FCC's UWB regulations (as will be explained in Chapter 4). In this contribution, a novel reading method to increase the reading range of the frequency signature based chipless RFID systems is proposed. The FCC's regulation states that the Effective Isotropic Radiated Power (EIRP) for an UWB device operating in the range 3.1–10.6 GHz must not exceed -41.3 dBm/MHz. However, the FCC's regulations allow a peak level of emission with a maximum of 0 dBm, contained within a bandwidth of 50 MHz centered at the frequency at which the highest emission occurs [73–75]. Therefore, the method depends on detecting the

presence of a tag in a spectrum using frequency sweeping and hopping techniques instead of sending a UWB impulse signal. The reflected power from either logic-0 "no-notch" or logic-1 "notch" detection in case of narrowband transmission is 400 times the power reflected in the case of UWB transmission at a distance of 30 cm [76, 77].

Detecting all the tags efficiently by scanning the whole RFID bandwidth in the traditional way is time consuming, energy inefficient, and computationally expensive. The reader's transmitted signal using the NPM-Gen-1 protocol to identify the chipless tags consists of two parts. The first one is the sweeping of the preamble bandwidth to determine the existence of the tags and the unique frequency shift code corresponding to each tag. The second part is dedicated to identifying the chipless tags as represented in Equation (3.10).

$$X_{\text{inventory}}(f) = X_{\text{preamble}}(f) + X_{\text{identification}}(f) \tag{3.10}$$

Equation (3.11) illustrates the scanning of the preamble bandwidth necessary to calculate the unique frequency shift defined for the n^{th} tag (ε_n). In addition, this scan enables the reader to determine the number of chipless tags available in the reader's interrogation zone.

$$X_{\text{preamble}}(f) = \sum_{m=0}^{M-1} A.\delta(f - m.\xi) \tag{3.11}$$

where M represents the hopping frequencies in the preamble bandwidth, A is the amplitude of the transmitted signal of the preamble, and ξ is the frequency sweeping step used to scan the preamble band.

The identification of the transmitted signal is divided into two parts as described in Equation (3.12). The first part is the identification of the n^{th} tag's ID ($X_{\text{ID-n}}(f)$) and the second part is determining the beginning of the bit bandwidths (Δf), $X_{\text{frame-start}}(f)$. After the preamble bandwidth spectrum sweeping, the number of tags is determined and each tag is assigned its own ε_n (frequency notch position parameter). The reader sweeps the k^{th} bit of the n^{th} chipless tag by hopping the frequencies in the spectrum of the predefined frequency locations according to the tags' unique shift parameters ε_n. Furthermore, the reader sweeps each start of the bit bandwidth Δf in order to obtain better results for environmental clutter removal using the empty

room calibration process described in the measurements section.

$$X_{\text{identification-n}}(f) = X_{\text{ID-n}}(f) + X_{\text{frame-start}}(f) \tag{3.12a}$$

$$= \sum_{k=1}^{K} A.\delta(f - k\Delta f - \varepsilon_n) + \sum_{k=1}^{K} A.\delta(f - k.\Delta f) \tag{3.12b}$$

where Δf is the frame (bit) bandwidth and K is the maximum number of bits as illustrated in Equation (3.4)

The frequency response of the received signal is represented by Equation (3.13).

$$Y(f) = X_{\text{inventory}}(f).[(\sum_{n=1}^{N} H_{\text{f}n}(f).\Gamma_n^{\text{Gen-1}}(f).H_{\text{b}n}(f)) + H_{\text{c}}(f)] + N(f) \tag{3.13}$$

where $X_{\text{inventory}}(f)$ is the reader's transmitted signal, $H_{\text{f}n}(f)$ is the forward channel to identify tag-n with a frequency response $\Gamma_n^{\text{Gen-1}}(f)$, $H_{\text{b}n}(f)$) is the backward channel for tag-n, $H_{\text{c}}(f)$ is the environmental clutter that is expected at the start of each frame bandwidth (expressed in Equation 3.14), and $N(f)$ is the noise response.

$$\tilde{H}_{\text{c}} = \sum_{i=1}^{K} H_{\text{c}}(f - \Delta f_i) \tag{3.14}$$

3.4.2 Mathematical Framework of the Gen-2 Protocol

A. Chipless Tag Frequency Response

Based on the LUT-Gen-2 anti-collision protocol, the chipless tag consists of two notches. The first one is the same for all chipless tags working with the Gen-2 protocol. The other one is unique for each tag as described in Equation (3.15).

$$\Gamma_n^{\text{Gen-2}}(f) = S(f)|_{f_{\text{r}}=f_{\text{pre}}} + S(f)|_{f_{\text{r}}=f_n-f_{\text{pre}}} \tag{3.15}$$

B. Signaling Schemes

The reader sweeps the overall operating frequency using either fixed or adaptive hopping techniques in order to reduce the overall system latency (as will be described in Chapter 4).

$$X_{\text{Gen-2}}(f) = \sum_{m=0}^{M-1} A.\delta(f - m.f_{\text{h}}) \qquad f_{\text{start}} \leq f \leq f_{\text{stop}} \tag{3.16}$$

where $X_{\text{Gen-2}}(f)$ is the transmitted signal based on the Gen-2 protocol and M is the number of frequency hops with a step of f_{h}. The frequency step estimation is made more precise by using an adaptive technique for the sweeping process as will be explained in Chapter 4. This improves the system latency significantly. In addition, $f_{\text{stop}} - f_{\text{start}}$ represents the spectrum of possible operating frequencies. Furthermore, the ID of the chipless tags is stored in the look-up-table of the main memory at the reader. The address of the memory location is obtained by the frequency shift between the tag's unique signature and the preamble frequency as in Equation (3.17). Thus, each tag is represented by a unique address in the memory.

$$a_n = f_n - f_{\text{pre}} \tag{3.17}$$

The received signal's frequency response is represented by Equation (3.18).

$$Y_{\text{Gen-2}}(f) = X_{\text{Gen-2}}(f).[(\sum_{n=1}^{N} H_{\text{f}n}(f).\Gamma_n^{\text{Gen-2}}(f).H_{\text{b}n}(f)) + H_{\text{c}}(f)] + N(f) \tag{3.18}$$

The description and implementation of the LUT-Gen-2 anti-collision MAC protocol is much easier than that of the Gen-1 algorithm.

3.5 Simulation Results and Discussions

In this section, the simulation results showing the validity of the proposed multi-tag anti-collision protocols are outlined. The utilized simulation environment is presented in Fig. 3.6. A model of the RFID chipless tags will be described in chapter 5 using a second-order notch filter approach which matches the simulated chipless tags using CST-Microwave Studio. Equations (3.9 and 3.15) are used to represent the chipless tags in the simulations. Afterwards, the two proposed protocols are evaluated by estimating the probability of error deriving from the variation of the signal-to-noise ratio on the receiver's side. The simulations are performed for 10-tags and the

corresponding results with regard to the key performance indicators are discussed. Furthermore, overhead and spectrum usage are studied for both of the proposed protocols. In addition, the effect of increasing the operating frequency during the performance of the chipless tag employing Gen-1 and Gen-2 protocols is discussed. The simulation is implemented using the MATLAB M-file simulation tool.

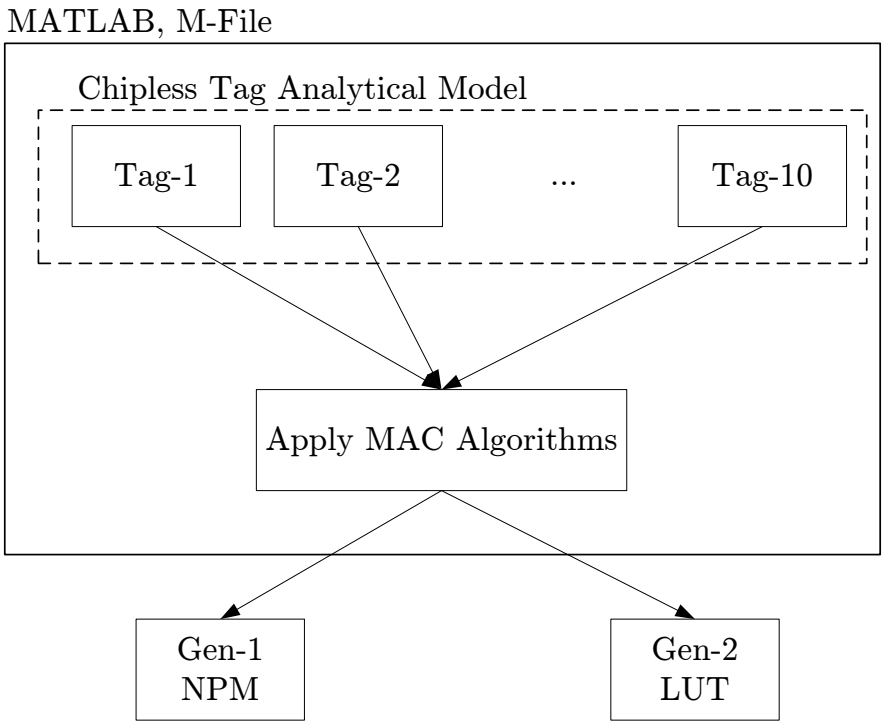

Figure 3.6: Block diagram of simulation environment.

3.5.1 Gen-1 Protocol Simulation

A. Chipless Tag Response

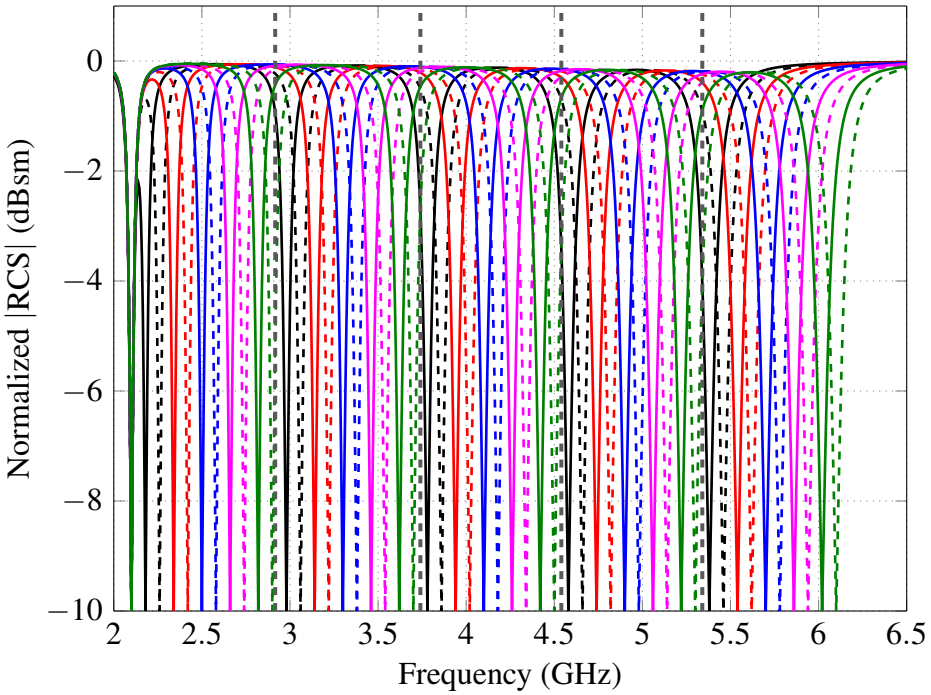

Figure 3.7: Simulation of 10-tags using Gen-1 MAC.

Fig. 3.7 shows the normalized RCS magnitude for ten 4-bit chipless tag responses with the Gen-1 protocol. Each tag is represented by a different color. The dashed vertical lines indicate the preamble bandwidth and the 4-coding bandwidths. Therefore, the representation of the 10 chipless tags with 4-bit coding capacity each is implemented within a 4.5 GHz operating bandwidth by means of utilizing the proposed NPM technique.

B. Probability of Error

The probability of error is estimated by varying the signal-to-noise ratio per bit to study the behavior of the proposed technique at low SNR values. The low SNR causes a deformation in the notch pattern due to the effect of the noise. Hence, it is important to study the robustness of the proposed protocols considering the deformation error of the notch pattern.

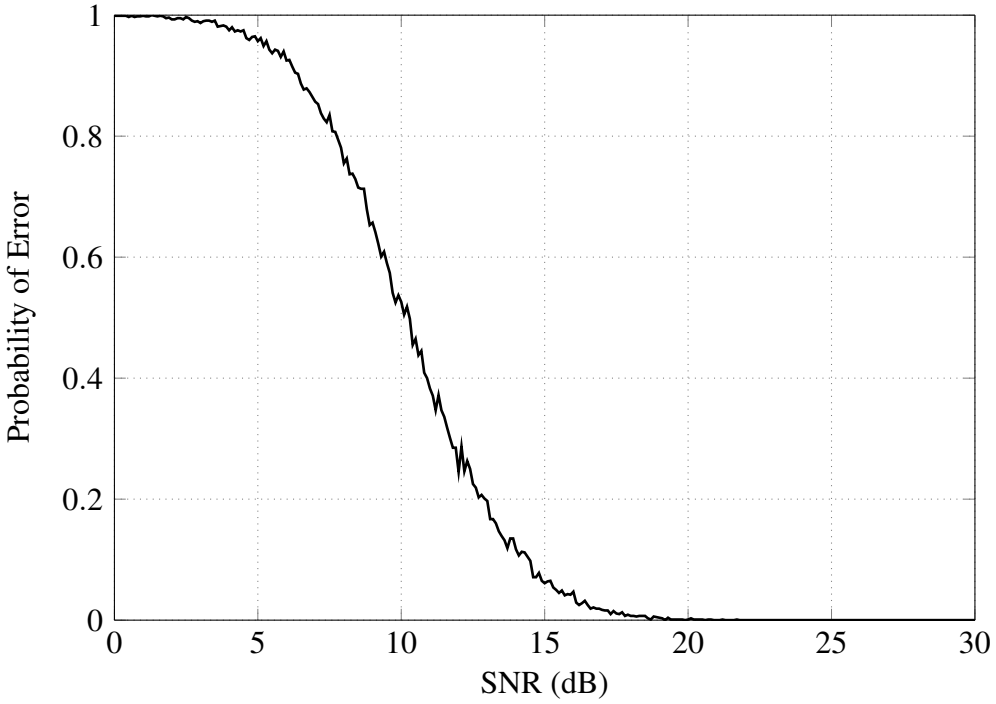

Figure 3.8: Probability of error for 10-chipless tags with 4-bits coding capacity when employing the Gen-1 protocol.

The probability of error for the identification of 10-chipless tags using the Gen-1 protocol is illustrated in Fig. 3.8. It shows that at lower SNR/bit values the probability of error is high. This is due to the fact that if any bit is received wrongly, the overall tag code is wrongly detected. Also, there are two sources of errors in the identification of tags using the Gen-1 protocol. The first one is caused by a wrong decision at the preamble bandwidth (which determines the tag's existence). The second one derives from the extraction of the tag's ID (from the coding bandwidth). The detection technique used in the simulation process is called window-based energy detection and is outlined in [36].

C. Overhead

The overhead parameter is calculated by using Equation (3.6). Fig. 3.9 illustrates the relationship between the overhead, the number of data bits, and the number of tags. The overhead is dramatically reduced when the number of coding bits (tags' data capacity) is much higher than the number of preamble bits as illustrated in Equation (3.19b). Moreover, the network's overhead is enhanced with a higher number of tags within the same interrogation zone as expressed in Equation (3.19a).

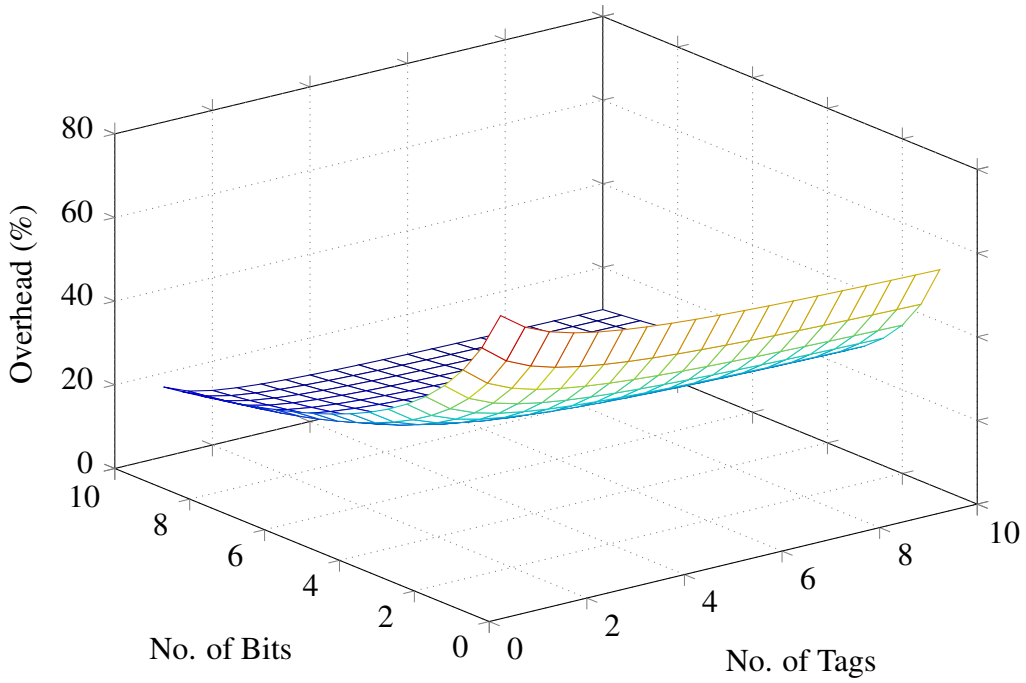

Figure 3.9: Overhead simulation when applying the Gen-1 protocol.

$$V = \frac{P}{T} \tag{3.19a}$$

$$= \frac{P}{P+C} \tag{3.19b}$$

where V is the overhead, P is the number of preamble bits, T is the total number of bits, and C is the number of coding bits (tag-ID).

3.5.2 Gen-2 Protocol Simulation

A. Chipless Tag Response

The normalized RCS magnitude of the 10-chipless tags using the Gen-2 LUT-based protocol is shown in Fig. 3.10. As mentioned in Section 3.3, the chipless tags' IDs are stored in a look-up-table as shown in Table 3.2. The frequency shift between the notches is 80 MHz. Each tag is represented by a different color. The 10-chipless tags are perceived at 0.9 GHz by applying the look-up-table based on the Gen-2 protocol, since that overall tag's ID is stored in the main memory on the reader.

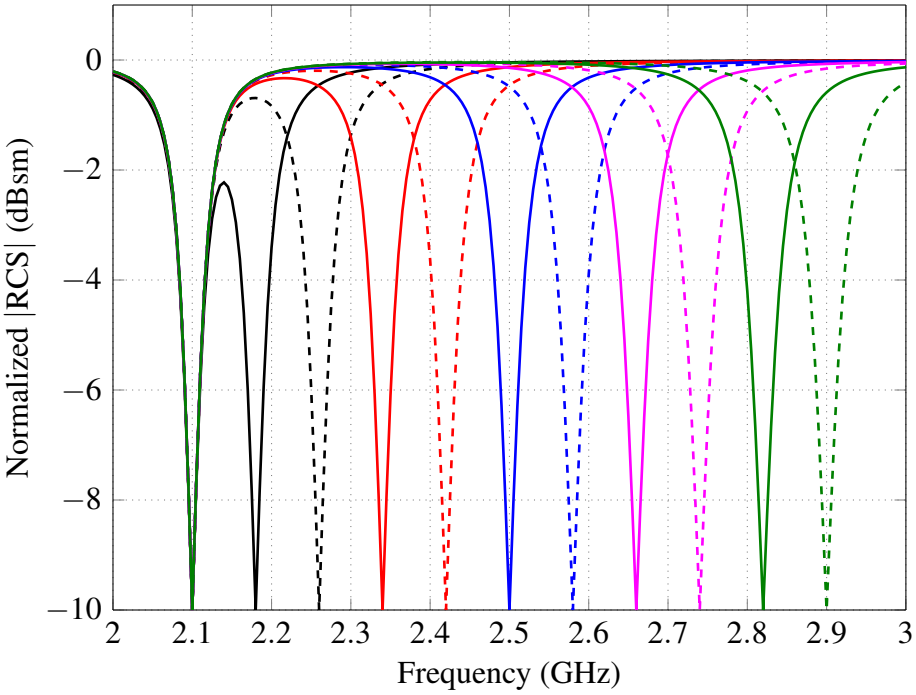

Figure 3.10: Simulation of 10-tags using Gen-2 MAC.

Table 3.2: Look-Up-Table (LUT) showing the IDs of the simulated chipless tags.

Frequency Shift (MHz)	Tag ID			
	b3	b2	b1	b0
80	1	0	0	1
160	1	1	1	1
240	X	X	X	X
...	...	...	...	...
800	X	X	X	X

B. Probability of Error

The probability of error is estimated for the identification of 10-chipless tags based on the look-up-table of the Gen-2 protocol and the window-based energy detection described in [36]. Fig. 3.11 shows that the Gen-2 protocol performs better as it shows a much lower probability of error. This is due to the fact that the Gen-2-tag's response is assigned a much lower spectrum than the Gen-1-tag's response.

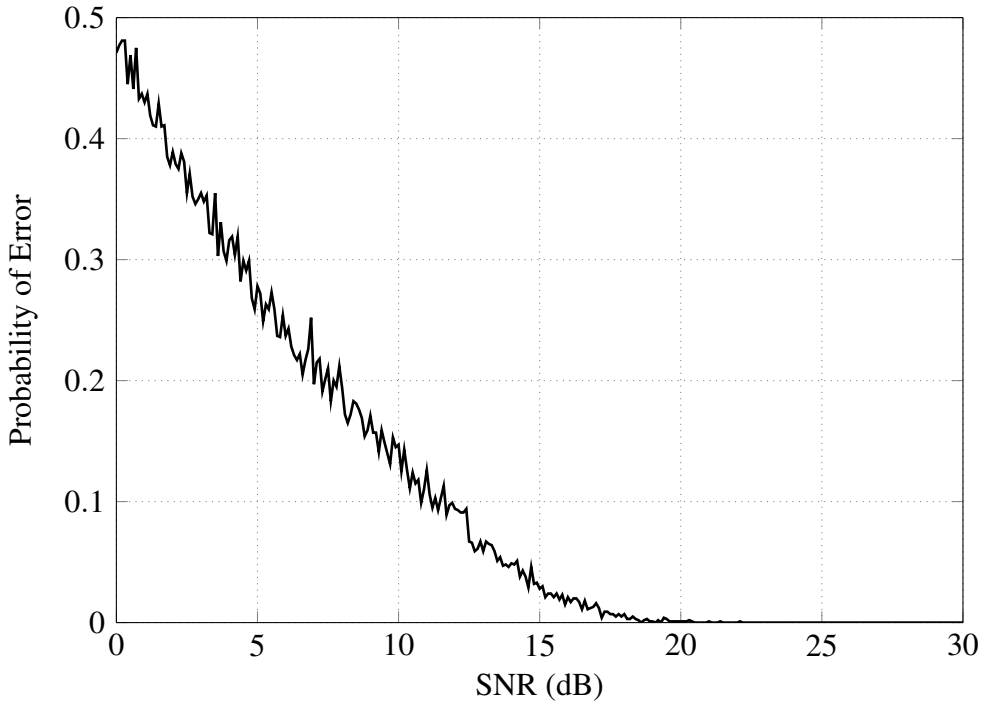

Figure 3.11: Probability of error for 10-chipless tags with 4-bits coding capacity when applying the Gen-2 protocol.

C. Overhead

The benefit of the look-up-table method is that it combines identification and coding process. Therefore, there is no overhead when using the Gen-2 protocol because the same notches are used for both identification (unique identifier) and coding (address to the ID at the LUT).

3.5.3 Effect on the Protocols' Performances when Increasing the Carrier Frequency

The influence on the performance of the chipless RFID system when increasing the operating frequency is studied considering multi-tag systems in order to determine whether or not it is beneficial to operate at higher frequencies. The consequences of increasing the operating frequency are as follows:

1. The notch bandwidth is increased as a result of increasing the frequency. This is shown in Chapter 4. It will require an increase of the operating frequency's bandwidth to identify the same number of chipless tags. For example:

- For Gen-1, 10-tags represented with an operating frequency of 2–6.5 GHz are represented in the range of an operating frequency of 4–12 GHz in order to avoid interference between adjacent notches.
- For Gen-2, the 10-tags are represented by an operating frequency of 2–3 GHz. These tags can be represented in a frequency range of 8–10 GHz.

2. The probability of error to identify the 10-tags represented by a higher carrier frequency is shown in Fig. 3.12. It can be seen that the probability of error is lower when operating at higher frequencies. This is due to the fact that notches with a wider bandwidth are more accurately detected than the narrower ones. This is discussed in Chapter 5. Consequently, the detection of tags operating at higher frequencies is much better than of those that are working at lower frequencies. Furthermore, the Gen-2 protocol performs very well at a higher operating frequency. This directly impacts the reading range which is increased for operation at higher frequencies.

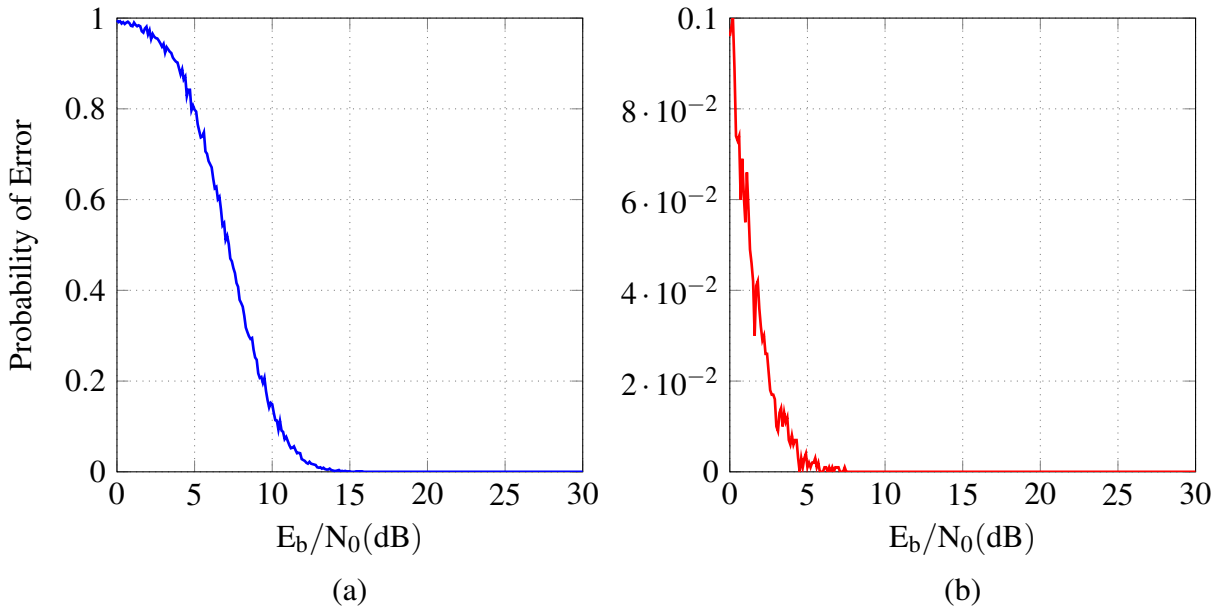

Figure 3.12: Probability of error for the identification of 10-chipless tags operating at a higher carrier frequency: (a) Gen-1. (b) Gen-2.

3.6 Measurements

In order to validate the proposed chipless RFID collision avoidance protocols, two chipless tags (with 3-coding bits that represent the tag's ID) are designed and manufactured based on Gen-1

and Gen-2 using the CST-Microwave Studio EM simulation tool. Then, a real-world testbed is designed based on a software defined radio platform (USRP) to identify the chipless tags when applying the Gen-1 and Gen-2 protocols.

3.6.1 Protocol Based Chipless Tags

Designing chipless RFID tags with the frequency responses as shown in Figs. 3.3 and 3.5 is crucial. They require a uniform spacing between resonances, a high coding capacity, no harmonics within the frequency band of interest, easy coding, and a compact size. Herein, the orientation independent tag presented in [78] is employed to fit the protocol's requirements. Hence, the slot ring resonators are optimized using CST-MWS [79] to present different codes that satisfy the Gen-1 and Gen-2 protocol's instructions as illustrated in Figs. 3.13 and 3.13, respectively. The operating frequency of the chipless tags is 4–6 GHz, which can be detected using the USRP, with 3-bits of coding data representing the tags' IDs. In order to increase the level of backscattered power, the tags are designed in a (2×2) array. Accordingly, different arrays of tags are designed, simulated, and evaluated. The substrate used in the design is RO4003C with a permittivity of 3.38, a loss tangent of 0.0027, and a thickness of 1.52 mm. Fig. 3.13 illustrates the response of the chipless tags based on the Gen-1 NPM protocol such that the ID of Tag-1 is "111" and that of Tag-2 is "110". The responses of the Gen-2 based tags are shown in Fig. 3.14, which uses IDs stored in the look-up-table. The manufactured chipless tags are depicted in Fig. 3.15. They are planar without ground plane. Therefore, the detection of these tags can either occur in the backscattering mode or the transmission-through mode.

3.6.2 Measurement Setup and Environment

A real time Software Defined Radio (SDR) hardware platform is employed in the measurement setup as a reader. For all experiments and tests an Ettus USRP N210 [80] with a CBX [81] daughter-board as RF front-end is used. This is a wide band transceiver that supports full duplex operation for a frequency band of 1.2 GHz to 6 GHz with an instantaneous bandwidth of 40 MHz. As illustrated in Fig. 3.16, a GNU Radio based chipless RFID reader is implemented to detect the frequency signature of the protocol based tags. The overall signal processing operations are implemented in the PC (written in Python including the designed protocols) and then transferred to the FPGA and the RF frontend at the USRP by means of an Ethernet connection.

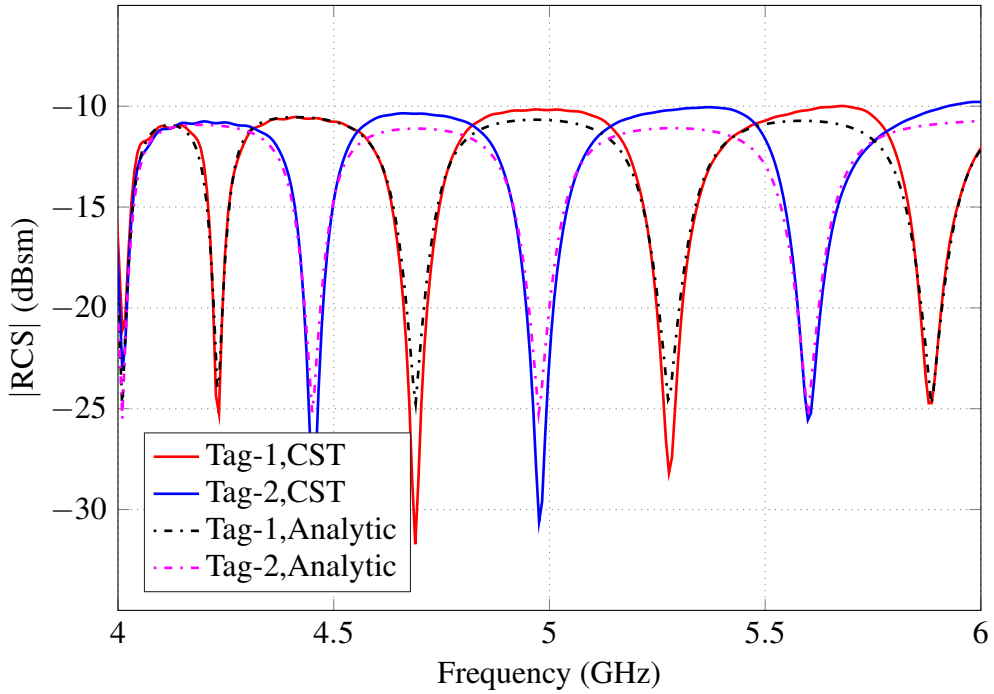

Figure 3.13: The RCS frequency response simulation of two RFID chipless tags using CST-MWS and an analytic method based on Equation (3.9) when applying the Gen-1 NPM protocol.

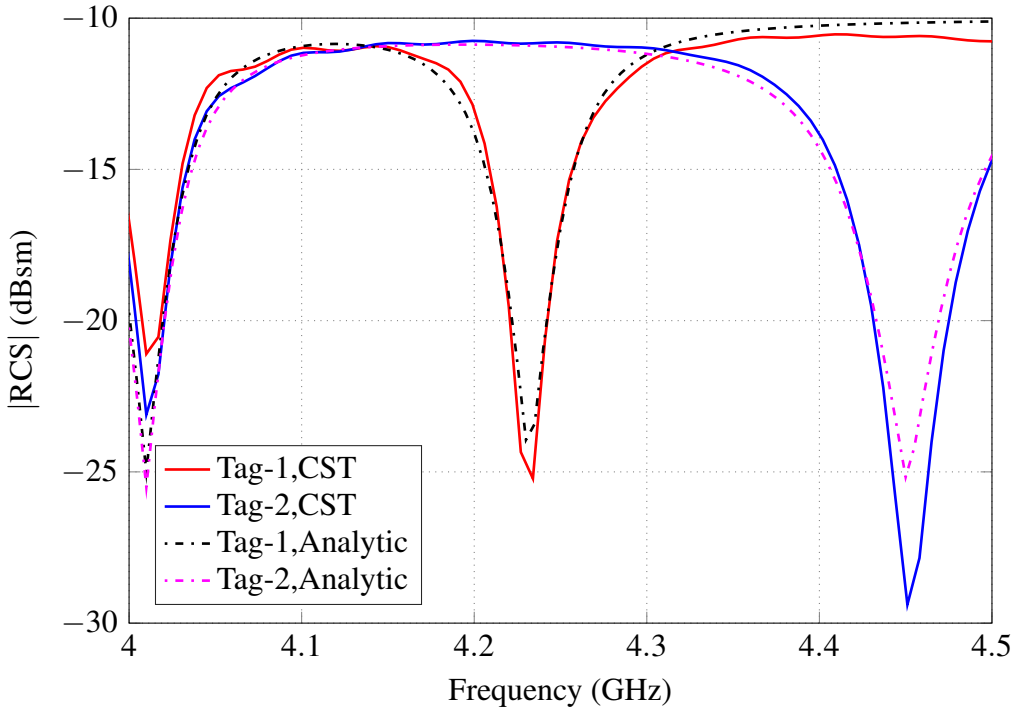

Figure 3.14: The RCS frequency response simulation of two RFID chipless tags using CST-MWS and an analytic method based on Equation (3.15) when applying the Gen-2 LUT protocol.

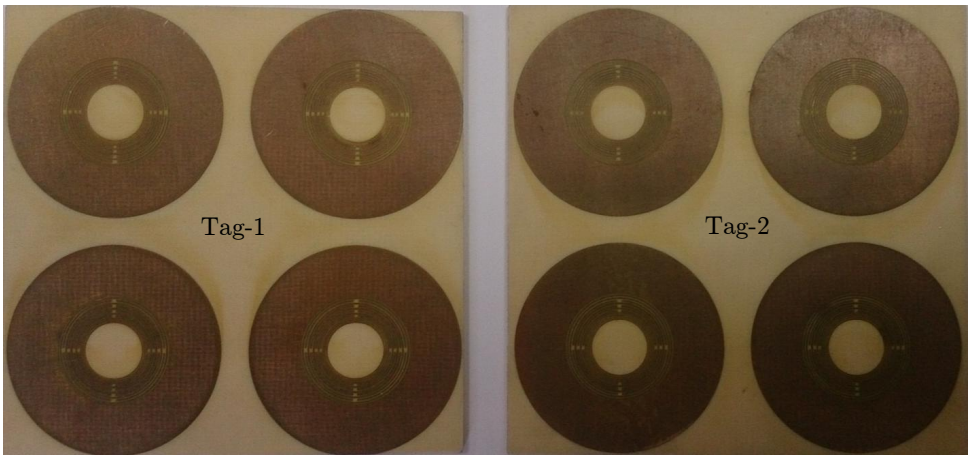

Figure 3.15: Manufactured tags.

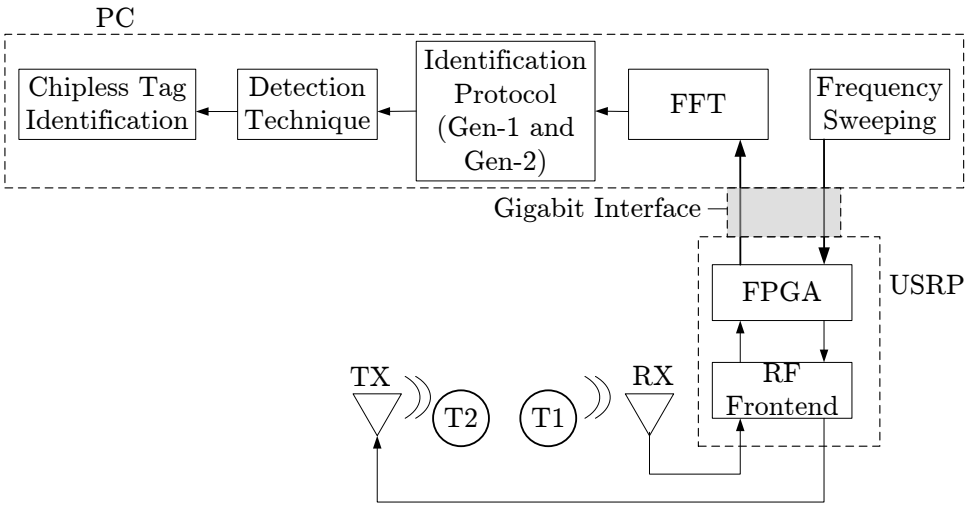

Figure 3.16: Block diagram of the measurement setup.

Specifications for the USRP N210, CBX, and the frequency sweep parameters are given in Table 3.3. Two directional horn antennas are used in a frequency range of 4 GHz to 6 GHz. The setup in Fig. 3.17 indicates that the USRP is connected via Ethernet cable to the laptop where the advanced signal processing techniques are implemented. Additionally, the laptop also sends commands to the USRP to control the transmitted and received signals. In the designed testbed, the Tx and the Rx antennas are in a line-of-sight distance of $D_{\mathbf{ant}} = 30$ cm. Moreover, the two protocol based tags (Gen-1 and Gen-2) are placed in the middle of the interrogation zone of the two antennas. The measured signal $Y(f)$ does contain the backscattered tag response, in addition to the clutter effects, the antennas' transfer functions, and the additive noise. In order to extract

Table 3.3: USRP Parameters.

Parameter	Value
FPGA	Spartan 3A-DSP 3400
Sampling Rate	1 M samples / second
Transmitter Gain	31.5 dB
Receiver Gain	0 dB
Start Frequency	4 GHz
End Frequency	6 GHz
Frequency Step	10 MHz
Output Power	12 dBm
Interface	Gigabit Ethernet
Frequency Sweep	
Averaging	100
FFT size	1024
Notch detection algorithm	Energy detection
Reader Antenna	
Type	Horn
Gain	5 dBi

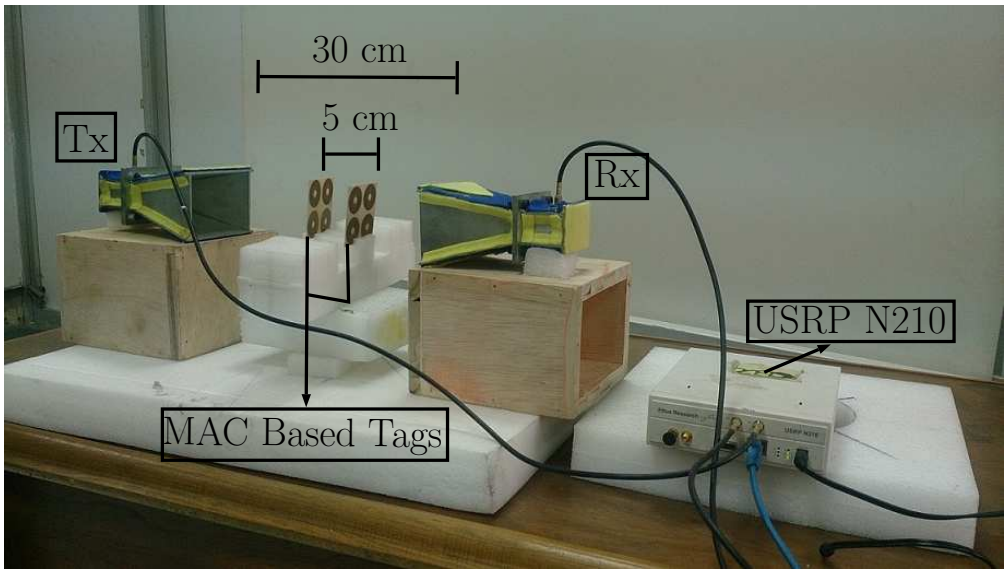

Figure 3.17: Real scenario for multi-tag identification using a software defined radio platform (USRPN210).

the tags' signature accurately, an empty room calibration has to be performed, then a subtraction process takes place as illustrated in Equation 3.20.

$$|Y_{\mathrm{R}}(f)|_{\mathrm{dB}} = \frac{1}{A}\sum_{a=1}^{A}[|Y^{a}(f)|_{\mathrm{dB}} - |Y^{a}_{\mathrm{Empty}}(f)|_{\mathrm{dB}}] \tag{3.20}$$

where $Y^{a}_{\text{Empty}}(f)|_{\text{dB}}$ describes the empty room measurements on a dB scale and $Y_{\text{R}}(f)|_{\text{dB}}$ represents the backscattered received power from the two tags after applying an empty-room calibration, clutter removal, and a noise averaging process as presented in Figs. 3.18 and 3.19. Moreover, A represents the maximum amount of averaging done for noise suppression as it increases the dynamic range of the signal above the noise levels.

3.6.3 Measurement Results

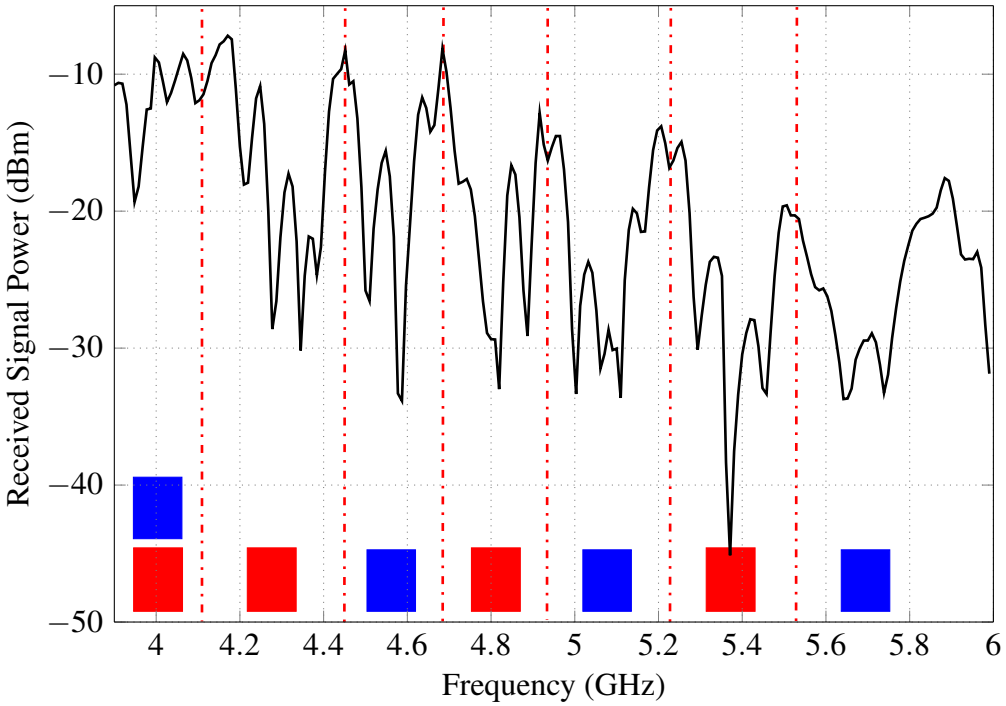

Figure 3.18: Detected signal using USRP after applying a real-time clutter removal and equalization process utilizing the Gen-1 protocol. (Red: Notches of Tag-1, Blue: Notches of Tag-2)

Fig. 3.18 shows the measurements of the backscattered received power from the two tags based on the Gen-1 NPM anti-collision protocol after applying an empty-room calibration, clutter removal, and a noise averaging process. Furthermore, Fig. 3.18 illustrates a noticeable decay in the received signal power for operating frequencies greater than 5 GHz. This is because the utilized CBX daughter board's functionality decreases for high operating frequencies which is observed during the experiments. This is why most of the tags designed and described in the following chapters are working at an operating frequency of 2–5 GHz.

The measurement result of the received signal when using the two Gen-2 based chipless tags is illustrated in Fig 3.19 taking into consideration environmental effects by also applying the

empty-room calibration process. Furthermore, the experiment with the two chipless tags is now performed within a much lower bandwidth and with a lower complexity than the Gen-1 NPM protocol. This means that:

1. The CBX-RF-daughter board performs at a frequency range lower than 5 GHz so that the average power of the received signal does not decay.
2. It is much easier to identify the chipless tags when using the LUT-Gen-2 protocol and the accuracy of detection is much greater.
3. The utilized LUT stored in the reader's main memory is illustrated in Table 3.4 for the two identified tags.
4. There is a frequency shift of 40 MHz between the measured and the simulated tags. This is due to manufacturing issues.

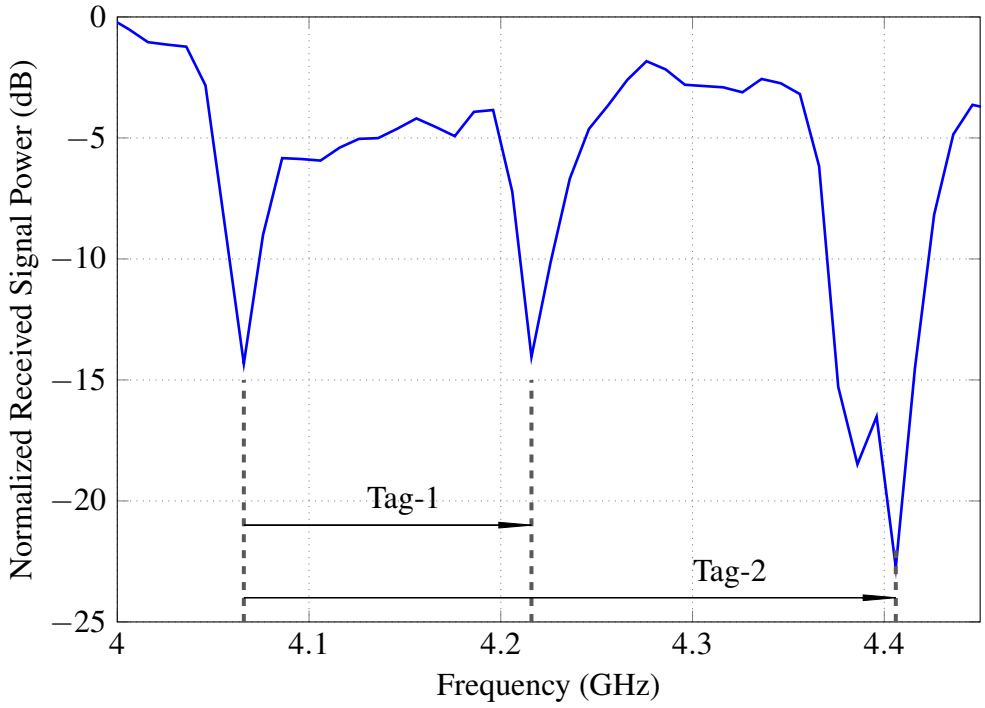

Figure 3.19: Detected signal using USRP after applying a real-time clutter removal and equalization process when using the Gen-2 protocol.

Table 3.4: Stored LUT in the reader's main memory.

Unique Frequency Shift (MHz)	Tag-ID
150	Tag-1-ID
340	Tag-2-ID

3.7 Conclusion

In this work, new protocols for anti-collision avoidance between tags in a chipless RFID network have been proposed. The introduced algorithms are not only able to identify the number of tags in the reader's interrogation zone but they also effectively identify the ID of each tag. The first generation of the protocol is based on unique frequency shifts hard coded in every chipless tag based on an NPM technique that represents the tag's ID. An advanced frequency sweeping signaling scheme is applied for tag identification meeting the FCC UWB regulations and increasing the backscattered power by a factor of 400 compared to the traditional UWB-IR signaling scheme.

The second generation of the protocol enhances the spectrum's utilization efficiency and the coding capacity. The Gen-2 protocol uses the unique frequency shifts of each tag as addresses to their IDs which are stored in a table in the main memory of the reader. In addition, the influence of increasing the operating frequency on the performance of the chipless RFID system is investigated from the multi-tag identification point of view. It was shown that the probability of detection is enhanced when operating at higher frequencies because the notch bandwidth is increased. Thus, the detection process is improved. However, a greater operating frequency bandwidth is required to identify the chipless tags.

In order to imitate the real-world characteristics of the chipless RFID system, an SDR platform is used as a real time reader for two MAC based manufactured chipless tags. For these the empty room calibration and equalization processes were performed to obtain the ID of the tags successfully. As expected, both collision free tag IDs were promptly identified on the reader's side in an indoor scenario at a distance of 30 cm. Finally, the comparison between the two proposed anti-collision protocols is listed in Table (3.5).

Table 3.5: Comparison between the proposed anti-collision protocols, Gen-1 and Gen-2, and the introduced techniques in the literature

Key Performance Indication	**Evaluation**			
	LUT-Gen-2	NPM-Gen-1	[63]	[65]
Probability of Error	Low	Low	-	-
Spectrum Utilization	Low	High	High	High
Multiple-Tags Multiple-Bits	Yes	Yes	No	No
Complexity	Low	Moderate	High	High
Hardware Implementation	Yes	Yes	No	No

4 Adaptive Frequency Sweeping Techniques to Reduce System Latency

The main objective of Chapter 4 is to introduce novel techniques to reduce the time taken by the reader to identify the Frequency Coded (FC) chipless RFID tags existent in the reader's interrogation region. This delay is called *system latency*. The frequency scanning method, the number of spectrum sweeping iterations to remove the environmental clutter, and the hop duration are the three main parameters that significantly affect the overall system latency. Consequently, the Adaptive Frequency Hopping (AFH) and Adaptive Sliding Window (ASW) methodologies are introduced and shown to be efficient for the chipless RFID systems to reduce the latency and to improve the accuracy. Likewise, the performance of the designed AFH and ASW techniques is compared to the classical Fixed Frequency Hopping (FFH) method with a small frequency step to validate the accuracy of the proposed techniques. Moreover, four differently coded FC chipless tags are manufactured and used in the measurements. A real-world testbed is designed which includes a Software Defined Radio (SDR) platform in which the proposed adaptive algorithms and the traditional FFH method are implemented. All the measurements are performed in an indoor scenario. It also includes all environmental effects. The experiments show that the proposed AFH combined with ASW algorithms reduces the system latency by 58%. A section of this chapter is already published in [82].

4.1 Introduction

The time required to identify the chipless RFID tags, called *system latency*, is critical in the design of chipless RFID systems. In order to achieve a realistic system, the tagged objects need

to be accurately classified in a short time. Therefore, the technique at the reader's side used for recognizing the chipless tags has to take into consideration all the other system latency parameters besides the accuracy of detection as presented in [36]. Reducing the system latency leads the chipless RFID scheme to be more reliable, robust, and efficient for real-world applications. Consequently, a new method will be presented to decrease the system latency for chipless RFIDs. It is worth noting that most of the studies dealing with the latency of RFID systems focus on the chipped RFID technologies (RFID-with-chip). In [83–88], the identification time is studied resulting from several modifications of the Medium Access Control (MAC) protocols that are not applicable to the chipless RFID systems. Therefore, the factors that are taken into consideration to reduce the latency of chipless RFID systems are quite different.

The Adaptive Frequency Hopping (AFH) technique is described in several studies such as [89]. Here the hopping rate is considered in an adhoc network [90–92] and adapted according to the channel quality after applying a spectrum sensing process. Likewise, the research in [93] adapts the hopping rate according to a feedback system with a quality measure for frequencies that avoids the bad frequency components. In addition, the research in [94, 95] utilizes the AFH technique to reduce interference and to obtain a better performance at the Bluetooth application. The aforementioned studies related to the AFH differ from the currently proposed technique for the chipless RFID systems such that:

- The hop rate is determined by the PN sequence used, which is different from the proposed AFH technique.
- The hop rate is adapted according to the channel quality where it is not the case with the introduced AFH scheme which is adapted according to the notch pattern. This will be explained in Section 4.3.
- The presented AFH technique for the chipless RFID system is not a spread spectrum scheme, but it is only used for the identification of the chipless tag during the process of spectrum scanning.

Therefore, this chapter explores the system latency of the chipless RFID system which, as far as the author knows, has not been mentioned in any of the prior studies on the chipless RFID. Two novel adaptive techniques, AFH and the Adaptive Sliding Window (ASW), are designed to match the requirements of the chipless RFID tags so they can be identified using the adaptive frequency sweeping methodology. The adaptive techniques are implemented in a real-world testbed utilizing a Software Defined Radio (SDR) platform.

This chapter is organized as follows. The system latency and the factors affecting the chipless RFID's system latency are listed in Section 4.2. The core functionality of the adaptive frequency hopping and of the adaptive sliding window are illustrated in Section 4.3. In order to verify the proposed method, real FC chipless RFID tags are designed and manufactured based on the description in Section 4.4. The proposed AFH and ASW techniques are simulated in Section 4.5 and evaluated using a real-world testbed based on an SDR platform (USRP N210). The measurement results are explained and verified in Section 4.6. Finally, a comparison is performed between the proposed techniques and concluded in Section 4.7.

4.2 Latency of Chipless RFID Systems

In this section, the system latency of the chipless RFID is evaluated. Furthermore, the factors that affect the system latency are discussed and modeled.

4.2.1 Factors Affecting the System Latency of Chipless RFID

The system latency is interpreted as the time it takes the reader to identify the chipless tags existent in the reader's interrogation region. It is considered to be one of the most important KPIs of the chipless RFID systems. The factors that affect the system latency can be summarized as:

1. Spectrum scanning T_{scan}: this is the time required to sweep the overall operating frequency in order to identify the tag's Identification number (ID).

2. Hop duration T_{hop}: which is the time in which a certain frequency occupies the channel before switching to the other hop (frequency). This factor is controlled by the Voltage Controlled Oscillator (VCO) used in the testbed because it has to remain at the same frequency for a certain time (hop-duration) before switching to the next one.

3. Number of reading iterations (N) required for the environmental clutter removal process.

The system latency can be mathematically expressed by Equation (4.1a).

$$\begin{aligned} T_{\text{sys-latency}} &= N \times T_{\text{scan}} \\ &= N \times n \times T_{\text{hop}} \end{aligned} \tag{4.1a}$$

with

$$T_{\text{scan}} = n \times T_{\text{hop}} \tag{4.1b}$$

where n is the number of hops required to sweep the spectrum. Therefore, the scanning method has a significant effect on the system latency.

4.2.2 Spectrum Scanning Method

The RFID reader's transmitter is responsible for the scanning mechanism at the operating frequency in order to identify the FC-chipless tags. There are two options to sweep the spectrum:

1. The operating frequencies are swept linearly starting at the lowest operating frequency and finishing with the highest operating frequency.
2. A UWB-RF pulse is sent which will cover the operating frequencies according to the Gaussian distribution criterion.

A. Linear Frequency Modulation

With the Linear Frequency Modulation (LFM), chirp, the signal sweeps the spectrum from low-to-high frequencies. This signal can be generated by sending a series of sinusoidal signals with an incremental sequence of frequencies [96–99]. This transmitting signaling scheme is well-known at Frequency Modulated Continuous Wave (FMCW) Radar systems [100–103]. The LFM signal can be represented as described in Equation (4.2).

$$x(t) = A\cos\left(2\pi(f_{\text{start}}t + \frac{k}{2}t^2)\right) \tag{4.2a}$$

when

$$k = \frac{f_{\text{stop}} - f_{\text{start}}}{T} \tag{4.2b}$$

where $x(t)$ is the transmitted signal, A is the amplitude of the signal, f_{start} is the start of the operating frequency, f_{stop} is the end of the operating frequency, T is the time taken to sweep from start to finish of the operating frequency, and k is the chirp rate.

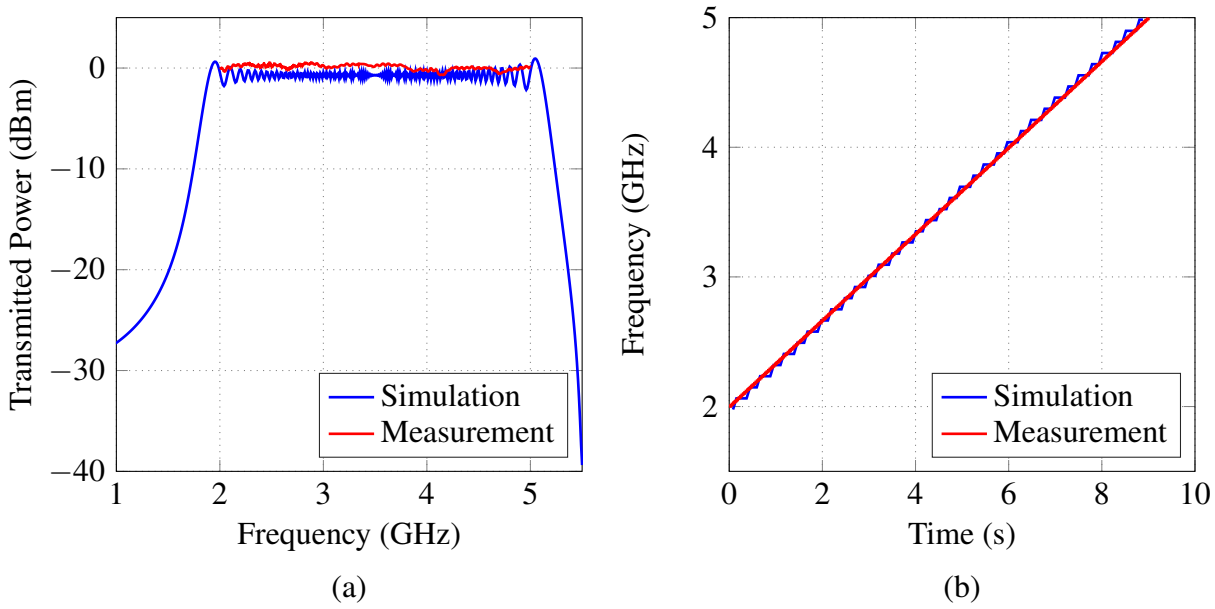

Figure 4.1: Simulation and measurement of the transmitted signal using the LFM scheme, the utilized hop duration is 30 ms: (a) Frequency response of the transmitted signal. (b) Frequency–Time graph for the LFM signal.

Fig. 4.1a shows the frequency domain of the LFM's transmitted signal which indicates a flat magnitude response. Moreover, the relation between frequency and time shows a linear relationship as depicted in Fig. 4.1b. Fig. 4.2 portrays the flowchart of transmitting an LFM signal using the SDR platform in the proposed testbed, which is represented by the red lines in Fig. 4.1.

B. UWB-RF Pulse

The second method of scanning the overall operating frequency is to transmit a UWB signal. This can be generated by transmitting an RF-Gaussian pulse which is represented in Equation (4.3).

$$x(t,\alpha) = Ae^{-t^2/(2\alpha^2)} \tag{4.3}$$

where α is the parameter used to control the width of the pulse. The full term of the normalized Gaussian pulse can be expressed as in Equation (4.4).

$$x(t,\delta t) = \left(\frac{2\sqrt{\log 2}}{\sqrt{\pi}\delta t}\right)^{1/2} e^{-2t^2\log 2/(\delta t^2)} \tag{4.4}$$

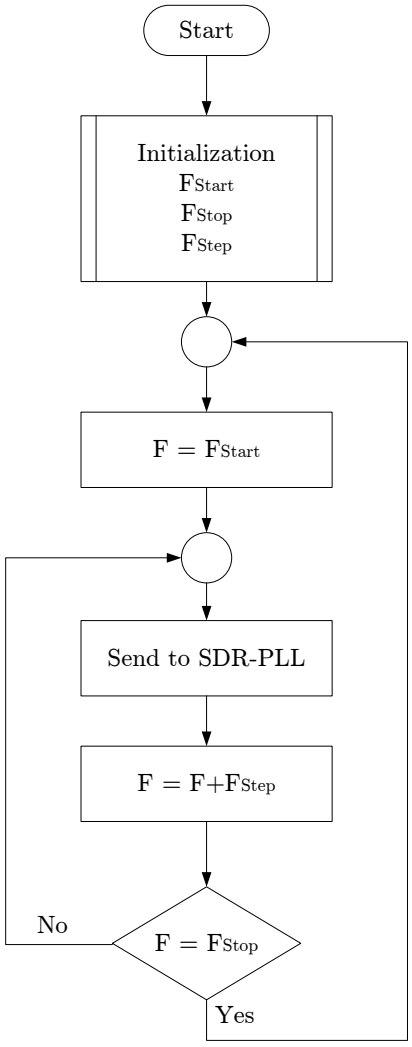

Figure 4.2: Flowchart of transmitting a signal using the LFM technique.

where δt is the full width of the pulse. Furthermore, the frequency domain representation of the normalized Gaussian pulse is expressed in Equation (4.5) and the entire mathematical derivation and framework are represented in [104].

$$x(\omega, \delta t) = \left(\frac{\sqrt{\pi}\delta t}{\sqrt{\log 2}} \right)^{1/2} e^{-\omega^2 \delta t^2/(8 \log 2)} \tag{4.5}$$

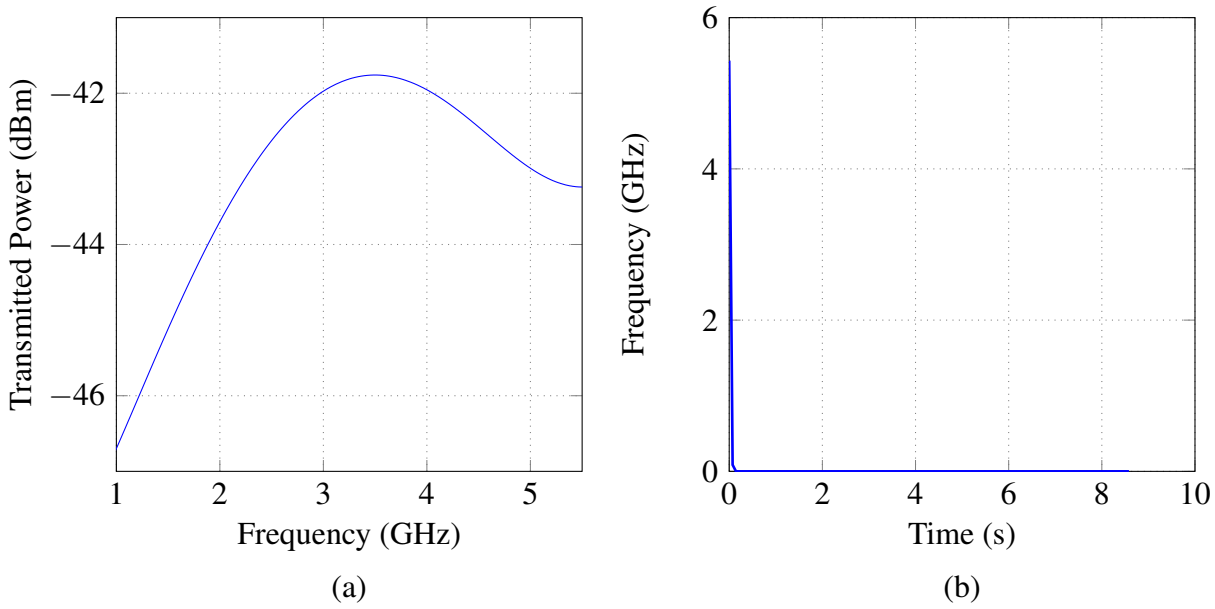

Figure 4.3: Illustration of the RF pulse (Gaussian RF pulse) method: (a) Frequency response of the signal. (b) Frequency–Time graph of the RF-Gaussian pulse.

Fig. 4.3 shows the simulation results of an UWB-RF Gaussian pulse in the range of (2–5 GHz) and the corresponding frequency–time relationship. It indicates that the UWB-RF Gaussian pulse, unlike the LFM scheme, is able to cover the overall operating frequency in a very short time. Still, there are some disadvantages for the UWB-RF pulse, for example:

1. The power transmitted is much lower according to the FCC regulations of both UWB indoor and outdoor scenarios, which in turn reduces the reading range of the chipless RFID system, as discussed in Chapter 3.

2. The cost of the hardware to be used for generating the UWB-RF pulse is much higher than that used in the proposed testbed when applying the LFM signaling schemes.

Therefore, the LFM method is used in the identification process of the chipless RFID system. Thus, the number of hops that are necessary to sweep the overall operating frequency can be reduced to obtain a lower system latency.

4.3 Core Functionality of Adaptive Frequency Hopping Techniques

This section explores the proposed adaptive techniques (AFH and ASW) that are designed to match the requirements of the FC chipless RFID systems and to reduce the system latency.

Furthermore, the traditional FFH method is discussed and compared to the proposed adaptive techniques.

4.3.1 Fixed Frequency Hopping

Before exploring the proposed techniques to reduce the system latency, the primary FFH has to be mentioned to illustrate the classical method of the FC chipless tag's identification process. The pseudo code that is used in the FFH methodology for the identification of chipless tags is described by Algorithm 4.1. With this technique, the overall spectrum (operating frequency) is scanned with a fixed frequency step (F_{step}), which is described in Equation (4.6).

$$F_{\text{hopping}} = F_{\text{start}} + k \times F_{\text{step}} \tag{4.6}$$

where F_{hopping} is the set of hopping frequencies, F_{start} is the start of the operating frequency, k is an integer number from $(0 \ldots k)$, and F_{step} is the step frequency.

Algorithm 4.1 Scanning with Fixed Frequency Hopping.

```
1: //F_start is the starting operating frequency
2: //F_step is the frequency step
3: //F_end is the end of operation frequency
4: //TX is the transmitter operation
5: //RX is the receiver operation
6: //N is the number of sweeping iterations to remove the clutter
7: while F_start < F_end do
8:     F_hopping ← F_start + k × F_step
9: end while
10: for each F_hopping do
11:     TX ← send_freq(F_hopping)
12:     RX ← get_amp(F_hopping)
13:     apply_averaging(N)
14: end for
```

4.3.2 Adaptive Frequency Hopping

The notch bandwidth BW is increased according to the frequency as illustrated in Fig. 4.4 which shows the RCS magnitude response of a real chipless tag using CST-Microwave Studio (as will be explained in Section 4.4).

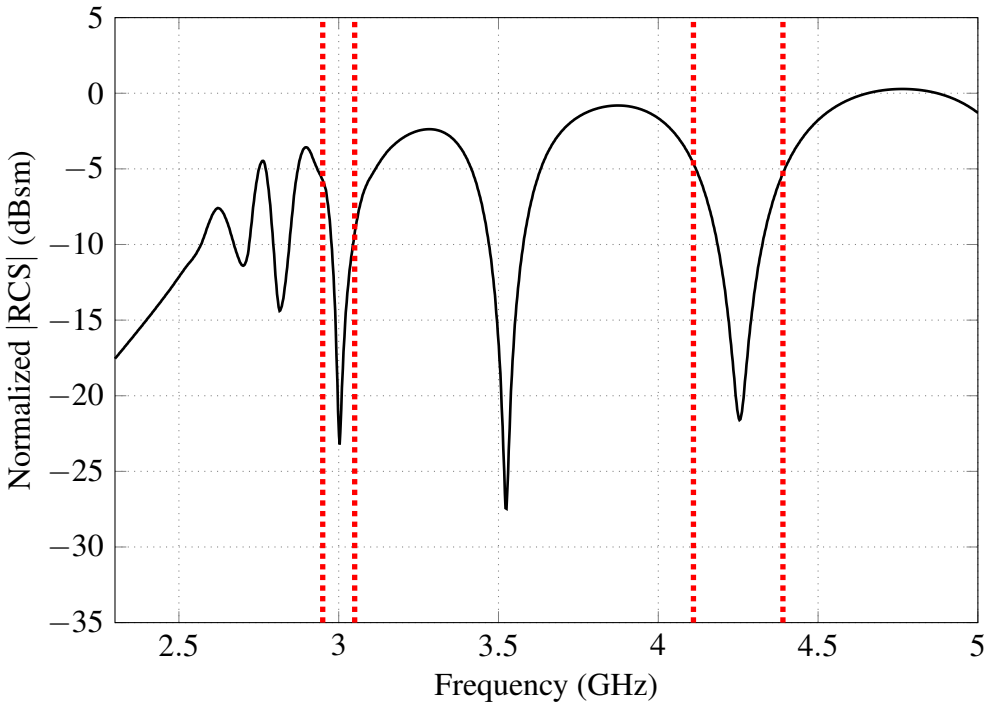

Figure 4.4: Illustration of the notch–bandwidth increment with operation frequency for a chipless tag designed using the CST-MW Studio EM simulator.

Thus, notches with wider bandwidths will be identified by a larger number of frequency hops than the narrower ones are as shown in Fig. 4.5a. Consequently, an adaptive technique is designed to diminish the number of hops which will reduce the system latency accordingly. The proposed AFH technique relies on scanning the notches with a narrow bandwidth using a fine frequency hopping rate (larger number of hops) and the wider-bandwidth notches with fewer frequency hops (with different frequency steps). Fig. 4.5b shows a simulation of the application of the proposed AFH technique (using MATLAB) for a designed FC chipless tag (with the Radar Cross Section (RCS) magnitude shown in Fig. 4.4). It also illustrates the dynamic hopping frequency allocation method which indicates that the number of hops is reduced. The number of hops used to identify the chipless tag is illustrated in Fig. 4.6 after applying the introduced AFH technique and the classical FFH methodology. It becomes clear that the AFH technique identifies the tag with a much lower number of hops than the classical FFH methodology. The pseudo code of the proposed AFH scanning method and its utilization in the chipless RFID systems are described by Algorithm 4.2. The different hop rates are calculated according to several frequency steps as expressed in Equations (4.7a–4.7c).

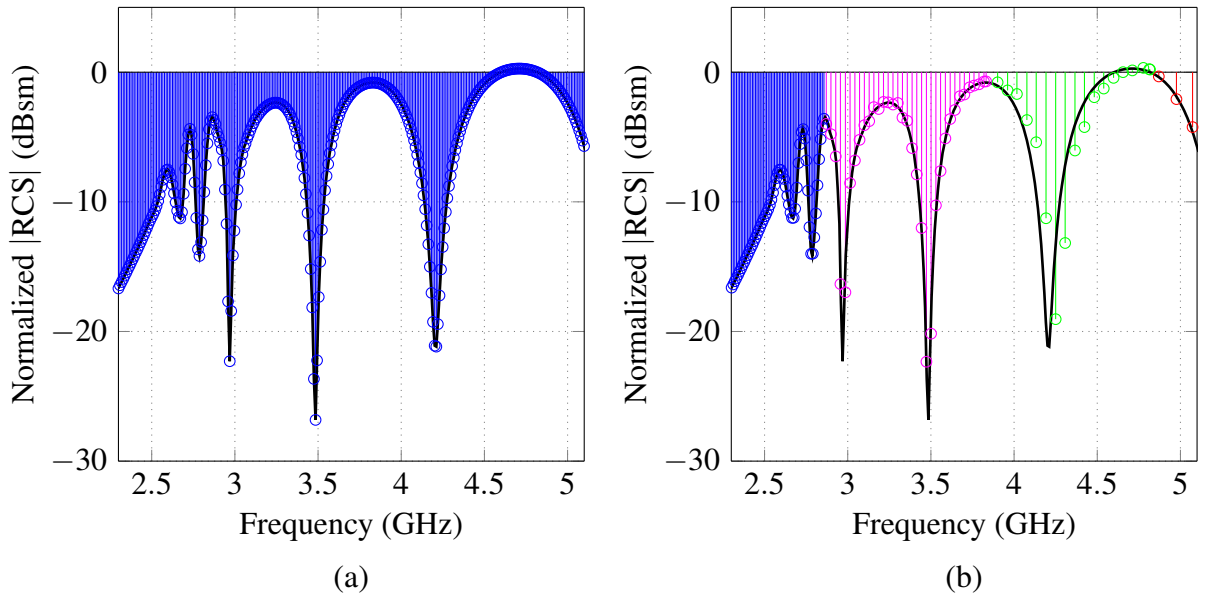

Figure 4.5: The functionality of the AFH technique compared to the FFH method: (a) Application of the FFH technique for a designed chipless tag. (b) Application of the proposed AFH for the same chipless tag.

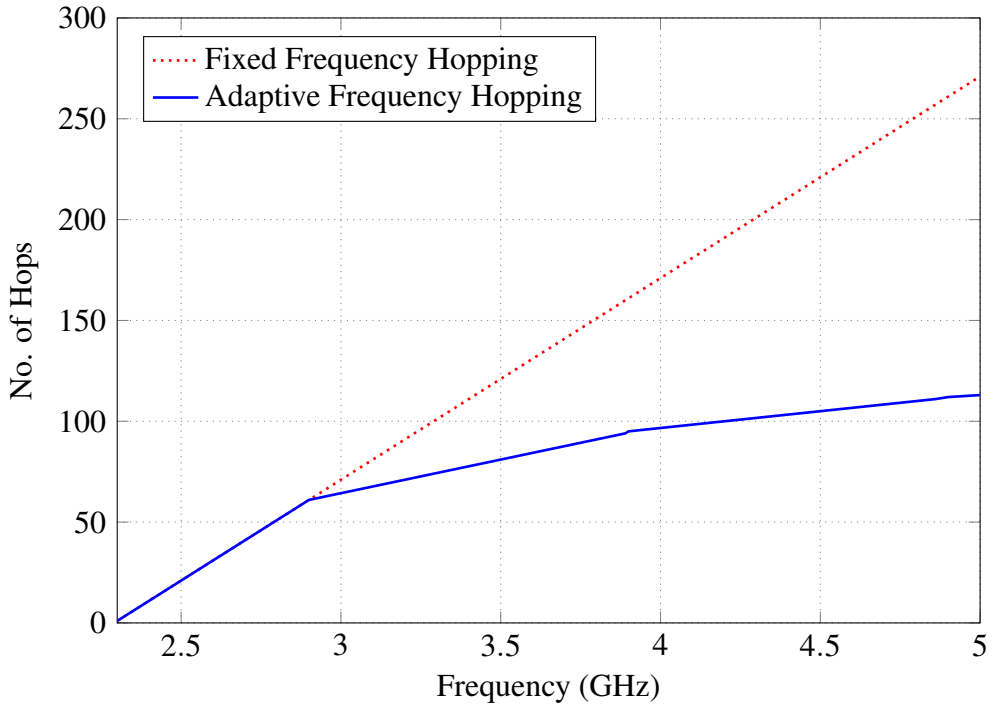

Figure 4.6: Simulation results for the number of hops used for AFH vs. FFH.

$$F_{\text{h-1}} = F_{\text{start}} + k_1 \times F_{\text{step}} \qquad F_{\text{start}} \leq F_{\text{h-1}} < F_{\text{e-1}} \tag{4.7a}$$

Algorithm 4.2 Scanning with Adaptive Frequency Hopping.

```
1: //F_start is the starting operating frequency
2: //F_step is the frequency step
3: //F_end1 is the end of fast hopping
4: //F_end2 is the end of moderate hopping
5: //F_end3 is the end of slow hopping
6: //k1&k2&k3 are the different hopping rates
7: //TX is the transmitter operation
8: //RX is the receiver operation
9: //N is the number of sweeping iterations to remove the clutter
10: while F_start < F_end1 do
11:     F_hopping ← F_start + k1 × F_step
12: end while
13: while F_end1 < F_end2 do
14:     F_hopping ← F_end1 + k2 × F_start
15: end while
16: while F_end2 < F_end3 do
17:     F_hopping ← F_end2 + k3 × F_start
18: end while
19: for each F_hopping do
20:     TX ← send_freq(F_hopping)
21:     RX ← get_amp(F_hopping)
22:     apply_averaging(N)
23: end for
```

$$F_{\text{h-2}} = F_{\text{e-1}} + k_2 \times F_{\text{step}} \qquad F_{\text{e-1}} \leq F_{\text{h-2}} < F_{\text{e-2}} \tag{4.7b}$$

$$F_{\text{h-3}} = F_{\text{e-2}} + k_3 \times F_{\text{step}} \qquad F_{\text{e-2}} \leq F_{\text{h-3}} \leq F_{\text{e-3}} \tag{4.7c}$$

where $F_{\text{h-1}}$ is the the set of frequency hops used for narrow notch bandwidths (at lower frequencies), F_{start} is the start of the operating frequency, k_1 is the rate used to identify the lower frequencies (high rate), F_{step} is the frequency step, $F_{\text{e-1}}$ is the end of the 1^{st} hopping rate, $F_{\text{h-2}}$ is the set of frequency hops used for notches with moderate bandwidths, k_2 is the rate used for moderate frequencies (medium rate), $F_{\text{e-2}}$ is the end of the 2^{nd} hopping rate, $F_{\text{h-3}}$ is the set of frequency hops used for wider notch bandwidths (low rate), k_3 is the rate used to identify the notches at higher frequencies, and $F_{\text{e-3}}$ is the end of the operating frequency spectrum.

The suitable hopping rates are estimated by obtaining the average notch bandwidths at lower, moderate, and higher frequencies. Thus, the equation ($\text{BW} = \frac{F_{\text{r}}}{Q}$) can be used to estimate the notch bandwidth; where BW is the notch bandwidth, F_{r} is the notch resonance frequency, and Q is the quality factor of the tag's resonator (notch filter). Thus, by changing the resonance frequency

the corresponding notch bandwidth can be calculated. Afterwards, the required frequency steps, used to identify the notch patterns based on the operating frequencies, are estimated and the corresponding hop rates are predefined. The proposed AFH technique yields a high accuracy for the identification of chipless RFID tags as will be shown by the measurements in (Section 4.6). In addition, a reduced system latency will be introduced which conserves the system's simplicity.

4.3.3 Adaptive Sliding Window

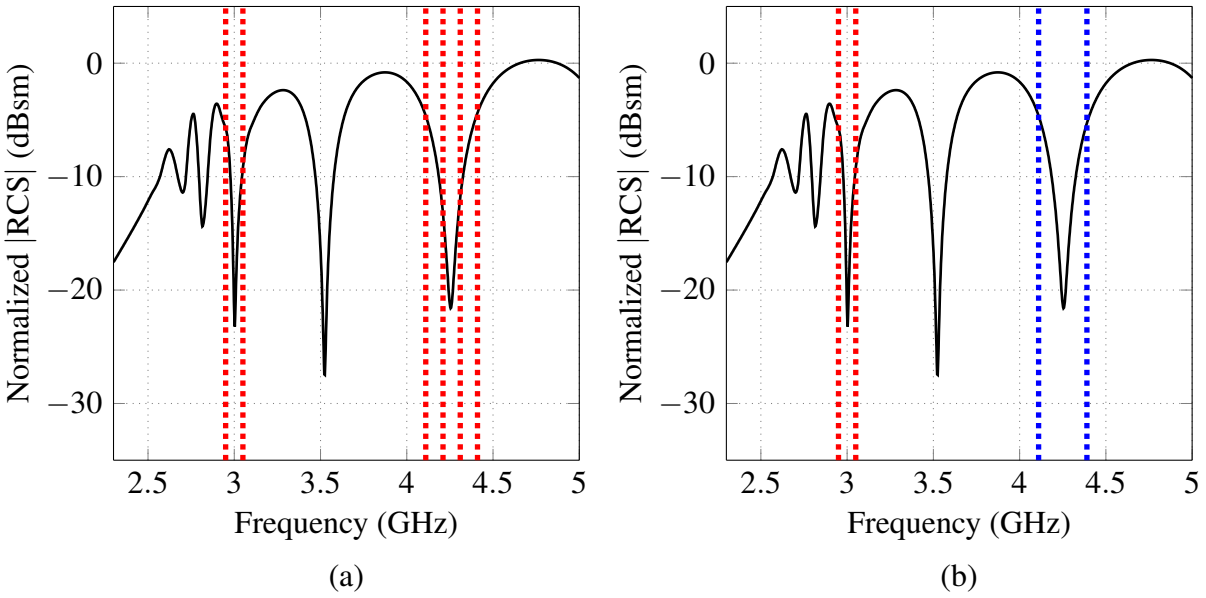

Figure 4.7: Illustration of the variation of size of the decision window and its adaption to fit the notch pattern: (a) Fixed window size. (b) Adaptive window size.

Since the notch bandwidth increases with the frequency as shown in Fig. 4.4, the adaptive window size is utilized. This technique is mainly introduced to fit the requirements of the Notch Position Modulation (NPM) MAC algorithm illustrated in Chapter 3. The NPM technique divides the operating frequency into two parts, the preamble bandwidth and the coding bandwidth. The first part is responsible for determining the tag's existence and the second part shows the frequency locations that represent the tag's ID making use of the unique frequency shifts extracted from the preamble bandwidth. The proposed Adaptive Sliding Window (ASW) algorithm starts scanning the preamble bandwidth with a fixed window size. Then it scans the rest of the band according to the estimated frequency position using an adapted window size. Consequently, the scanning time can be calculated as described in Equation (4.8). The traditional fixed window size method is shown in Fig. 4.7a where the window size is adapted to meet the increment in the notch BW,

as illustrated in Fig. 4.7b.

Algorithm 4.3 Scanning with Fixed Sliding Window

1: $//BW_{\text{pre}}$ is the preamble bandwidth
2: $//W$ is the window size
3: $//F_{\text{pre}}$ is the preamble frequency
4: $//Bit_{\text{BW}}$ is the bit bandwidth
5: $//\varepsilon_i$ is the i^{th} tag shift parameter
6: $//Fstart_i$ is the reference frequency of the i^{th} bit bandwidth
7: $//Ftag_m$ is the unique absorption frequency of tag m
8: $//Bit_{\text{position}}$ is the position of the bit
9: $//\zeta$ is the guard band between notches
10: $W = const\_value$;
11: **for all** BW_{pre} **do**
12: Locate the center of the window at F_{pre};
13: **if** F_{pre} is existent **then**
14: $\varepsilon_i \leftarrow Ftag_m - F_{\text{pre}} - \zeta$
15: Calculate the number of tags;
16: Switch to the k^{th} bit bandwidth;
17: **else**
18: Go to the idle state (at F_{pre} position);
19: **end if**
20: **end for**
21: **for all** Bit_{BW} **do**
22: $Bit_{\text{position}} \leftarrow Fstart_i + \varepsilon_i$;
23: $d1 \leftarrow Bit_{\text{position}} - W, d2 \leftarrow Bit_{\text{position}} - 0, d3 \leftarrow Bit_{\text{position}} + W$;
24: **if** $average(d1, d2, d3)$ is LOW **then**
25: This bit represents one of the i^{th} order;
26: **else**
27: This bit represents zero of the i^{th} order;
28: **end if**
29: **end for**
30: Arrange the tag's ID in a matrix;

Algorithm 4.3 describes the functionality of spectrum scanning with fixed window size based on the NPM-MAC protocol illustrated in Section 3.3. The notches at higher frequencies suffer under wider bandwidths which require several windows in order to detect the whole notch as shown in Fig. 4.7a. Here three windows are required to detect the notch, and the decision (notch or no notch) is based on the average of all decisions for each window. To improve processing efficiency and to reduce latency, the window's size is adapted to the notch bandwidth as illustrated in Algorithm 4.4 and shown in Fig. 4.7b. Accordingly, the detection of each notch is done once for each window as described in [36].

Algorithm 4.4 Scanning with Adaptive Sliding Window

```
1: //BW_pre is the preamble bandwidth
2: //W is the window size
3: //F_pre is the preamble frequency
4: //Bit_BW is the bit bandwidth
5: //ε_i is the i^th tag shift parameter
6: //Fstart_i is the reference frequency of the i^th bit bandwidth
7: //Ftag_m is the unique absorption frequency of tag m
8: //Bit_position is the position of the bit
9: //ζ is the guard band between notches
10: //Q is the quality factor of the notch
11: for all BW_pre do
12:    W = initial_value ;
13:    wndow_position ← F_pre ;
14:    if F_pre is existed then
15:       ε_i ← Ftag_m − F_pre − ζ
16:       Calculate the number of tags;
17:       Switch to the k^th bit bandwidth;
18:    else
19:       Go to the idle state (at F_pre position);
20:    end if
21: end for
22: for all Bit_BW do
23:    Bit_position ← Fstart_i + ε_i
24:    W ← Bit_position/Q;
25:    if (d inside W) is LOW then
26:       This bit represents one of the i^th order;
27:    else
28:       This bit represents zero of the i^th order;
29:    end if
30: end for
31: Arrange the tag's ID in a matrix;
```

$$T_{\text{scan}} = T_{\text{preamble}} + T_{\text{bitbw}} \tag{4.8}$$

where T_{preamble} is the time used to scan the preamble bandwidth and T_{bitbw} is the time required to scan the bit bandwidth.

4.4 Chipless Tag Design

As shown in Fig. 4.8, the created chipless tag relies on slot ring resonators without a ground plane illustrated in [105, 106]. This increases the flexibility of identifying the tag in backscattering mode or transmission through mode (the latter is used in the measurement setup). Each slot resonator is responsible for absorbing the signal at a certain frequency (notch filter) resulting in a notch with a particular resonant frequency that is decoded to represent a bit or several bits. This process will be described in Chapter 5.

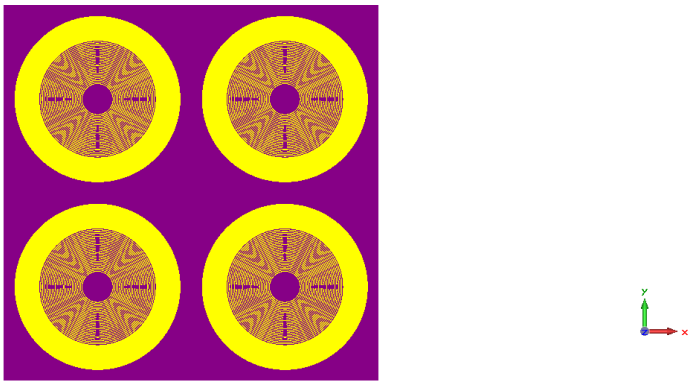

Figure 4.8: RFID chipless tag design using CST-Microwave Studio.

The utilized FC chipless tag has two advantages:

1. The level of backscattered power is increased by designing a (2×2) array which enhances the tag's detection and identification.

2. The detection of this tag is orientation independent since the frequency absorbing element is the circular resonator.

The designed tags are simulated using the CST-MW studio EM simulator. The simulations are conducted by exciting the tags using a plane wave and monitoring the backscattered signal of the tag. This setup is called backscattering mode because the backscattered signal is analyzed to extract the tag's signature. Fig. 4.9 shows the simulation results and the RCS magnitude response of the four designed chipless tags coded with different IDs (tag signature). The substrate used in the design is RO4003C with a permittivity of 3.38, a loss tangent of 0.0027, and a thickness of 1.52 mm.

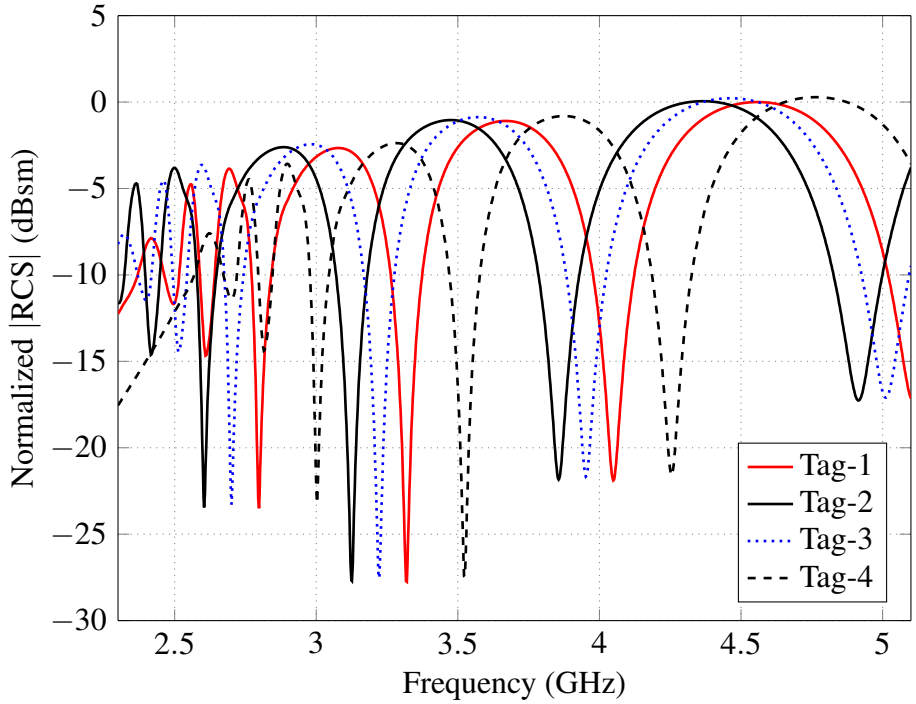

Figure 4.9: Simulation of FC-chipless tag using the CST-Microwave Studio EM simulator.

4.5 Simulation Environments and Results

In this section, the performance of the proposed adaptive techniques (AFH, ASW with fixed hopping, and ASW with adaptive hopping) is evaluated based on simulations that also take into consideration the real chipless tags. The obtained results are compared to the classical FFH to validate the accuracy and the latency reductions of the introduced techniques.

4.5.1 Simulation Environment

The proposed algorithms are implemented by using the MATLAB simulation tool and by applying it to chipless RFID tags (described in Section 4.4), which are designed and evaluated using the CST-Microwave Studio Electromagnetic (EM) simulator. A block diagram of the simulation environment is shown in Fig. 4.10.

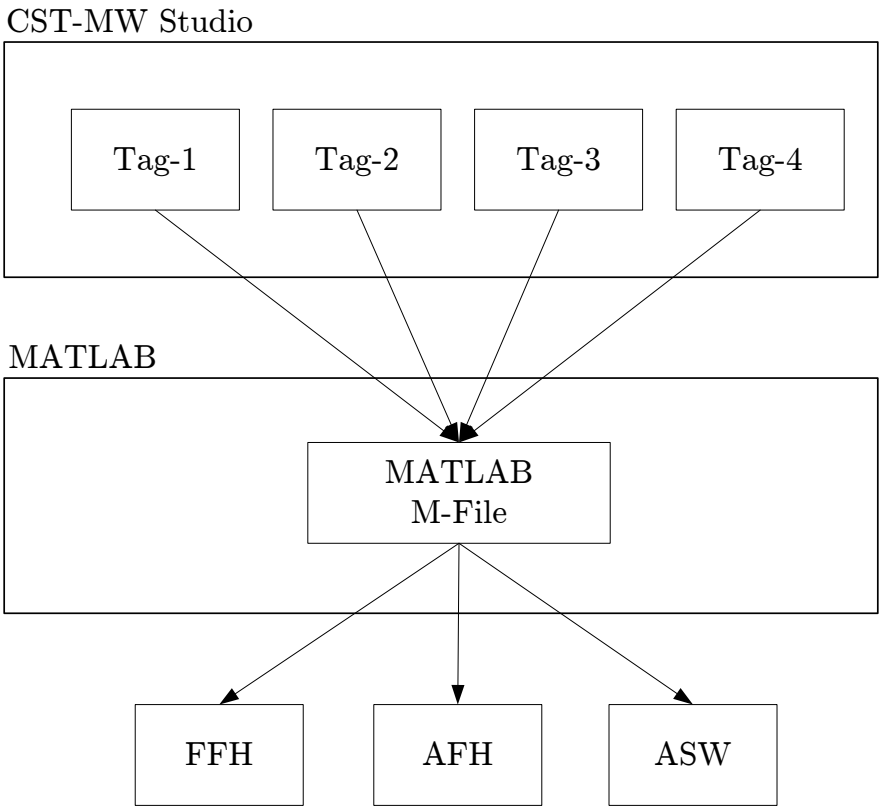

Figure 4.10: Block diagram of simulation environment.

Table 4.1: Frequency steps of the proposed AFH and of the classical FFH algorithm.

Frequency Range (GHz)	Value (GHz)
AFH	
2.3–2.9	0.01
2.9–3.9	0.03
3.9–4.9	0.06
4.9–5.00	0.1
FFH	
2.3–5.00	0.01

4.5.2 Simulation Results

A. Adaptive Frequency Hopping

The proposed AFH method defines different hopping rates to identify and detect the chipless RFID tags. Each hopping rate is defined for a certain operating frequency with a specific frequency step as illustrated in Table 4.1. The frequency step is selected to meet the increment of the notch bandwidth when the frequency is increased. For the designed chipless tags shown in

Fig. 4.9, the average notch bandwidths for the predefined frequency ranges (defined in Table 4.1) are 0.1, 0.22, and 0.35 GHz, respectively. Therefore, the estimated frequency steps are suitable to accurately detect the notch patterns using the operating frequency. The AFH technique is compared to the classical FFH methodology which employs a frequency step of 0.01 GHz for the operating frequency (2.3–5 GHz) to ensure a high accuracy of notch detection.

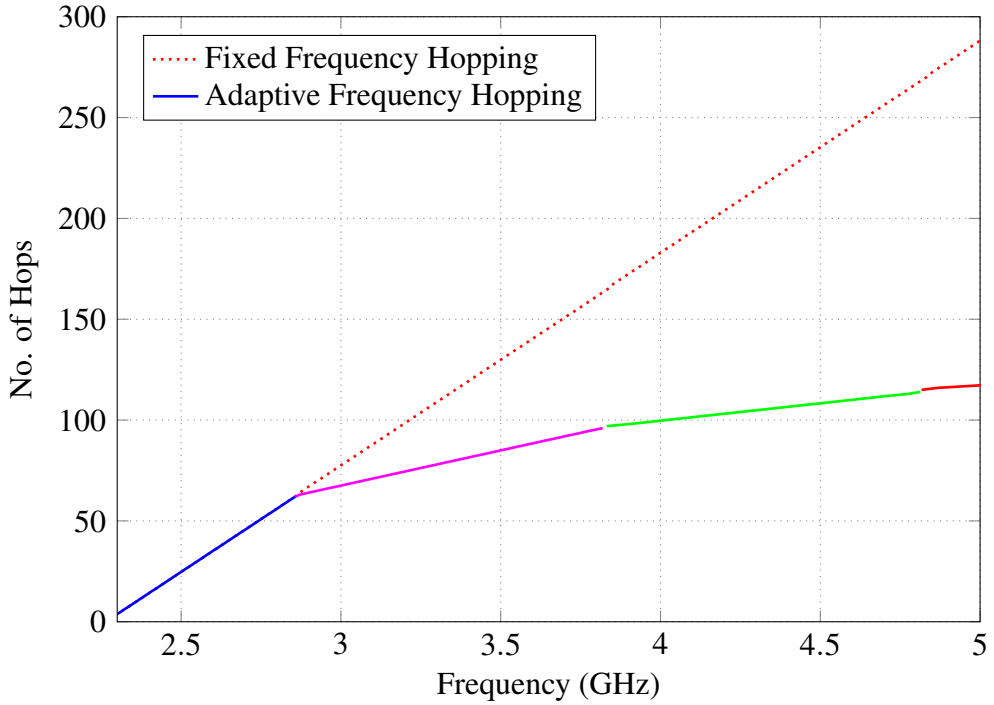

Figure 4.11: Simulation results with regard to the number of hops for the proposed AFH technique and for the classical FFH method (4-different frequency steps are used).

The number of hops of the primary FFH methodology is linearly proportional to the operating frequency since the hopping rate is constant in the entire range of the operating frequency as shown in Fig. 4.11 by the red-dotted line. Equation (4.6) is used to estimate the hopping frequencies necessary to identify the four chipless tags.

Unlike the FFH, the proposed AFH technique offers different hopping rates to identify and detect the chipless RFID tags. Therefore, the number of hops is significantly reduced over the entire operating frequency. Fig. 4.11, the multi-colored curve, illustrates the reduction of the number of hops as a result of the adaptation of the hopping rates. This can be explained as follows:

1. The red curve shows a hopping rate with a frequency step of 0.01 GHz to identify the notches with narrow bandwidths.

2. The magenta line illustrates a hopping rate with a frequency step of 0.03 GHz, which is suitable for notch patterns with moderate bandwidths.

3. The green part of the curve presents a hopping rate with a frequency step of 0.06 GHz in order to match the increase in the notch bandwidth.

4. the red curve presents a hopping rate with a frequency step of 0.1 GHz that is convenient for notches with high bandwidths.

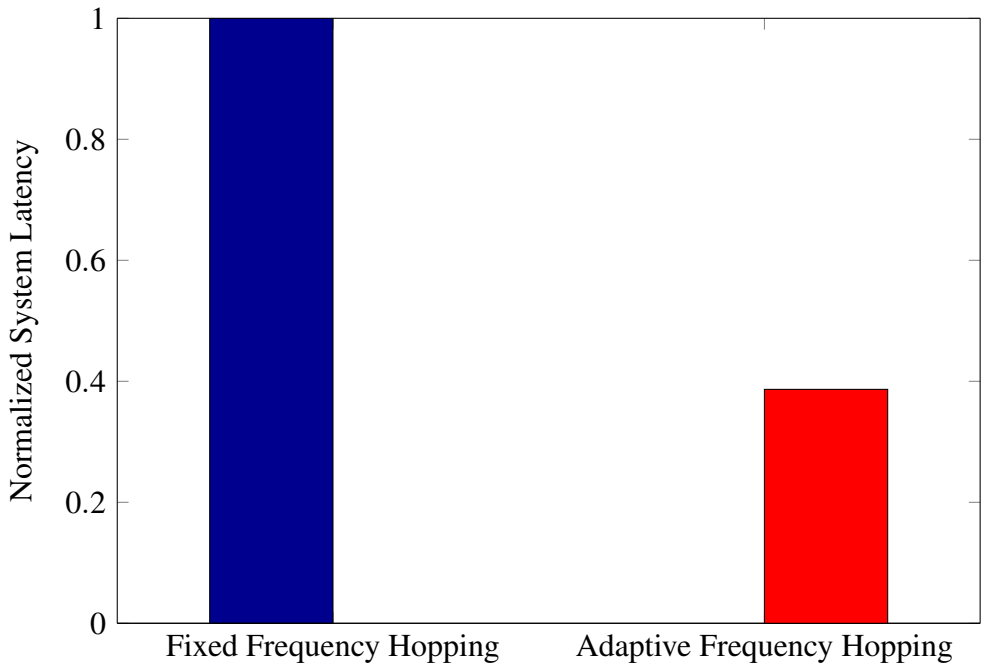

Figure 4.12: System latency simulation results based on Equation (4.1a).

As explained in Section 4.3, the number of hops directly influences the overall system latency. Furthermore, the system latency can be modeled using Equation (4.1). In order to illustrate the improvement, the system latency of the proposed algorithms is normalized for the fixed frequency hopping method according to Equation (4.9) considering a hop duration of 30 ms and 100-iterations for the clutter removal parameter.

$$\begin{aligned} T_{\text{sys-latency-normalized}} &= \frac{T_{\text{sys-latency-AFH}}}{T_{\text{sys-latency-FFH}}} \\ &= \frac{n_{\text{AFH}}}{n_{\text{FFH}}} \end{aligned} \tag{4.9}$$

where $T_{\text{sys-latency-normalized}}$ is the normalized system latency, $T_{\text{sys-latency-AFH}}$ is the system latency for the adaptive frequency hopping technique, $T_{\text{sys-latency-FFH}}$ is the system latency for the basic

fixed frequency hopping method, n_{AFH} is the number of hops necessary with the AFH technique, and n_{FFH} is the number of hops necessary with the FFH methodology. The simulation results for the normalized system latency are shown in Fig. 4.12 which indicates a satisfactory improvement with regard to the system latency when applying the AFH technique. Now, the number of hops for FFH and AFH are 271-hops and 113-hops, respectively which means more than 58% reduction of the overall system latency.

B. Adaptive Sliding Window

The normalized system latency for the ASW algorithm is evaluated by estimating the number of hops inside the windows which are used to identify the designed chipless tags. Moreover, two scenarios of the adaptive sliding window are simulated and compared to one another:

1. The Adaptive Sliding Window with Fixed Hopping rate (ASW-FH) uses the concept of variable window size, but with fixed frequency steps inside the detection window (frequency step of 0.01 GHz).

2. The Adaptive Sliding Window with Adaptive Hopping rates (ASW-AH) makes use of the benefit of the adaptive hopping technique to reduce the overall system latency (frequency steps of 0.01, 0.03, 0.06, and 0.1 GHz).

The ASW algorithm is specifically designed to meet the NPM-MAC protocol's requirements which are applied to identify the four chipless tags. Likewise, the system latency for the ASW algorithms (ASW-FH and ASW-AH) are normalized over the FFH technique, using Equation (4.9). Fig. 4.13 shows a comparison of the normalized system latency of the FFH, ASW-FH, and ASW-AH algorithms. The number of hops for the ASW-FH technique is 230, however, the number of hops for the ASW-AH algorithm is 112 after using the concept of the presented adaptive hopping criterion.

4.6 Measurements and Real-World Testbed

In this section, a real-world testbed is described based on an SDR platform and real manufactured chipless tags (shown in Fig. 4.14) in an indoor scenario. In addition, the adaptive algorithms are compared to the traditional FFH method in order to validate the performance of the proposed algorithms.

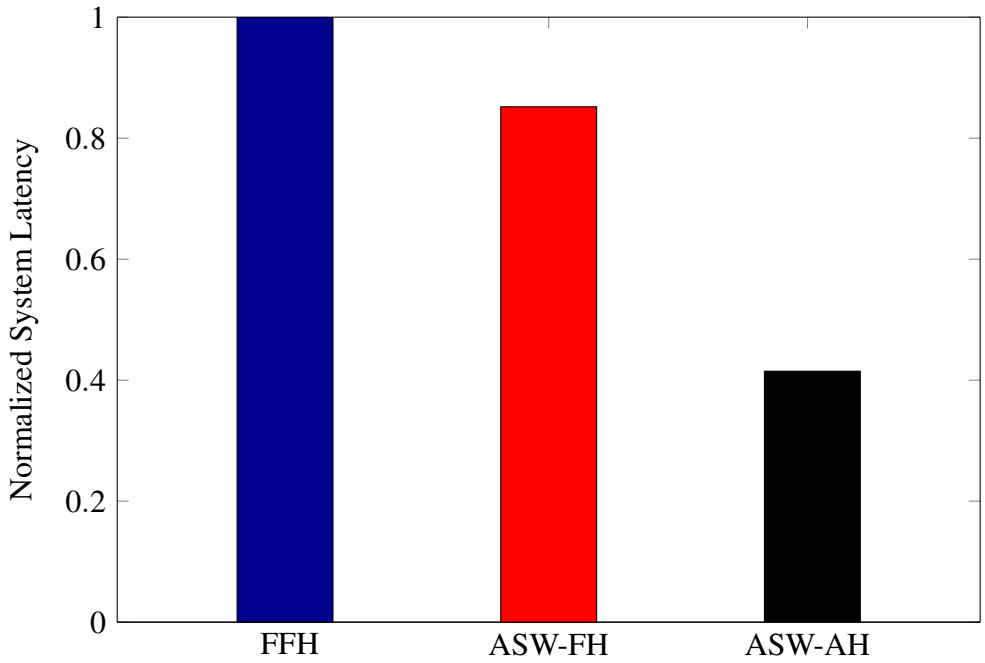

Figure 4.13: System latency simulation results for the Adaptive Sliding Window with Fixed Hopping (ASW-FH) and for the Adaptive Sliding Window with Adaptive Hopping (ASW-AH).

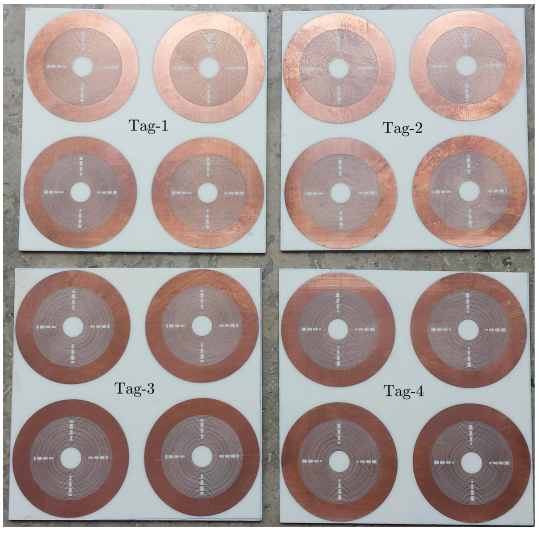

Figure 4.14: Manufactured RFID chipless tags.

4.6.1 Measurement Setup

The measurements are implemented using Universal Software Radio Peripheral (USRP) N210 [80] and a CBX daughter-board [81] operating in a frequency range of (1.2–6 GHz), the instantaneous bandwidth of the CBX daughter-board is 40 MHz. The parameters of the measurement setup are summarized in Table 5.2. Fig. 4.15 shows the block diagram of the designed testbed in which

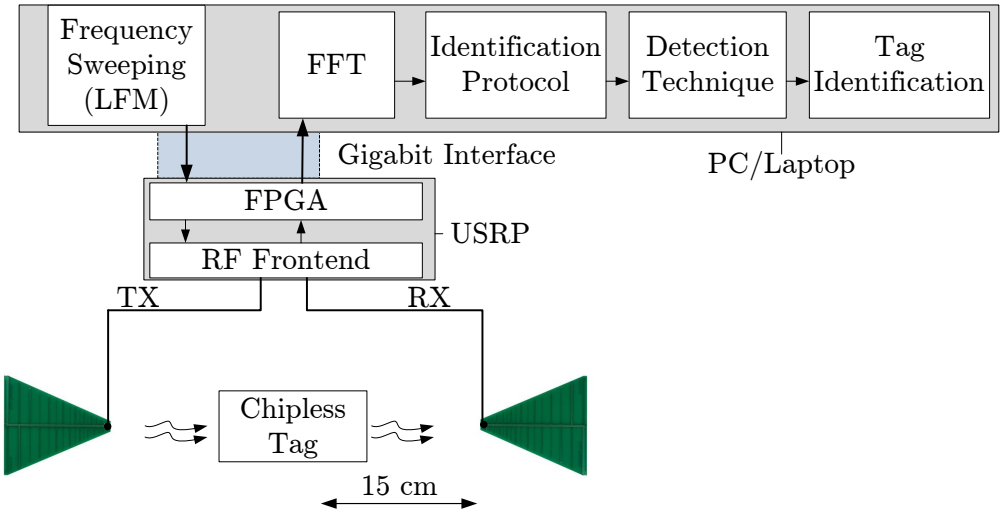

Figure 4.15: Block diagram of the measurement setup.

the laptop is connected to the USRP using a Gigabit Ethernet interface.

The measurements are performed in a real environment (indoor scenario) in order to validate the proposed AFH technique in a setup that includes environmental effects and multipath components.

A Linear Frequency Modulated (LFM) scheme, also known as linear chirp, is applied to generate a UWB-like signal at the transmitter's side which is described in Equation (4.2). The USRP baseband signal is up-converted by a variable carrier frequency (2.3–5 GHz) by means of the CBX daughter-board. Due to hardware limitations, a pure UWB-impulse cannot be generated because the CBX daughter board possesses a bandwidth of 40 MHz. Furthermore, the disadvantage of UWB impulse generation is its limited power constraints (-41.3 dBm/MHz according to the UWB-FCC regulations for indoor scenarios [107]). However, the frequency sweeping mechanism does not suffer from the same problem as the transmitted power can be 0 dBm within a bandwidth of 50 MHz [73]. So, in the proposed testbed, the transmitted power can be increased up to 0 dBm. The designed testbed is shown in Fig. 4.16. Moreover, the hop duration is set to be 30 ms (which is recommended by the supplier) and the number of sweeping iterations is 100 to remove the environmental clutter. This could also be removed by using PN-sequence schemes to speed up the process without using all the iterations as explained in [106]. All algorithms (classical FFH and Adaptive hopping) are performed in Python and can be applied to the USRP platform. The frequency steps used for the AFH algorithm are illustrated in Table 4.1. A room calibration process is performed at the beginning by subtracting

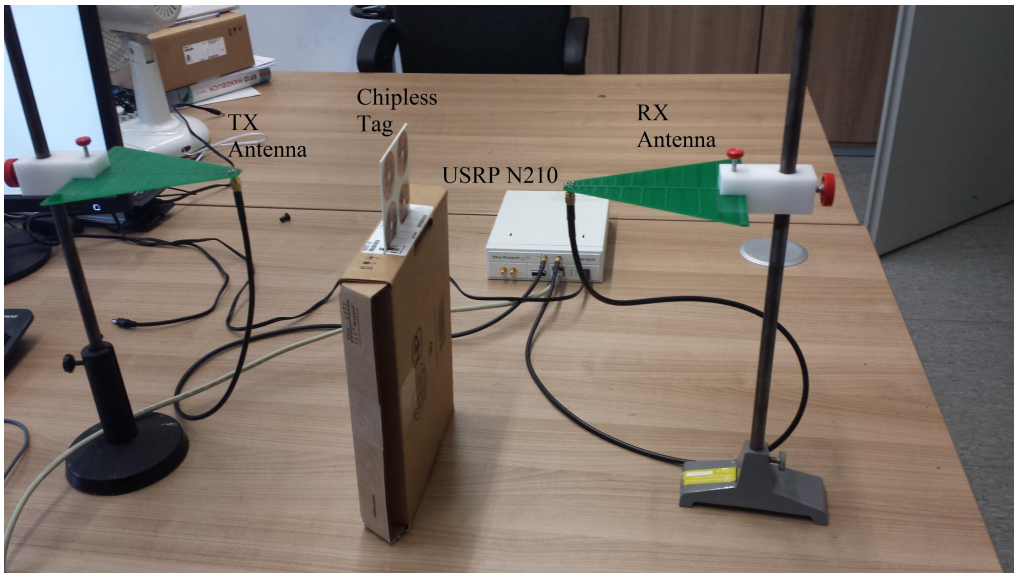

Figure 4.16: The real-world measurement setup based on SDR (USRP N210).

Table 4.2: USRP Parameters.

Parameter	**Value**
Sampling Rate	1 M samples / second
Transmitter Gain	31.5 dB
Receiver Gain	0 dB
Start Frequency	2.3 GHz
End Frequency	5 GHz
Frequency Step	10, 30, 60, 100 MHz
Frequency Sweep	
Averaging	100
Hop Duration	30 ms
Reader Antenna	
Type	Log-Periodic Antenna Array
Gain	2–5 dBi

the backscattered signal power of the tag from the received signal without any tags existent in the detection area as illustrated in Equation (4.10). This removes all environmental effects.

$$R^i_{\text{measured}} = R^i_{\text{tag}} - R_{\text{air}} \qquad \text{(dB)} \tag{4.10}$$

where R^i_{measured} is the total measured backscattered signal power of tag i, R^i_{tag} is the backscattered signal power of tag i, and R_{air} is the backscattered signal power of the environment. This last component is calculated once in the beginning.

4.6.2 Measurement Results

The measurement results for the system latency are obtained by estimating the time it takes to identify the chipless tags when the proposed algorithms are applied to the USRP device. Also, the hardware restrictions are taken into consideration in the proposed measurements. In order to validate the proposed techniques, the following key performance indicators are examined:

1. Detection accuracy: this parameter indicates the accuracy of identifying the chipless tags when applying frequency sweeping.

2. The number of hops: this parameter guarantees that the hardware used is able to vary the hop rates to fit the requirements of the proposed algorithms.

3. Normalized system latency: this is measured by normalizing the time it takes to identify the tags when applying the proposed adaptive techniques and comparing it to the time taken by the FFH method.

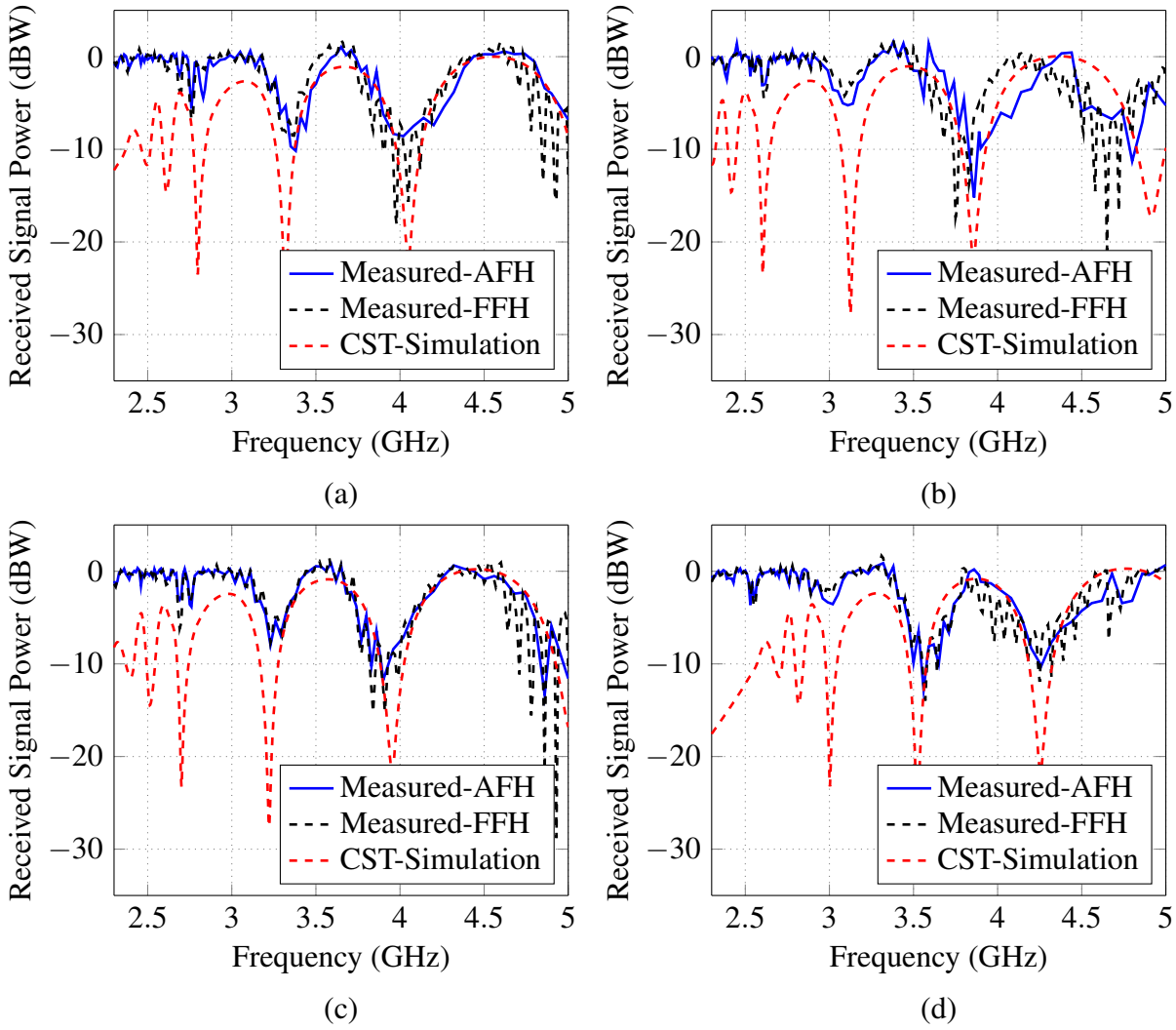

Figure 4.17: Measurement results for the backscattered signal from the chipless RFID tags after applying the proposed AFH technique and comparing it to the classical FFH methodology using USRP: (a) Tag-1. (b) Tag-2. (c) Tag-3. (d) Tag-4.

Fig. 4.17 shows a great similarity between the proposed AFH technique and the classical FFH method (used with a fine frequency resolution of 0.01 GHz). The received signals from the tags are compared to the simulation results obtained by the CST-MW studio EM simulator (shown in Fig. 4.8) in order to determine the accuracy of the proposed technique. The absorption of the notch is different due to channel effects. Moreover, the FFH methodology shows a greater number of fluctuations because the utilized averaging process is applied to each adjacent frequency step to remove environmental clutter. This results in higher error points than it does for the newly developed adaptive technique.

Fig. 4.18 illustrates the different hopping rates used to identify the chipless tags.

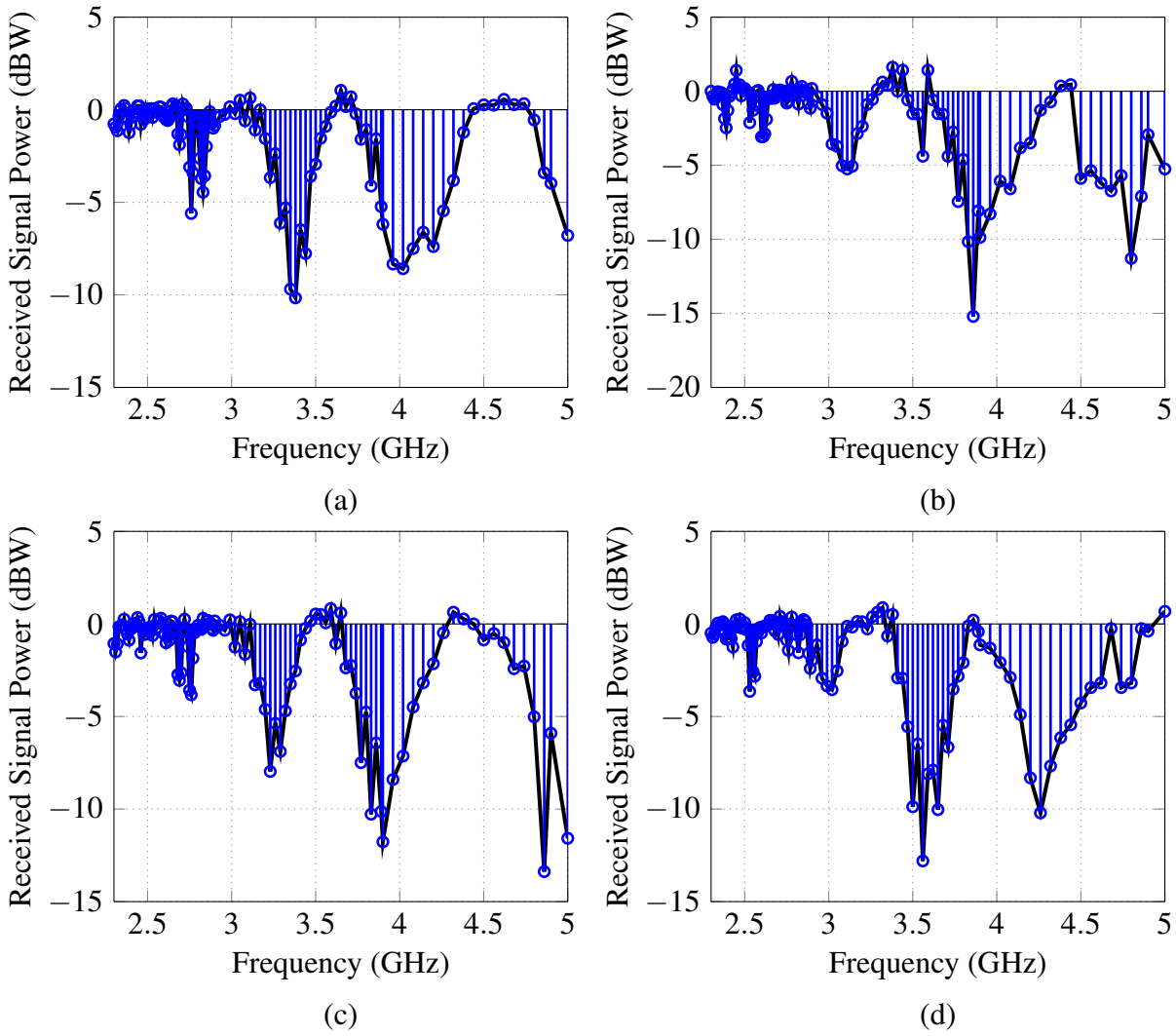

Figure 4.18: Measurement results for the backscattered signal from the chipless RFID tags illustrating the four frequency steps used to identify the chipless tags: (a) Tag-1. (b) Tag-2. (c) Tag-3. (d) Tag-4.

The USRP-transmitter generates a sweeping signal based on the predefined hopping rates (with different frequency steps as presented in Table 4.1). The backscattered signal from the tag is received by the USRP-receiver as shown in Fig. 4.17. Then, the signal processing techniques are executed including the adaptive sliding window criterion and the energy detection technique in order to translate these patterns into the corresponding bit stream.

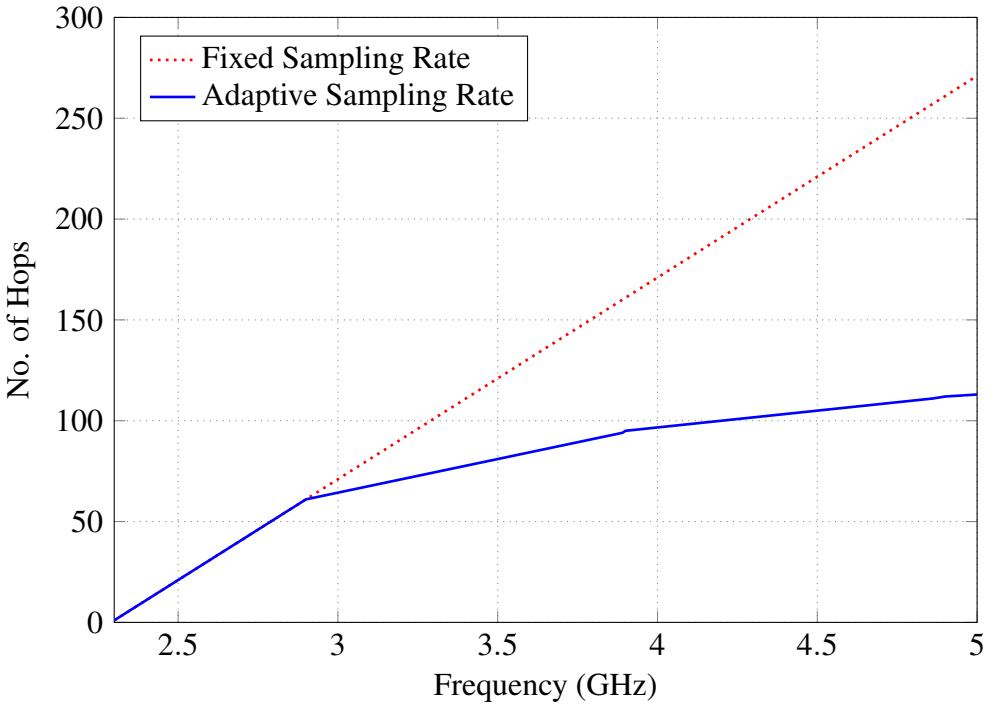

Figure 4.19: The measured number of hops after applying the AFH and the FFH spectrum scanning technique using the USRP.

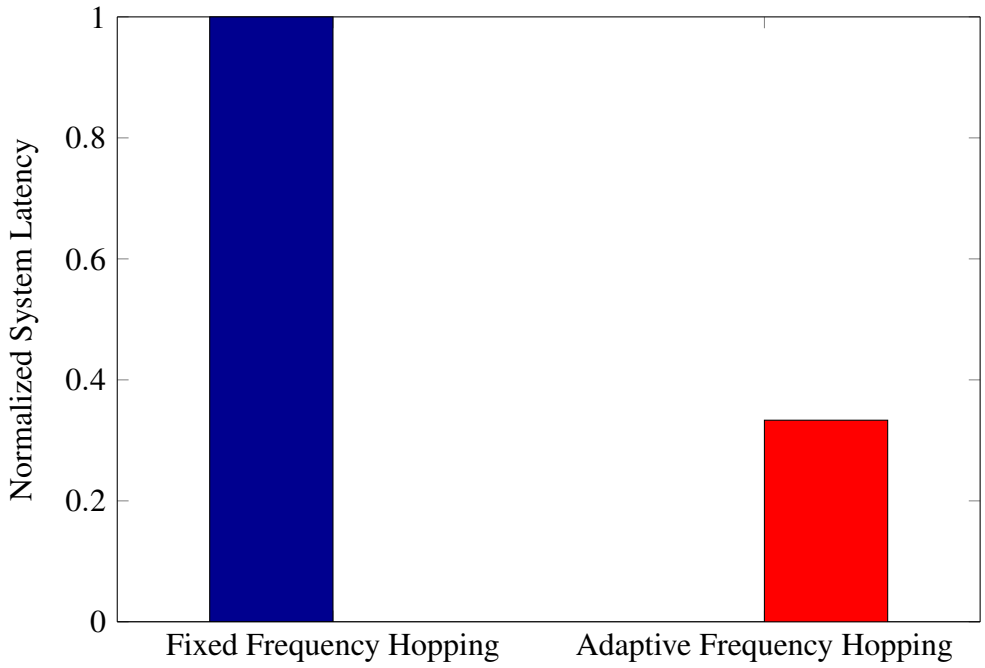

Figure 4.20: Normalized measured system latency.

The number of hops needed by the USRP for the classical FFH method and the proposed AFH technique is shown in Fig. 4.19 (the number of hops for both AFH and FFH are 113 hops

and 271 hops, respectively). Furthermore, the overall system latency is measured by estimating the time taken to scan the operating frequency when applying the AFH and FFH techniques. The normalized latency is calculated by dividing the latency for the adaptive algorithms by the latency for the classical FFH methodology. Fig. 4.20 shows that the proposed AFH technique reduces the system latency by more than 58% considering the hardware issues, which excellently matches the simulation results obtained by the latency modeling, shown in Fig. 4.12.

4.7 Conclusions

In this chapter, novel techniques to reduce the *system latency* of the reader, which is the time needed to identify the Frequency Coded chipless RFID tags, are proposed. It could be shown that the overall system latency is affected by the chosen frequency scanning method, the number of scanning iterations to remove clutter, and the frequency-hop duration. Therefore, a method of Adaptive Frequency Hopping (with variable detection window size) is designed, simulated, and implemented in a real-world testbed using a Software Defined Radio platform (USRP N210, with CBX daughter-board). Furthermore, the measurement setup relies on real manufactured FC chipless tags. The proposed algorithms are written in Python and introduced over the USRP. The measurements are performed outside the anechoic chamber, so that environmental effects can be included. The designed AFH algorithm is compared to the classical FFH method and the results show that the AFH algorithm works efficiently in the FC chipless RFID systems. When applying the proposed AFH technique, the overall system latency can be reduced by more than 58% and the chipless tag is accurately detected with the help of the adaptive sliding window criterion. A close match between simulation and measurement results can be seen throughout the results. A comprehensive study is performed between the proposed AFH algorithm, the classical FFH methodology, and the ASW techniques. The results are summarized in Table 4.3.

Table 4.3: Comparison of the proposed AFH, ASW-FH, ASW-AH, and FFH algorithms.

	FFH	**AFH**	**ASW-FH**	**ASW-AH**
Number of Hops	High	Low	High	Low
System Latency	High	Low	High	Low
Detection Accuracy	Moderate	High	Moderate	Moderate
Algorithm Complexity	Low	Low	High	High
Tag-Type Dependancy	No	No	Yes	Yes
Latency Increment with the No. of Tags	No	No	Yes	Yes

5 Coding Capacity

The main objective of this contribution is to introduce a novel technique that increases the coding capacity of the Frequency Coded (FC) chipless RFID system. The presented scheme encodes 4 bits per single resonator which employs the notch bandwidth and its corresponding frequency position. Hence, 80-bits can be achieved in the range of 2 to 5 GHz preserving the operating frequency bandwidth. Furthermore, a Smart Singular Value Decomposition (SSVD) technique is utilized to estimate the notch bandwidth and to ensure a low probability of error. Consequently, a high encoding efficiency and accurate detection can be achieved with a simplified reader design. In addition, the use of Error Correction Codes (ECC) is explored and applied to the chipless RFID system. This will enhance the system's performance due to the obtained coding gain. Likewise, a novel 4×5 cm^2 tag is designed to fit the requirements of the devised coding technique and to achieve a coding density of 4 bits/cm^2. Different tag configurations are manufactured and validated with measurements using a Software Defined Radio (SDR) platform. The introduced coding method is conclusively validated using Electromagnetic (EM) simulations and real-world testbed measurements. This work has already been partially published in [24].

5.1 Introduction

One of the most important applications of the chipless RFID system is the supermarket scenario, where the system is anticipated to replace the optical barcode by 2020 [71,108]. The conventional encoding schemes as mentioned in [109–111] are not applicable to the chipless RFID tags since they do not include memory and modulation modems [53]. The coding capacity and ease of chipless RFID tag detection are necessary functions to compete with the existing barcode systems

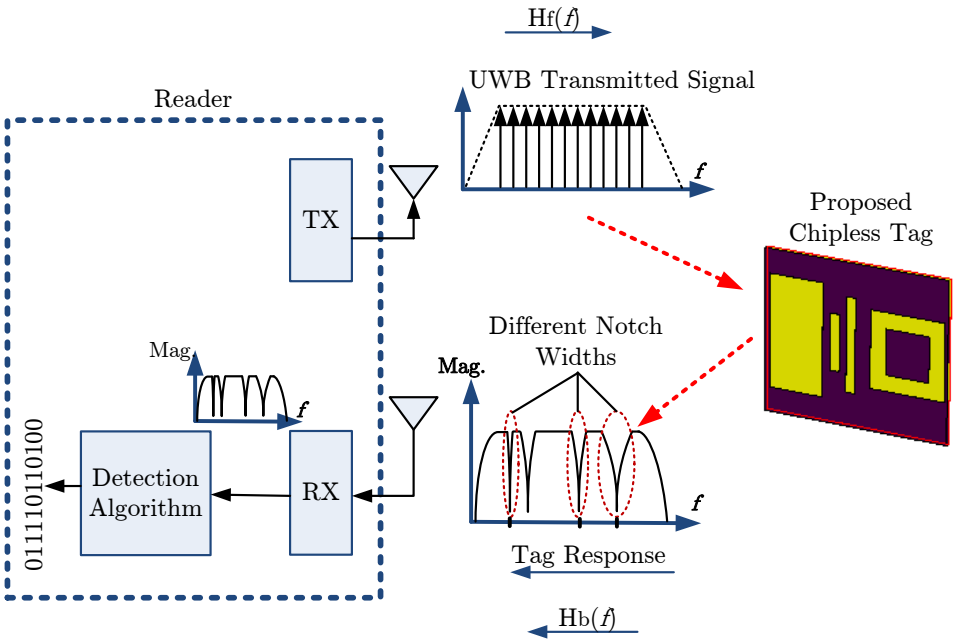

Figure 5.1: Block diagram of chipless RFID system.

and to simplify the reader's design. Chipless RFID tags are defined according to their coding method as time domain [112], frequency domain [105], image based [113], and hybrid. The hybrid tag uses more than one dimension for data encoding and decoding such as (frequency - phase) [114], (frequency - polarization) [53], and (frequency - time) [115] to increase the coding capacity.

The time domain based chipless RFID tags are evaluated by transmitting a pulse signal from the reader and listening to the reflected signal from the tag. The data is encoded by sending adjacent pulses at different time slots [23]. However, the tag employs only a low number of bits at a comparably large tag size.

The chipless Frequency Coded (FC) RFID system relies on a frequency signature induced by the tag on the transmitted signal with the aid of resonators. The chipless RFID tag is detected by analyzing the backscattered signal that constitutes the tag's ID. With the help of the proposed Notch Width Modulation (NWM) technique, the tag's response consisting of notches with different bandwidth and frequency locations can be detected as presented in Fig. 5.1. The involved signal processing for decoding and detecting the tag's ID is quite challenging as it is used for fast (reduced system latency) and accurate (minimum error of detection) identification. An increased number of data bits for chipless RFID tags is important to match the barcode

standards listed in [116] and the associated Electronic Product Code (EPC) [117].

Table 5.1 summarizes all previous studies dealing with the encoding techniques for chipless RFID tags and compares them to the proposed encoding technique.

Table 5.1: Comparison between existing chipless RFID encoding techniques.

Class	Resonator Type	Encoding Technique	No. of Bits per Single Resonator	Coding Density (bits/cm^2) No. of Bits / Total Area	Frequency Range (GHz)	Detection Technique
Frequency Domain	Spiral [118]	N	1	0.61	3–7	N
	Open Stub [119]	N	1	<1	2–4	N
	Dual Band [120]	N	1.5	<1	2.5–5.5	Y
	C-Shaped [121]	Y	1	2.9	2.5–7.5	N
	Dual Polarized [78]	N	1	>7	7–12	N
	Depolarization [37]	Y	1	0.66	3–7	Y
	Stepped Impedance [122]	Y	2	>7	3–9	Y
	C-Shaped, RCS level coding [123]	Y	3	1.25	2–5	N
	Proposed Technique	**Y**	**4**	**4**	**2–5**	**Y**
Time Domain	SAW [25]	Y	1	<1	2.44	N
	Delay Line [124]	N	1	0.17	2.44	N

For the prior studies listed in Table 5.1, the maximum number of bits encoded in each resonator is three while the proposed technique introduces 4 bits per single resonator, which represents the notch. Moreover, the approaches listed in the literature use a Vector Network Analyzer (VNA) and a horn antenna (at the reader's side) in the measurement setup. The newly developed measurement setup uses a Universal Software Radio Peripheral (USRP), which is responsible for decoding and detection, and a low-cost monopole reader antenna (gain of 2–5 dB). These improvements enable a realistic implementation of the chipless RFID system. Furthermore, the proposed coding technique yields a high coding capacity relying on a lower operating frequency (2–5 GHz). Likewise, so far no studies have been done that deal with the effect of coding/detection of the chosen techniques on the probability of error. Up to now it also has not been evaluated in how far the proposed solutions are simple and trustworthy in a

real-world environment.

In this chapter, a realistic novel hybrid coding technique is introduced. It is based on the notch bandwidth and its corresponding resonance frequency position. The proposed encoding method does not encode the bits in phase. Thus, it does not require any phase compensation methods at each tag as it is very sensitive to the channel effects [105]. Furthermore, a Smart Singular Value Decomposition (SSVD) detection technique is presented to ensure a low detection error and increased simplicity. Section 5.2 interprets the core functionality of the proposed coding, the mathematical framework, the introduced tag design, the detection/decoding techniques, and the utilization of error correcting codes in the chipless RFID system. Section 5.3 depicts the simulation results of decoding the chipless tags coded with the NWM scheme. Finally, Section 5.4 illustrates the measurement results to show the validity of the introduced approach.

5.2 Proposed Coding and Detection Techniques

This section introduces an encoding technique that represents several bits per notch depending on the notch bandwidth and the frequency location. The proposed technique has the advantage of simultaneously executing the decoding and detection processes for the chipless tags encoded with the NWM technique. Furthermore, it reduces the overall bandwidth of the system which lets it operate at lower cost and with reduced complexity. This is due to the fact that a larger number of bits can be achieved with a lower number of notches as each notch is represented by 4-bits. In addition, the utilization of error correction codes is investigated in this section.

5.2.1 Basic Operation and Core Functionality

The efficiency of the coding capacity is increased by encoding multiple bits for each notch (which is implemented using a resonator). The proposed coding technique is based on notch bandwidth and frequency location. The benefits of the proposed NWM approach are:

1. The ability to code with a high coding capacity within a smaller operating bandwidth (2–5 GHz). This can reduce the reader's cost due to lower hardware demands.

2. The use of a smart detection technique SSVD to reduce the detection error of the received chipless tag's ID while reducing the design complexity and detecting the notch widths and resonance frequencies.

3. Robustness against channel and multipath effects (no need for phase compensation for each tag as in [121]). Besides, the RCS level is not used in the encoding process (as in [123]) due to its sensitivity to environmental channel effects.

The first step to encode several bits per single notch based on the notch bandwidth and frequency location is illustrated in Fig. 5.2. The proposed coding technique comprises three notch bandwidths ($BW1$, $BW2$, and $BW3$) and frequency positions (F_r, $F_r + \Delta f$, and $F_r - \Delta f$) such that BW is the notch bandwidth, F_r is the notch resonant frequency, and Δf is the frequency shift used in the second dimension for coding.

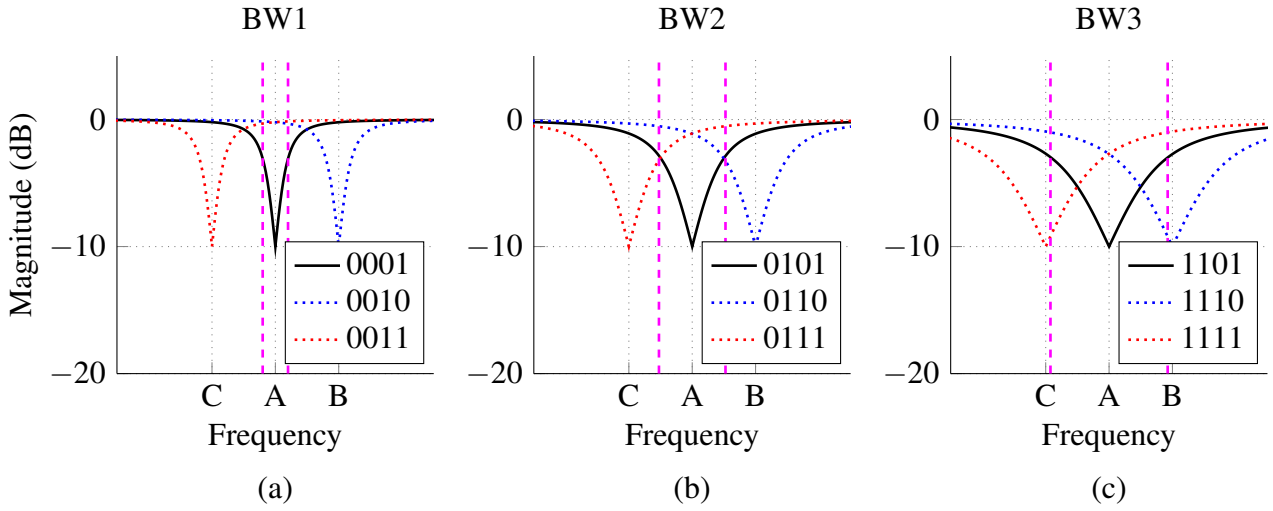

Figure 5.2: Basic principle of the coding technique: (a) Codes for notch with bandwidth BW1. (b) Codes for notch with bandwidth BW2. (c) Codes for notch with bandwidth BW3.

However, the total number of combinations for the method used in Fig. 5.2 that can be obtained is ten which will yield only 3-bits or 4-bits with six combinations that remain impossible to achieve. Consequently, two additional frequency shifts per notch bandwidth are required. Thus, the second step to obtain the unreachable combinations is to have five frequency locations for each notch bandwidth as illustrated in Fig. 5.3.

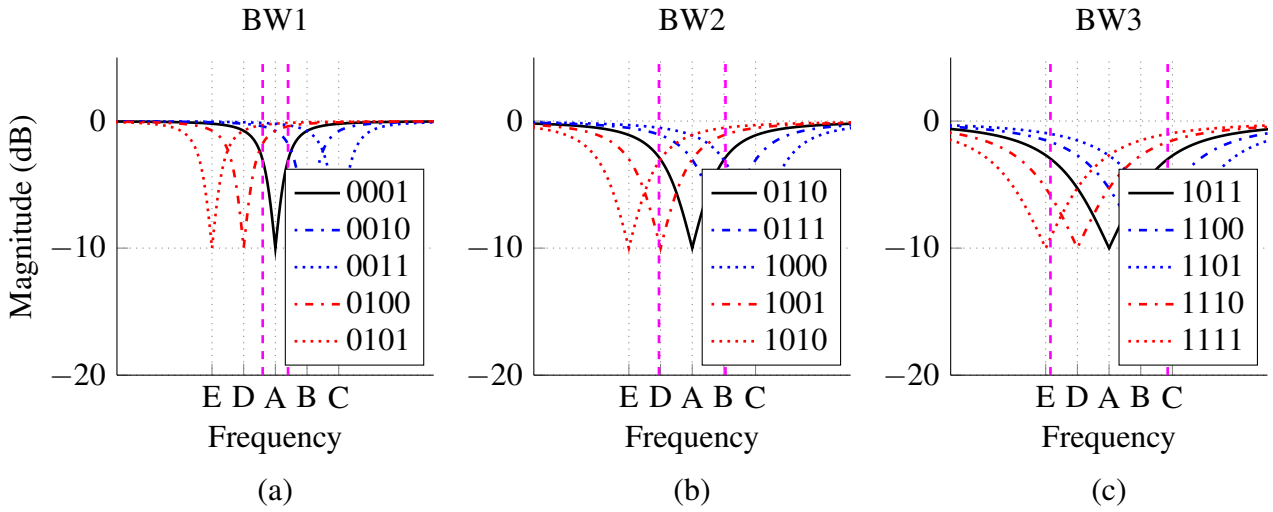

Figure 5.3: Basic principle of the coding technique: (a) Codes for notch with bandwidth BW1. (b) Codes for notch with bandwidth BW2. (c) Codes for notch with bandwidth BW3.

Hence, all 16 combinations can be obtained when encoding 4-bits per notch represented by the single resonator. Fig. 5.4 illustrates the 2D constellation diagram that describes the hybrid technique relying on both, notch bandwidth and frequency position. The notch bandwidths are estimated using the SSVD algorithm outlined in Section 5.2.4.

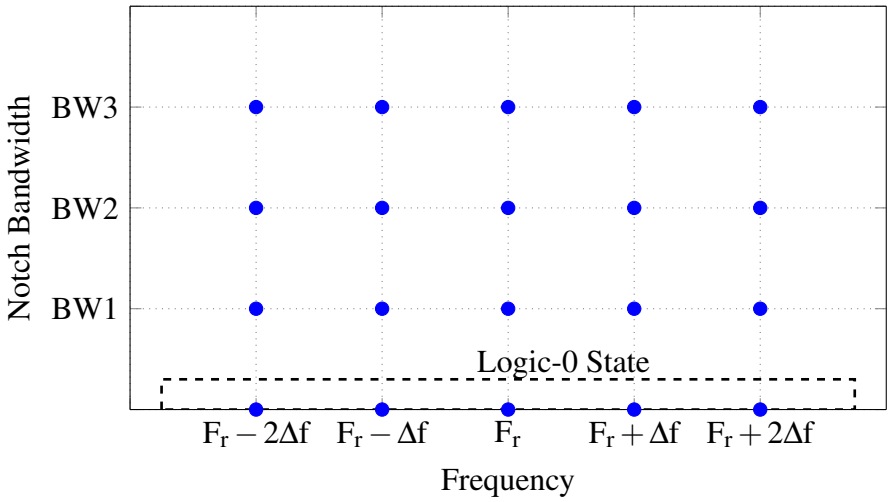

Figure 5.4: 2D constellation diagram for the proposed technique.

Fig. 5.5 illustrates the proposed coding principle for a real chipless tag using the CST-Microwave Studio EM simulator. The dashed magenta lines represent the windows that can include a notch with certain bandwidth and frequency location.

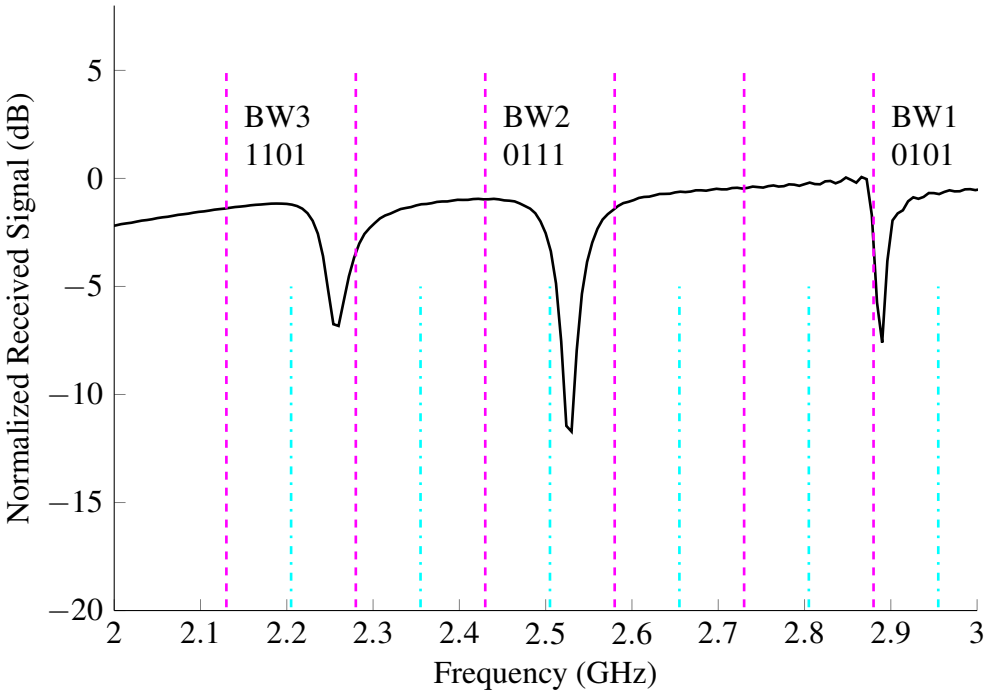

Figure 5.5: Basic principle of the coding technique.

The pseudo code describing the NWM decoding technique is illustrated by Algorithm 5.1. The SSVD technique is applied to each frequency location in order to estimate the notch pattern. Consequently, the notch coding pairs C_j (f_k,B_l) are obtained in order to be able to extract the corresponding ID which is stored in a look-up-table in the reader's main memory.

5.2.2 Mathematical Framework

The chipless RFID tag's response consists of several notches with predefined bandwidths and frequency positions. These represent a certain code as described before. The notch pattern can be expressed as a function of the frequency location (f_k) and the notch bandwidth (B_l). The notch pattern is modeled by a 2^{nd} order notch filter scheme [125] as described in Equations (5.1).

$$S(s) = \frac{s^2 + \omega_k^2}{s^2 + \frac{\omega_k}{Q_l}s + \omega_k^2} \tag{5.1a}$$

$$S(\omega) = \frac{\omega_k^2 - \omega^2}{(\omega_k^2 - \omega^2) + (\frac{\omega_k}{Q_l}\omega)i} \tag{5.1b}$$

$$S(f) = \frac{f_k^2 - f^2}{(f_k^2 - f^2) + (\frac{f_k}{Q_l}f)i} \tag{5.1c}$$

Algorithm 5.1 Proposed Coding Technique for Chipless RFID Tag

```
1: //BW1 is notch bandwidth with value BW1 used for coding
2: //BW2 is notch bandwidth with value BW2 used for coding
3: //BW3 is notch bandwidth with value BW3 used for coding
4: //Fr is notch resonant frequency
5: //Δf is the shift frequency used for coding
6: //f is notch frequency position
7: //ssvd_opt the output of SSVD algorithm
8: //d is the minimum distance to pre-calculated constellation points
9: for all f ← Fr do
10:    ssvd_output ← apply_ssvd_algorithm();
11:    d ← calculate_min_distance_constellation(ssvd_opt);
12:    if d is no_notch then
13:       f ← Fr + Δf;
14:       ssvd_opt ← apply_ssvd_algorithm();
15:       d ← calculate_min_distance_constellation(ssvd_opt)
16:       if d is no_notch then
17:          f ← Fr + 2Δf;
18:          ssvd_opt ← apply_ssvd_algorithm();
19:          d ← calculate_min_distance_constellation(ssvd_opt)
20:          if d is no_notch then
21:             f ← Fr − Δf;
22:             ssvd_output ← apply_ssvd_algorithm();
23:             d ← calculate_min_distance_constellation(ssvd_opt)
24:             if d is no_notch then
25:                f ← Fr − 2Δf;
26:                ssvd_output ← apply_ssvd_algorithm();
27:                d ← calculate_min_distance_constellation(ssvd_opt)
28:                if d is no_notch then
29:                   The code is 0000;
30:                else
31:                   get_code_from_LUT();
32:                end if
33:             end if
34:          end if
35:       end if
36:    end if
37: end for
```

where ω_k equals $2\pi f_k$ and represents the notch angular resonance frequency. Q_l is the quality factor of the notch filter. Furthermore, the notch bandwidth B_l is represented by Equation (5.2).

$$B_l = \frac{f_k}{Q_l} \tag{5.2}$$

Thus, the notch pattern $S(f)$ is expressed based on the notch bandwidth B_l and the frequency position f_k. Consequently, the notch is modulated by a specific bandwidth and frequency location that represents a certain code (bit stream).

$$S(f) = \frac{f_k^2 - f^2}{(f_k^2 - f^2) + (B_l \times f)i} \tag{5.3}$$

Thereafter, the chipless tag is illustrated by Equation (5.4) based on the proposed NWM encoding technique with the coding pairs C_j (f_k,B_l) .

$$\Gamma_{\mathrm{NWM}}(f) = \sum_{k=1}^{K} c_k . S_k(f)|_{(f_k, B_l)} \tag{5.4}$$

The chipless tag's response $\Gamma_{\mathrm{NWM}}(f)$ is analytically described based on the predefined frequency position f_k and the notch bandwidth B_l. Also, c_k is the code factor that shows whether or not there is a notch with a certain code existent in the interrogation area. The absence of this specific code is represented by code-0000.

In order to validate the suggested mathematical framework of the proposed notch with modulated tags, three chipless tags are designed based on the NWM technique using the CST-Microwave Studio EM simulator, as described in the "Tag Design" Section. The CST-simulation results are compared to the proposed mathematical framework. Fig. 5.6 shows a close match between the newly-developed analytic model and the simulation results.

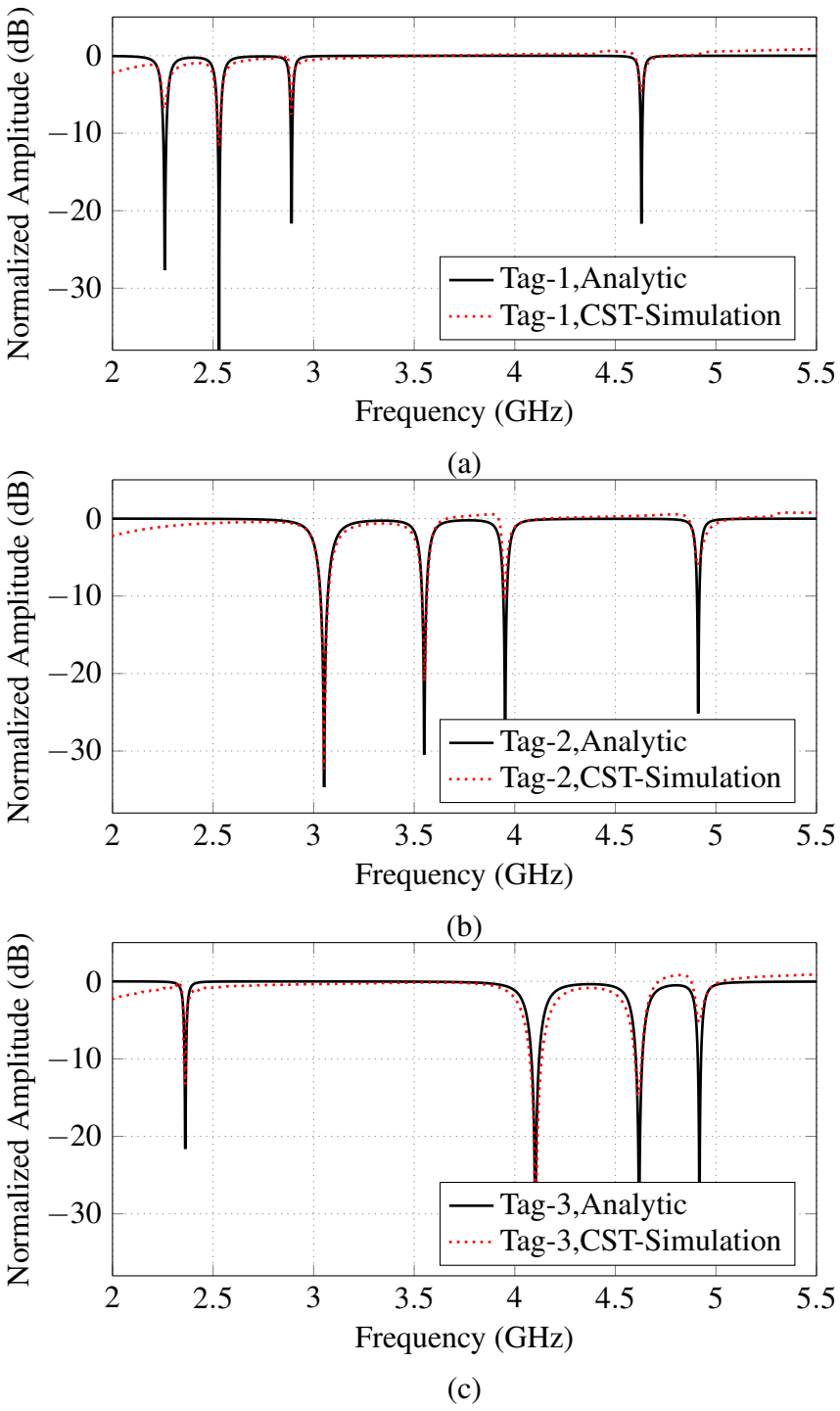

Figure 5.6: Results of analytic model and simulation: (a) Tag-1 analytic and simulation. (b) Tag-2 analytic and simulation. (c) Tag-3 analytic and simulation.

5.2.3 Tag Design

According to the proposed NWM coding technique, the tag is able to provide three different notch bandwidths at specified frequencies inside each window (the window definition is illustrated in

Section 5.2.4). However, it is still problematic that the quality factor of the same resonator over the same substrate is almost constant, thus the bandwidth is increased with increasing frequency (shown in Chapter 4) as expressed by Equation (5.2). Consequently, a novel tag structure is developed in order to meet the NWM's coding requirements. The tag relies on three different resonating elements specifying the three coding bandwidths. The coding elements are a dipole, a rectangular ring, and a rectangular patch which correspond to the first, the second, and the third coding bandwidth, respectively.

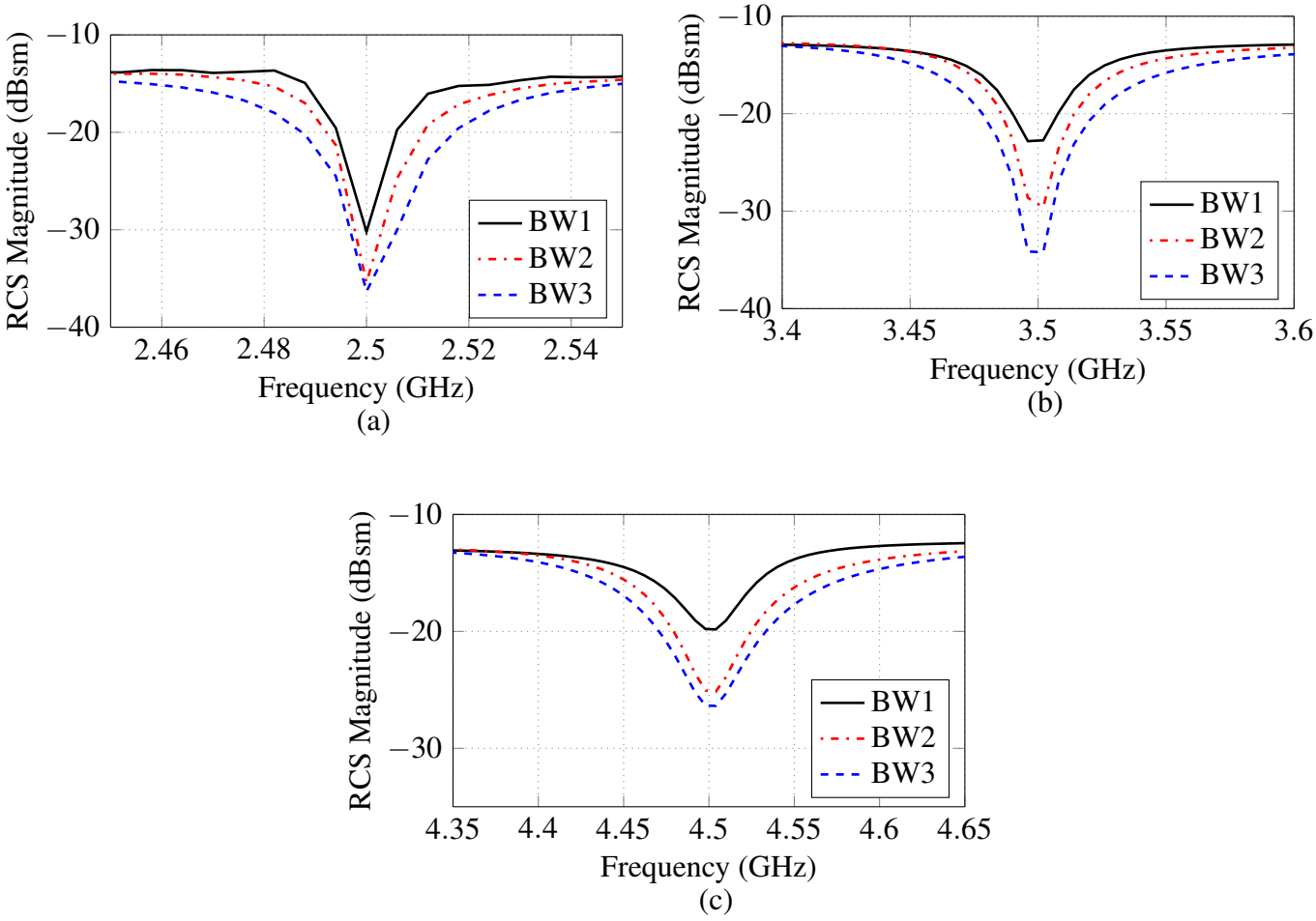

Figure 5.7: NWM based notch patterns at three different frequency bands using the CST-Microwave Studio EM simulator: (a) First window. (b) Second window. (c) Third window.

The average notch bandwidths for these elements are calculated using Equation (5.2) with the given quality factor value for each resonating element. They can also be estimated by using the CST-MW Studio simulator for each GHz of the operating frequency. Fig. 5.7 shows the pattern of the notches within the operating frequency in the ranges of 2–3, 3–4, and 4–5 GHz,

respectively. These values of notch bandwidths are used by the reader to decode the backscattered signal from the tag. Three different tags are designed to meet the requirements of the NWM technique as shown in Fig. 5.8.

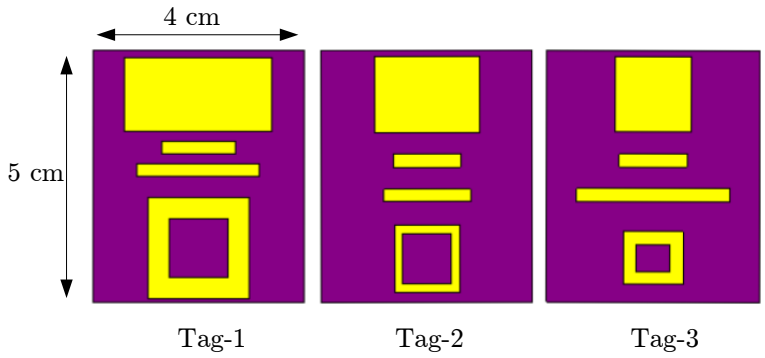

Figure 5.8: Proposed tag design.

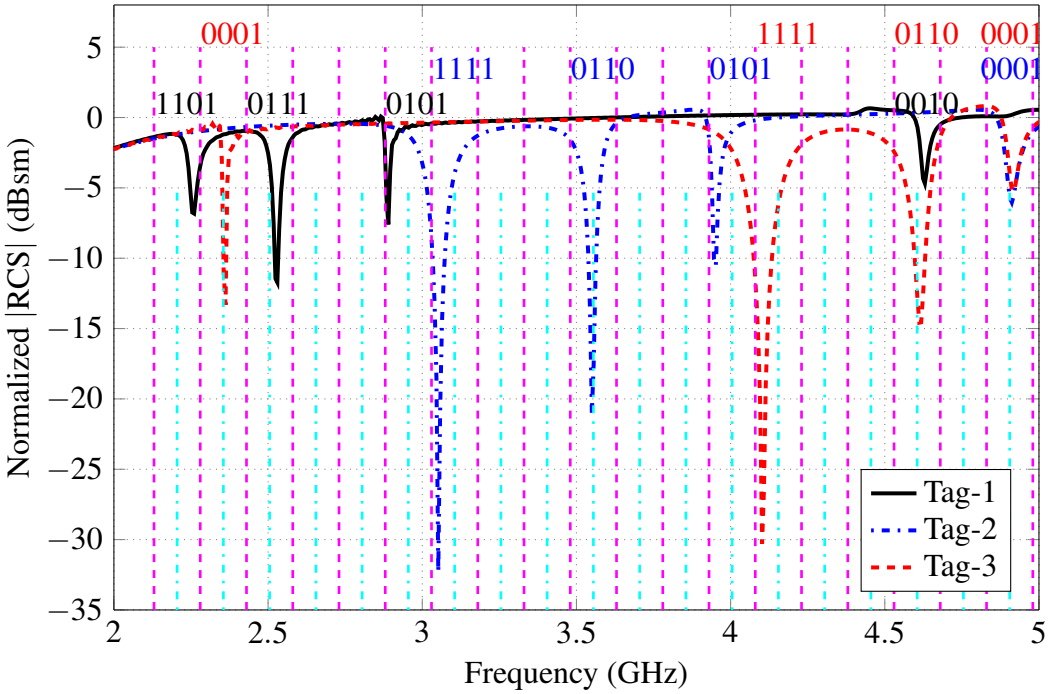

Figure 5.9: Simulation results of the designed chipless RFID tags using the CST-Microwave studio EM simulator.

The responses of the designed tags are shown in Fig. 5.9 which illustrates the flexibility of controlling both the notch bandwidth and the resonant frequency with the predefined values that represent a certain code. Likewise, the notch arrangement of these tags yields results contrary to

all previously known phenomena with regard to the notch bandwidth's increment with rising frequency. This is due to the fact that here each tag's response starts with the wider notch bandwidth and continues with the narrower ones. Additionally, it is observed that up to 20 notches can be allocated in an operating frequency range of 2–5 GHz representing around 80-bits. The dotted magenta lines represent the coding window and each dotted cyan line shows the center of this coding window. Thus, the notch can be located on these cyan lines or, in order to represent a specific code, it can be shifted to the left or to the right.

5.2.4 Proposed Smart Singular Value Decomposition Detection Technique

In this section, the use of the SSVD algorithm proposed in [36] is briefly described to estimate the notch bandwidth in order to meet the encoding requirements.

A. Windowing

Windowing is an essential process that is part of the proposed detection technique. In this work, windowing is done in the frequency domain by multiplying the received signal $Y(f)$ with a shifting window function as illustrated by Equation (5.5).

$$Y_k(f) = Y(f).\text{rect}(\frac{N}{f_{\max} - f_{\min}} - k.N) \tag{5.5}$$

where N is the number of frequency points in the window and k is the k^{th} window in the whole band. Moreover, $f_{\max} - f_{\min}$ is the bandwidth of the window. These windows are represented by the dashed magenta lines shown in Fig. 5.9 with a bandwidth of 150 MHz.

B. Smart-SVD

The classical Singular Value Decomposition (SVD) algorithm mentioned in [126] uses 2^b combinations to create the detection constellation points, where b is the total number of bits for each chipless tag. When the number of bits is increased, the number of constellation points also rises, thus decreasing the probability of detection (accordingly, this increases the probability of error). Moreover, the size of the matrix used to calculate the constellation coordinates rapidly expands, making the detection very computationally expensive.

The SSVD is a fast and improved method to detect the notch using Signal Space Representation (SSR). In the SSVD, only four training sequences are considered for any number of total

notches, creating a rank four matrix **M** as illustrated by Equation (5.6).

$$\mathbf{M} = \mathbf{U}\Sigma\mathbf{V}^{\mathbf{T}} = [\gamma_1, \gamma_2, \gamma_3, \gamma_4]_{m\times 4} \tag{5.6}$$

where $[\gamma_1, \gamma_2, \gamma_3]$ represents the three predefined notches with different pattern bandwidths (according to the coding technique requirements, $BW1$, $BW2$, and $BW3$) and γ_4 constitutes a no-notch representation. **U** and **V** are unitary matrices composed of orthonormal column vectors $\mathbf{u_i}$ and $\mathbf{v_i}$. Moreover, Σ is a diagonal matrix consisting of four constant values of σ_i as presented in Equation (5.7).

$$\mathbf{M} = \begin{bmatrix} \mathbf{u}_1 & \dots & \mathbf{u}_4 \end{bmatrix}_{N\times 4} \begin{bmatrix} \sigma_1 & 0 & 0 & 0 \\ 0 & \sigma_2 & 0 & 0 \\ 0 & 0 & \sigma_3 & 0 \\ 0 & 0 & 0 & \sigma_4 \end{bmatrix}_{4\times 4} \begin{bmatrix} \mathbf{v}_1^T \\ . \\ . \\ . \\ \mathbf{v}_4^T \end{bmatrix}_{4\times 4} \tag{5.7}$$

Using the orthonormal property of the SVD matrix, the four constellation points are calculated off-line.

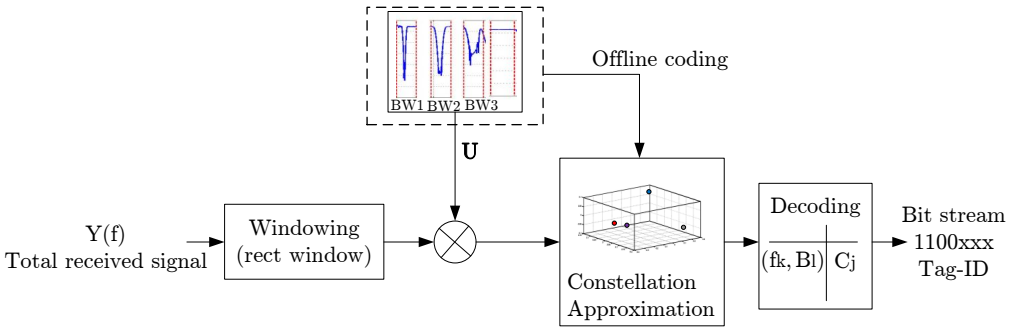

Figure 5.10: Block diagram of Smart-SVD.

Fig. 5.10 shows the block diagram of the decoding cycle for the received signal $Y(f)$ which is reflected from the tag and decoded with the proposed NWM coding technique. The received signal is windowed $Y_k(f)$ and then compared to the previously calculated constellation points c_j. The minimum distance vector criterion is applied as described in Equation (5.8). Afterwards, the notch pattern that is defined by the frequency and bandwidth pairs, called *coding pairs* (f_k,B_l), is

decoded to a specific code C_j.

$$d_k = \min \left\{ || \langle Y_k(f), U \rangle - c_j ||^2 \right\} \; j = 1..4 \tag{5.8}$$

Therefore, utilizing the already introduced SSVD algorithm, the notch bandwidth can be estimated according to the predefined bandwidths derived from the offline coding. Furthermore, the notch frequency location is determined inside each window by applying the SSVD within narrow frequency location ranges.

5.2.5 Error Correction Coding

In this section, the utilization of a linear block code (i.e., Hamming codes) as an error correction code for the chipless RFID system is presented. Within a block code, a block of k data digits is encoded by a codeword of n digits such that ($n > k$). Here, the number of bits used for error correction is m with $m = n - k$. They are called parity check digits $p_{(1\times m)}$. Fig. 5.11a shows the structure of the systematic codeword for a linear block coded chipless tag. The tag-ID, the codeword, and the parity check bits are represented as follows [127]:

$$\mathbf{d} = [d_1, \cdots, d_k] \tag{5.9a}$$

$$\mathbf{c} = [c_1, \cdots, c_n] \tag{5.9b}$$

$$\mathbf{p} = [p_1, \cdots, p_m] \tag{5.9c}$$

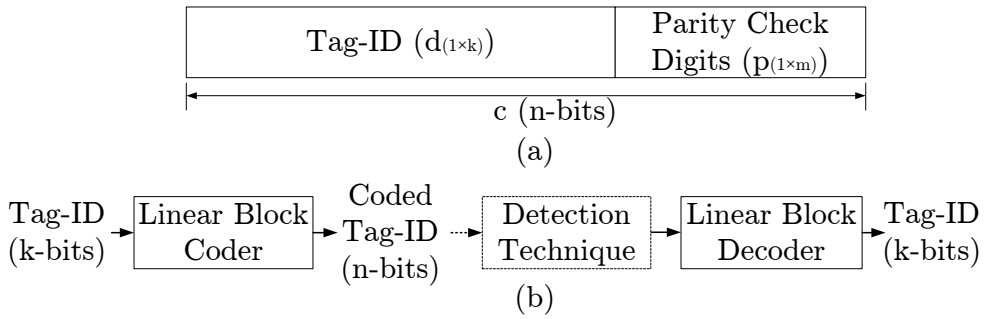

Figure 5.11: Illustration of the utilization of error correction coding in the chipless RFID system: (a) Structure of the systematic codeword. (b) Block diagram of coding/decoding the chipless tag using linear block codes.

In addition, the relationship between the number of bits in the codeword n and the number of parity check bits m is formulated by Equation (5.10) [128]. Furthermore, the coding efficiency

(also known as code rate R) is expressed as k/n.

$$n = 2^m - 1 \tag{5.10}$$

A. Coding

For the general case that uses linear block codes, all the n digits of the codeword are formed by linear combinations (modulo-2 additions) of k data digits. The special case where $c_1 = d_1$, $c_2 = d_2, \cdots, c_k = d_k$ and the remaining digits from c_{k+1} to c_n are linear combinations of $d_1, \cdots, d_k$ is known as a systematic code [128]. The structure of the systematic codeword is illustrated in Fig. 5.11a and the parity check digits are formed by linear combinations of the data digits.

$$\begin{aligned}
c_1 &= d_1 \\
c_2 &= d_2 \\
&\vdots \\
c_k &= d_k \\
c_{k+1} &= p_{11}d_1 \oplus p_{12}d_2 \oplus \cdots \oplus p_{1k}d_k \\
c_{k+2} &= p_{21}d_1 \oplus p_{22}d_2 \oplus \cdots \oplus p_{2k}d_k \\
&\vdots \\
c_n &= p_{m1}d_1 \oplus p_{m2}d_2 \oplus \cdots \oplus p_{mk}d_k
\end{aligned} \tag{5.11a}$$

$$\mathbf{c} = \mathbf{dG} \tag{5.11b}$$

where

$$\begin{aligned}
\mathbf{G} &= [\mathbf{I}_{(k\times k)} \vdots \mathbf{P}_{(k\times m)}] \\
&= \begin{bmatrix}
1 & 0 & 0 & \cdots & 0 & p_{11} & p_{12} & \cdots & p_{m1} \\
0 & 1 & 0 & \cdots & 0 & p_{21} & p_{22} & \cdots & p_{m2} \\
 & & & \vdots & & & & \vdots & \\
0 & 0 & 0 & \cdots & 1 & p_{1k} & p_{2k} & \cdots & p_{mk}
\end{bmatrix}
\end{aligned} \tag{5.12}$$

The $k \times n$ matrix $\mathbf{G}$ is known as the generator matrix and can be separated into a $k \times k$ identity matrix and a $k \times m$ parity check digits matrix as expressed by Equation (5.12). Thus, in order to code the chipless tag-ID with a linear block code, Equation (5.11b) is employed.

B. Decoding

When considering some of the codeword's properties that are necessary for the decoding purpose, Equation (5.13) is obtained by the derivation depicted in [127–129].

$$\mathbf{c}\mathbf{H}^T = 0 \tag{5.13a}$$

where

$$\mathbf{H}^T = \begin{bmatrix} \mathbf{P} \\ \mathbf{I}_m \end{bmatrix}$$

and its transpose

$$\mathbf{H} = [\mathbf{P}^T \ \ \mathbf{I}_m] \tag{5.13b}$$

is called the parity check matrix. Each codeword must satisfy Equation (5.13a). Due to the channel noise, possible errors ($\mathbf{e}$) can be expected when decoding the received word ($\mathbf{r}$) which can be written as:

$$\mathbf{r} = \mathbf{c} \oplus \mathbf{e} \tag{5.14}$$

Moreover, the syndrome ($\mathbf{s}$) is used to detect the position of the error bit as illustrated in [128] and expressed in Equation (5.15).

$$\mathbf{s} = \mathbf{r}\mathbf{H}^T \tag{5.15}$$

where $\mathbf{s}$ is a nonzero row vector called syndrome. After obtaining the syndrome vector $\mathbf{s}$ to the received word $\mathbf{r}$, the corresponding error $\mathbf{e}$ is extracted from the decoding table. The complete description of the linear codes and the syndrome decoding is illustrated in [127–131].

C. Coding Gain

Coding gain is a measure for the difference of the signal-to-noise ratio (SNR) levels between the uncoded system and the coded system that is required to reach the same probability of error levels when used with the Error Correcting Code (ECC). Thus, it indicates the amount of SNR improvement after applying the ECC. The asymptotic coding gain G_a is expressed by Equation (5.16) [132, 133].

$$G_a = 10\log[d_{min}R] \tag{5.16}$$

where d_{min} is the minimum distance of a linear block code that represents the smallest Hamming distance between any pair of code vectors in the code. This is the same as the smallest Hamming weight. t is the number of errors that need to be corrected using the ECC. Likewise, d_{min} is expressed as $2t+1$ as discussed in [127, 128]. The coding gain is calculated for different Hamming pairs and the corresponding parity check digits with $d_{min} = 3$ as shown in Fig. 5.12. Thus, the coding gain is increased when increasing the number of parity check digits.

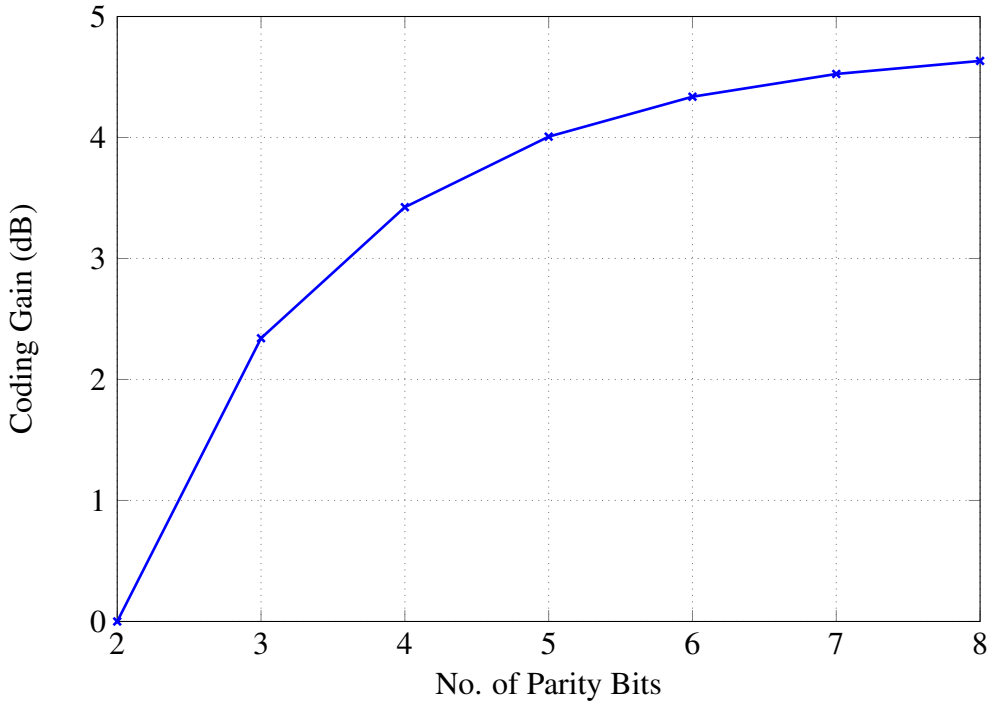

Figure 5.12: Asymptotic coding gain in relation to the number of parity bits.

In order to validate the usefulness of the ECC in the chipless RFID system, a 15-bit chipless tag is designed with the RCS magnitude response illustrated in Fig. 5.13a. The $(15, 11)$ error correction Hamming pair is applied. Furthermore, the probability of error is estimated for the designed chipless tag without and with the use of the ECC. As depicted in Fig. 5.13b, a coding

gain of 3.42 dB is obtained when applying the ECC with the $(15, 11)$ coding pair.

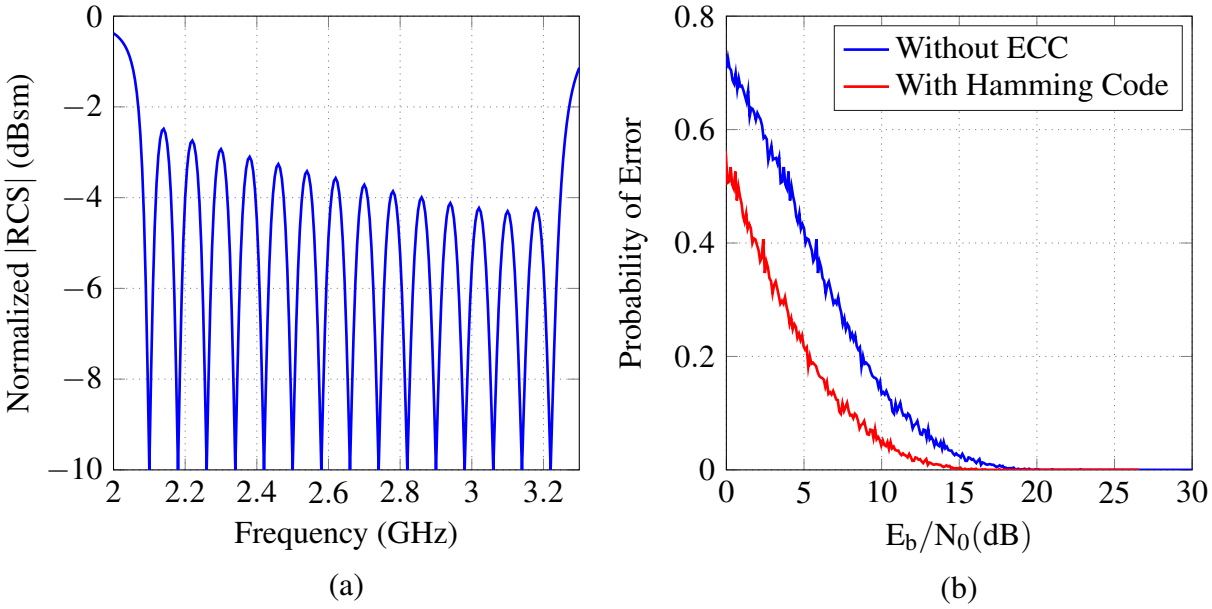

Figure 5.13: Illustration of the use of error correction coding: (a) 15-bits chipless tag. (b) Performance with and without error correction coding.

Consequently, the chipless tags in which each notch represents a single bit can successfully use the ECC technique to significantly enhance the system's performance. Since the proposed NWM technique encodes several bits for each notch in a particular window W, there is a need to design other coding techniques in order to obtain the appropriate combinations inside each W. This, however, will be the subject of future studies.

5.3 Simulation and System Performance

In this section, the simulation results of detecting/decoding the chipless tags based on the NWM coding technique will be discussed. The probability of error is estimated for the identification of the designed chipless tags.

5.3.1 Simulation Environment

The chipless RFID tags are designed and implemented using the CST Microwave Studio EM simulator. The output files from the CST are then used in MATLAB in order to apply the proposed decoding algorithm and the detection techniques as illustrated in Fig. 5.14.

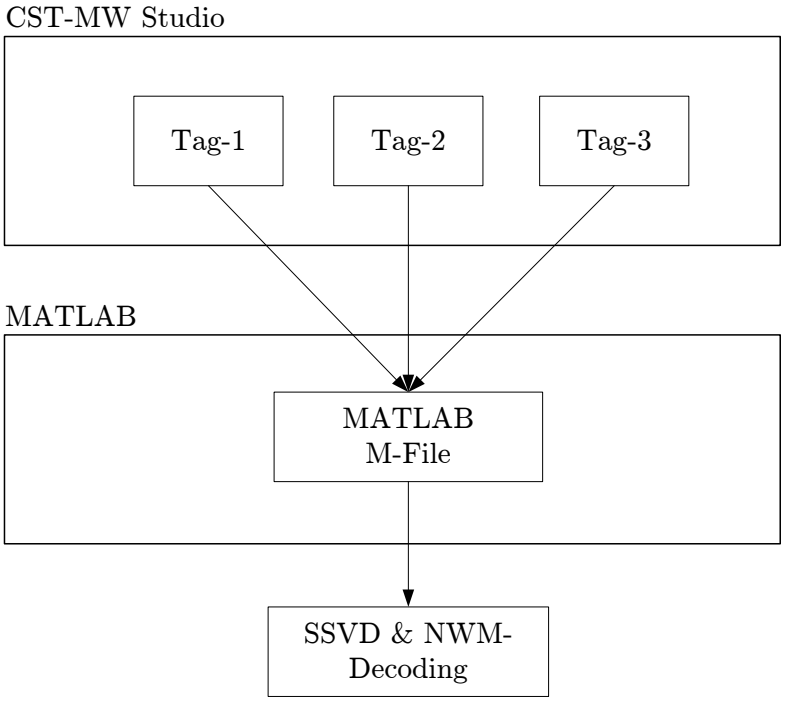

Figure 5.14: Block diagram of simulation environment.

The three designed chipless tags coded with the NWM technique are illustrated in Fig. 5.9. The range of the operating frequency is from 2 GHz to 5 GHz, the window size (bandwidth) is 150 MHz. This is illustrated by the magenta dashed lines. The Monte-Carlo iterations are 1500.

5.3.2 Simulation Results

The proposed algorithm defines three values for the notch bandwidths and five frequency positions for each window as illustrated in the 2D-constellation diagram shown in Fig. 5.4. As mentioned previously, the notch bandwidth is estimated using the SSVD algorithm, which is designed to match the nature of the received signal. Moreover, the frequency location of the notch is determined by sweeping each window with a narrow frequency step so that the coding pairs $C_j(f_k,B_l)$ can be obtained. In order to evaluate the overall system's efficiency when applying the NWM coding/decoding technique, the probability of error is estimated by changing the signal-to-noise ratio per symbol (energy per symbol to noise power spectral density ratio, E_s/N_0, because each notch represents a symbol with 4-bits). Additionally, the probability of error is determined for the:

1. Detection of notches using predefined bandwidths.

2. Detection of all the chipless tags coded using the proposed NWM coding technique.

A. Notch Bandwidth Detection Performance

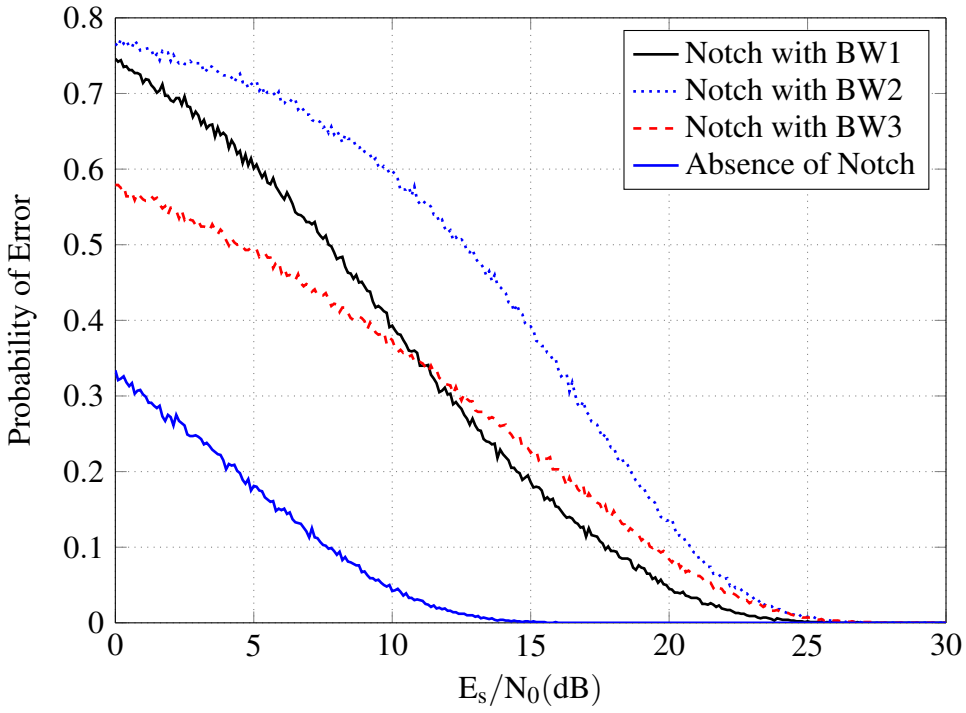

Figure 5.15: Probability of error for the received notch bandwidths.

The probability of error is evaluated for each detected notch bandwidth ($BW1$, $BW2$, $BW3$, and absence of notch) as shown in Fig. 5.15. It illustrates that when no notch is present, the error of detection is at its minimum because no code needs to be detected correctly. Moreover, the detection of the intermediate notch bandwidth $BW2$ shows the highest error. This is because it is enclosed between two values ($BW1$ and $BW3$). Therefore, there is a probability of detecting the notch of $BW2$ as if it was $BW1$ and to detect $BW2$ as if it was $BW3$. Furthermore, the detection error decreases with increasing notch bandwidth (at lower Signal to Noise Ratio per symbol values, less than 10 dB). This is due to the fact that the SVD algorithm yields a smaller error at a higher signal bandwidth (for $BW1$ and $BW3$). Only three values of notch bandwidths are examined in order to create a realistic design with regard to the implementation issues. The 3D constellation diagram that illustrates the results of the discussion above is shown in Fig. 5.16.

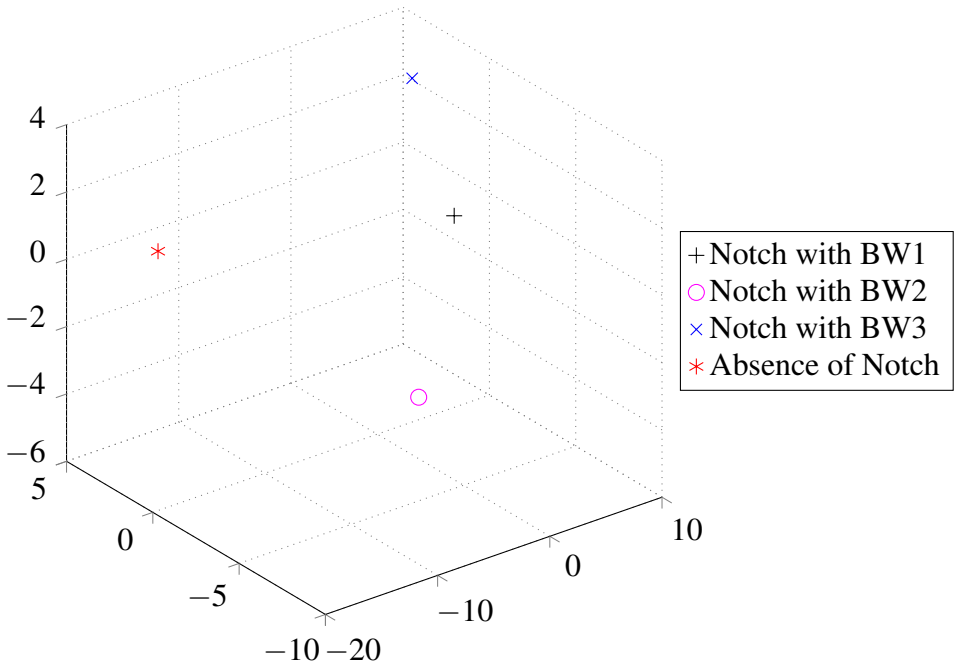

Figure 5.16: Constellation diagram for the notch bandwidths.

B. Overall NWM-Based System Performance

The general performance of the tags is illustrated in Fig. 5.16. It is shown that Tag-3 has the better performance at a lower SNR (less than 10 dB). This is due to the fact that it contains three notches in the higher frequency band (4–5 GHz) as shown in Fig. 5.9. They are relatively high bandwidths as illustrated in Fig. 5.7c. Also, Tag-2 has a higher probability of error since its response is mainly located in the intermediate bandwidth range (3–4 GHz). Tag-1, however, shows a higher probability of error because its response is located in the range of the lowest frequency bandwidth (2–3 GHz). Thus, its notches are positioned at the smallest bandwidths as shown in Fig. 5.7a.

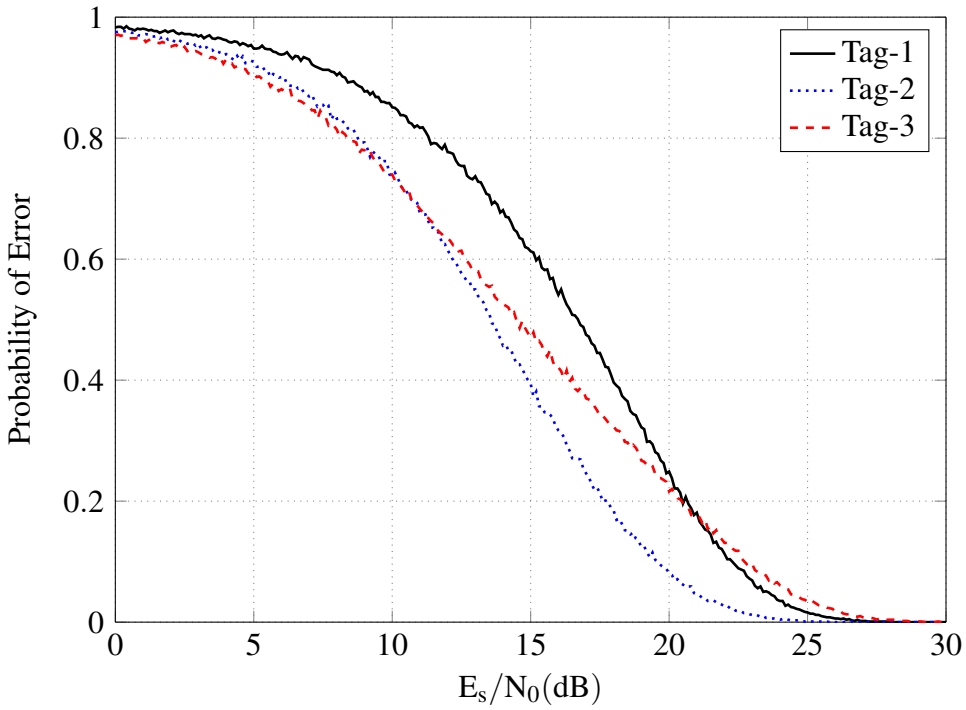

Figure 5.17: Probability of error for notch detection using the NWM method.

5.4 Measurements and Real-World Implementation

The real-world implementation for the proposed chipless RFID system working with the NWM encoding/decoding technique is described in this section.

5.4.1 Measurement Setup

The measurements are obtained by using an SDR platform based on USRP N210 [80] and a CBX RF-daughter board with an operating frequency of (1.2–6 GHz) [81], as illustrated in Fig. 5.18. The testbed setup parameters are summarized in Table 5.2. The tag is positioned at a distance of 30 cm from the reader's monopole antenna. A copper plate is placed between the two interrogator's antennas in order to isolate the effect of each one on the other, whereas the reader's antenna is omni-directional. Nevertheless, if a directive antenna is used, then the isolating plate can be removed. Furthermore, in order to increase the reading range of the chipless RFID system, an UWB reflect antenna array can be used at the reader's side as described in [71]. A frequency sweeping mechanism is applied in such a way that a sinusoidal wave is transmitted in a range of 2 GHz to 5 GHz with a frequency step of 10 MHz, as described in Chapters 3 and 4, respectively. At the same time, the receiver monitors the backscattered signal from the tag

Table 5.2: USRP Parameters.

Parameter	Value
Sampling Rate	1 M samples / second
Transmitter Gain	31.5 dB
Receiver Gain	0 dB
Start Frequency	2 GHz
End Frequency	5 GHz
Frequency Step	10 MHz
Frequency Sweep	
Averaging	100
Reader Antenna	
Type	Monopole
Gain	2-5 dBi

(because the CBX daughter board is full-duplex). Subsequently, the reader starts the processing phase by applying the SSVD algorithm and the designed decoding technique. The code for the N210 USRP platform is written in Python. The measurements are performed by subtracting the reflected signal power from the front of the tag and the received one from the tag's copper side as illustrated in Equation (5.17).

$$R^i_{\text{measured}}|_{\text{dB}} = R^i_{\text{front}}|_{\text{dB}} - R^i_{\text{back}}|_{\text{dB}} \tag{5.17}$$

where $R^i_{\text{measured}}|_{\text{dB}}$ is the total backscattered signal power measured from tag i, $R^i_{\text{front}}|_{\text{dB}}$ is the backscattered signal power from the front of tag i, and $R^i_{\text{back}}|_{\text{dB}}$ is the backscattered signal power from the back of tag i (the copper side).

After employing the normalization process represented by Equation 5.17, the signal is transferred to the frequency domain by applying the FFT operation. Afterwards, the signal is windowed and the SSVD technique is used to decode and estimate the coding pairs C_j (f_k,B_l) as described in the testbed block diagram, Fig. 5.18a. Finally, the tag-ID is extracted from the look-up-table stored in the reader's main memory.

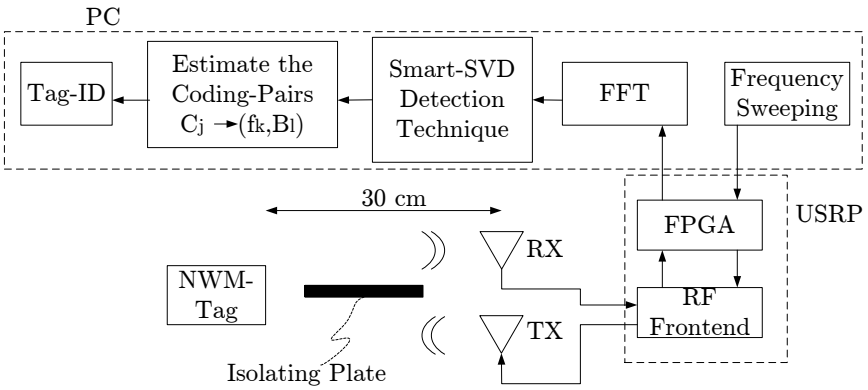

(a)

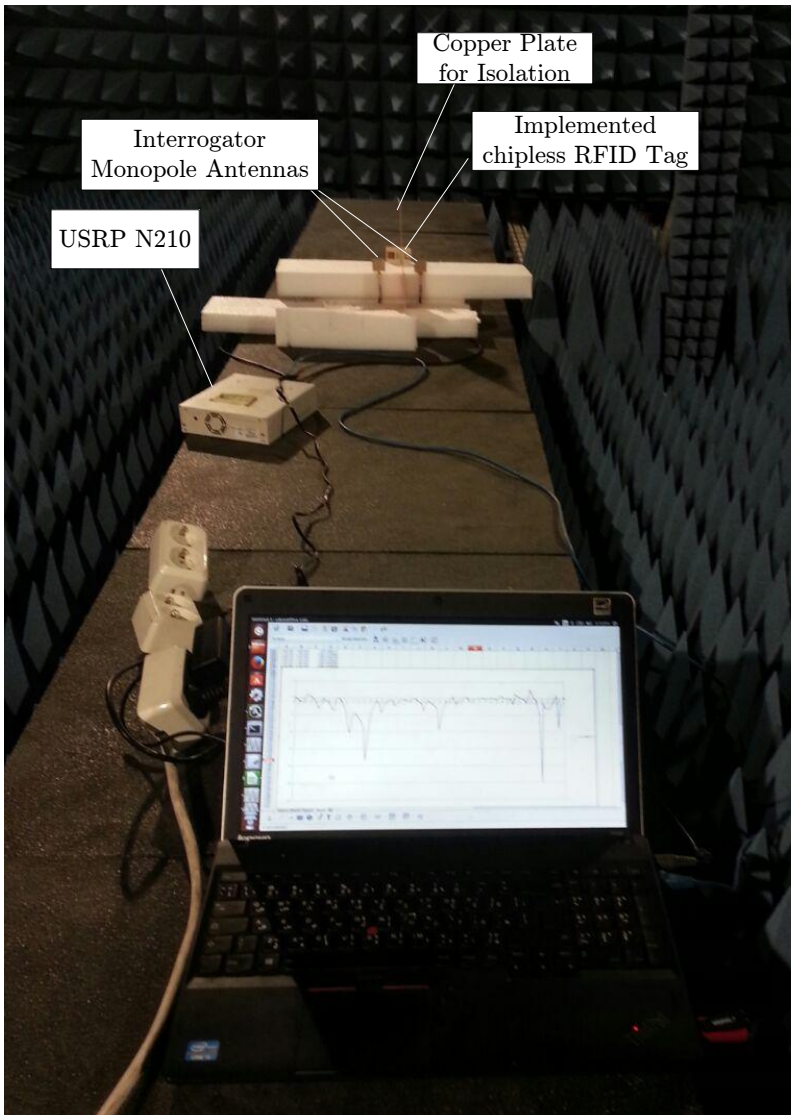

(b)

Figure 5.18: Measurement setup inside the anechoic chamber: (a) Testbed block diagram. (b) Real testbed.

5.4.2 Measurement Results

In order to validate the usefulness of the proposed NWM encoding and decoding techniques, the RFID chipless tags illustrated in Fig. 5.8 are employed (shown in Fig. 5.19), detected, and measured. Each tag consists of four resonators. Each resonator can individually encode 4 bits based on the notch bandwidth and the frequency position as mentioned in Section 5.2.1. The material used is RO4003 Rogers material with a thickness of 1.52 mm.

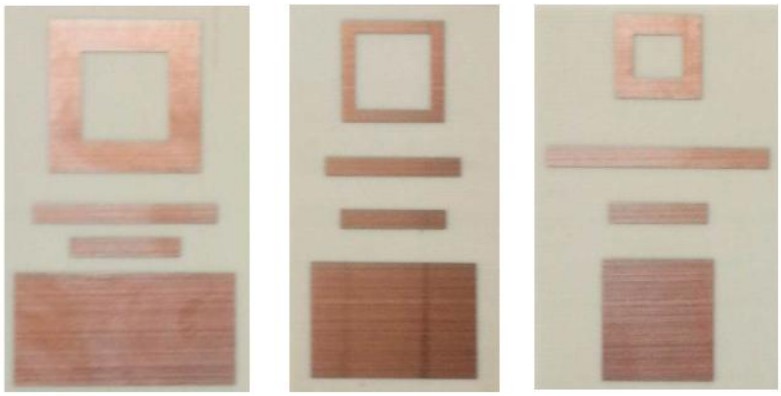

Figure 5.19: Manufactured chipless RFID tags employing the proposed encoding technique (The material used is RO4003 Rogers material with a thickness of 1.52 mm).

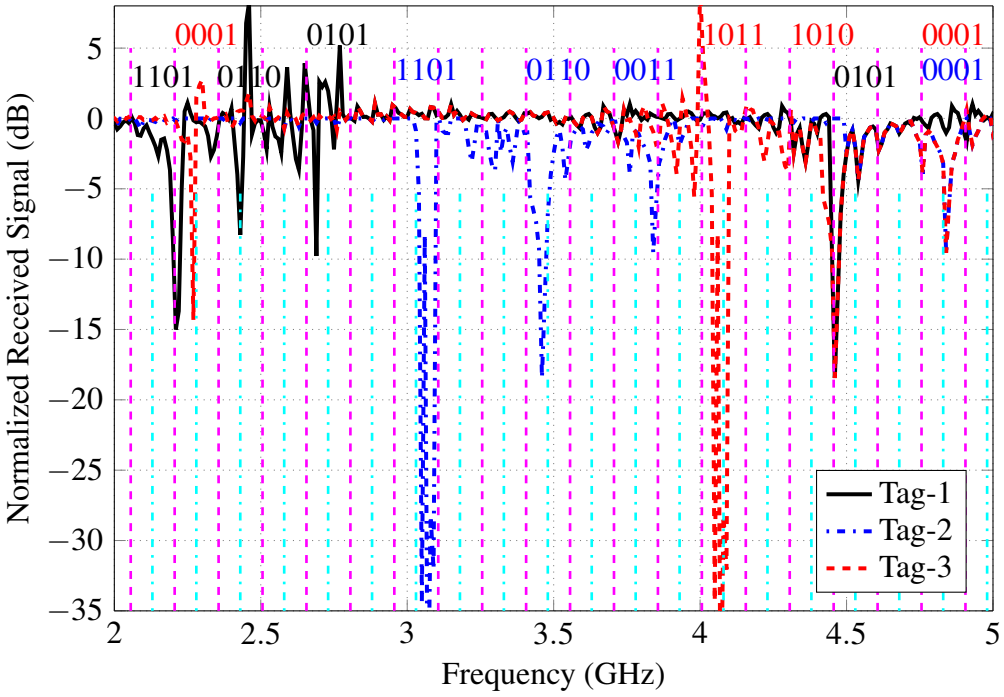

Figure 5.20: Normalized received signal power of the implemented NWM-tags using USRP-N210.

Fig. 5.20 illustrates all the backscattered signals received from each tag at the reader's side (USRP). Further, the obtained measurement results are normalized using Equation (5.17). Then, the proposed decoding technique is applied to the received signal and the SSVD algorithm is employed. The measurement results offer a close match to the simulation shown in Fig. 5.9. This highlights the validity of the proposed encoding and detection method in comparison to a real system.

Moreover, the comparison between the response of the received signal reflected from the chipless NWM-tags and the simulation results is shown in Fig. 5.21.

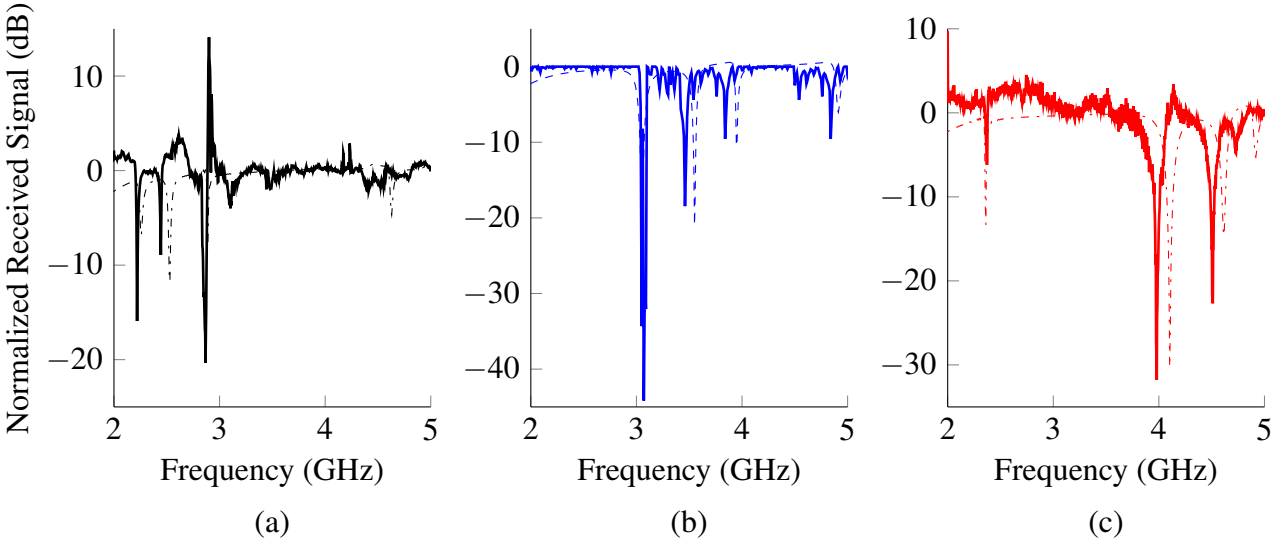

Figure 5.21: The measured tags' responses outside the anechoic chamber in reference to the simulation results obtained from CST-Microwave Studio: (a) Tag-1. (b) Tag-2. (c) Tag-3.

5.5 Conclusion

In this chapter, a novel technique to improve the coding efficiency of a chipless RFID system is proposed. The introduced coding technique relies on the precoded notch bandwidth and frequency position achieving 4 bits per resonator that uses the estimated coding pairs $C_j(f_k,B_l)$.

The notch pattern is analytically described to fit the proposed NWM-coding method. It yields a close match to the designed chipless tags using the CST-Microwave Studio EM simulator.

Also, the tags are intentionally designed to have the wider notch bandwidth at lower frequencies and the lower notch bandwidth at higher frequencies, which is contrary to the well-known phenomenon that the notch bandwidth increases with rising frequency (as shown in the previous chapters). This demonstrates the ability of the proposed new tag structure to control the

bandwidth.

Furthermore, a smart singular value decomposition detection algorithm is customized and realized to estimate the notch bandwidth, to decode the predefined notches, and to ensure accurate detection.

Subsequently, the utilization of the error correction codes in the chipless RFID system is discussed, in particular, the use of linear block codes. The (15,11) Hamming pair is applied to a designed frequency coded chipless tag with 1-bit per notch coding scheme and the corresponding coding gain is estimated. In order to obtain a higher coding gain, the minimum distance of the designed ECC code needs to be increased. Some studies aim at finding the optimum distance profiles for the linear block codes as introduced in [134, 135].

Moreover, the proffered NWM approach is realized using the commercial USRP platform and a low-cost monopole antenna to validate the presented system.

6 Conclusions and Future work

In this chapter, the achieved contributions throughout the thesis are concluded and summarized. Furthermore, future research aims based on the accumulated experience regarding the difficulties of implementing the proposed chipless system will be discussed.

6.1 Conclusions

In Chapter 3, novel MAC protocols to prevent the collision of backscattered signals from the chipless RFID tags were proposed. The introduced algorithms efficiently identify the number of tags located in the reader's interrogation region and effectively identify the tags' IDs.

- The first generation of the protocol (Gen-1) is based on unique frequency shifts hardcoded into every chipless tag based on the presented NPM technique that decodes the tag-ID and demonstrates the tag's existence. The Gen-1 protocol divides the overall spectrum into two parts; the first one includes the unique frequency shift for each tag. The second contains the tag-ID. The tag-ID is obtained by using the tag's unique frequency shift value which is obtained by hopping the corresponding locations with a step equal to the unique frequency shift. Afterwards, the tag-ID is derived utilizing the basic energy detection technique. Furthermore, an advanced frequency sweeping signaling scheme is applied for the tag's identification meeting the FCC UWB regulations and increasing the backscattered power by a factor of 400 compared to the traditional UWB-IR signaling scheme.
- The second generation of the protocol (Gen-2) enhances the spectrum's utilization efficiency and the coding capacity. The Gen-2 protocol makes use of the unique frequency shifts serving as addresses to their IDs which are stored in a table in the main memory

on the reader's side. Consequently, the information can be transferred from the tag to the reader only requiring the tag's address.

In order to reflect the real-world aspects of the chipless RFID system, an SDR platform is used as a real-time reader for two MAC based manufactured chipless tags. The empty room calibration and equalization processes were performed to obtain the ID of the tags successfully. In this setup, the collision free tags' IDs were promptly identified on the reader's side in an indoor scenario at a distance of 30 cm.

In Chapter 4, novel adaptive techniques are proposed to reduce the required time to identify the Frequency Coded chipless RFID tags existent in the reader's interrogation region. This time is called *system latency*. The overall system latency is shown to be affected by the frequency scanning methodology, the number of spectrum sweeping iterations to reduce the clutter, and the frequency-hop duration. Therefore, the introduced adaptive techniques sweep the operating frequency range with a lower number of frequency hops while conserving the detection accuracy. Moreover, two adaptive hopping techniques are designed to meet the requirements of both Gen-1 and Gen-2 multi-tag protocols. Furthermore, the proposed techniques are designed to meet the notch pattern variation phenomenon, which shows that the notch bandwidth increases with a rise of the resonating frequency.

- First of all, the classical Fixed Frequency Hopping (FFH) technique is examined with a narrow frequency step in order to perform an accurate detection and identification of the chipless tags.

- The first adaptive technique is called Adaptive Frequency Hopping (AFH). With the AFH method, the reader sweeps the operating frequency range with a variable frequency step, according to the notch pattern variation. The average frequency steps are found when analyzing the relationship of the notch bandwidth and the resonant frequency at a given quality factor as in ($\mathrm{BW} = F_\mathrm{r}/Q$). The benefit of the AFH sweeping method is that it is not only suitable for Gen-2 based tags, but it can be used for all FC chipless tag's detections.

- The second adaptive technique is designed to meet the requirement of the Gen-1 protocol is the Adaptive Sliding Window (ASW) method. The reader starts scanning the preamble bandwidth with a fixed window size and then scans the rest of the band according to the estimated frequency position with an adapted window size. The scanning inside the window is preferred to be done with an adaptive hopping rate, in order to also make use

of the benefits obtained from the proposed AFH technique that reduces the number of frequency hops and, accordingly, the overall system latency.

The FFH, AFH, and ASW techniques are modeled, simulated, and implemented in a real-world testbed using a Software Defined Radio platform (USRP N210, with a CBX daughter-board). Furthermore, the measurement setup relies on real manufactured FC chipless tags. The measurements are performed outside the anechoic chamber to include environmental effects. The designed AFH algorithm is compared to the classical FFH method. This comparison shows that the AFH algorithm can be efficiently applied to the FC chipless RFID systems. As a result of applying the newly-developed AFH technique, the overall system latency is reduced by more than 58% and the chipless tag is accurately detected utilizing the adaptive sliding window criterion. A close match between the simulation and the measurements can be seen throughout the results. A comprehensive study is performed to compare the proposed AFH algorithm, the classical FFH method, and the ASW techniques.

In Chapter 5, a novel technique to increase the coding capacity of the chipless RFID tag is described. The introduced coding technique depends on the precoded notch bandwidth and the frequency position achieving 4 bits per single resonator when utilizing the estimated coding pairs $C_j(f_k,B_l)$. The notch pattern is analytically represented to describe the proposed Notch Width Modulation (NWM) coding methodology which relates the notch pattern to the required code. It shows a close match to the real chipless tags using the CST-Microwave Studio EM simulator. Also, the tags are intentionally designed to have the wider notch bandwidth at lower frequencies and the lower notch bandwidth at higher frequencies. This is contrary to the well-known phenomenon that the notch bandwidth increases with the frequency. This demonstrates that the newly-developed tag structure can control the bandwidth. Furthermore, a Smart Singular Value Decomposition (SSVD) detection algorithm is customized and realized to estimate the notch bandwidth, to decode the predefined notches, and to ensure accurate detection. Additionally, the usefulness of Error Correction Codes (ECC) is explored when they are used in chipless RFID systems. Moreover, the proffered approach is realized using the commercial USRP platform and a low-cost monopole antenna at the reader's side to assess the presented system.

6.2 Future Work

In this section, some possible solutions to enhance the chipless RFID's robustness are proposed.

- **For multi-tag identification**: While preventing negative influences from clutter and environmental effects, a good performance can be achieved when the reader transmits signals at certain frequencies and the tag receives these signals but responds with a signal at other frequencies. The element used at the tag's side that is responsible for transforming its response into other frequencies is the Diode. However, as these tags are passive, the diode needs to be able to operate with a very small biasing voltage. Consequently, the zero-bias Schottky diodes with low convergence loss values are the ones most likely to be used in this application [136]. This technique to identify the tags is called a nonlinear chipless RFID system. The following techniques are used in the nonlinear chipless RFID system.

  - Harmonic RADAR: The basic architecture of a 1 bit harmonic RFID system consists of a reader transmitting a signal at a fundamental frequency f_0 while having the receiver tuned to $2f_0$. At the tag's side, it receives the signal transmitted by the reader at the predefined fundamental frequency. Then, the signal is passed to the Schottky diode that generates the fundamental frequency and the harmonics. The signal is filtered by an antenna with a center frequency tuned to the 1^{st} harmonic. Finally the filtered signal is reflected back to the reader that identifies the tag. Consequently, the clutter related to the fundamental frequency is avoided by receiving the tag's response at another frequency. The disadvantage of this technique is that it cannot identify several tags existent within the reader's interrogation region at the same time, since each tag will only respond to a particular fundamental frequency from the reader [137].

  - Dual frequency selective multiple access to RFID mixer tags: In this setup, two RF signals with different frequencies are transmitted by a reader and downconverted in the tag by an unbiased Schottky diode mixer after reception only when the interrogation frequencies of both signals match the filter characteristics of the two narrow-band receiving antennas. The downconverted RF signal (the lower component of the mixer's output) is backscattered to the reader by a third narrow-band antenna. Thus, several tags can be accessed with the help of individual frequency pairs [138].

  - Intermodulation technique: This technique is an extension of the nonlinear RFID mixer tags since it makes use of the intermodulation components of two or more RF signals with different frequencies [139–141]. The selection of the intermodulation

components is executed by using a filter tuned to the required frequency components.

- **Regarding the overall system latency**: The time required to identify the chipless tags can be reduced by following these suggestions.

  - For the proposed chipless system: One of the factors that has an effect on the system latency is the hardware used. The SDR based reader uses an USRP which requires 30 ms to switch to another frequency (hop duration). Consequently, if hardware with a smaller hop duration is used, the overall system latency is reduced. In addition, employing the PN sequence to detect the chipless tag's response improves the latency because there is no more need for empty room calibration or an averaging process that removes the environmental clutter effect.
  - For the nonlinear chipless system: The system latency is supposed to be lower than for the proposed chipless RFID system because the nonlinear system works at a narrower bandwidth (especially for the intermodulation technique).

- **For the coding capacity**: Besides increasing the coding capacity of the chipless RFID tag, the probability of error for decoding these coded tags is a critical issue. This is due to the fact that more bits can be encoded to the tag, but few of them are correctly received. Consequently, our recommendation to reduce the probability of error for the decoded tags is to use the channel coding technique since it provides additional protection against ISI and fading. Moreover, the space-time coding for the RFID with chip is illustrated in [142]. Yet, no prior studies discuss the impact of channel coding on enhancing the coding efficiency. In addition, another detection technique can be used to detect/decode the proposed NWM-coded chipless tags, which is the Dynamic Time Warping (DTW) described in [143]. The benefit of utilizing the DTW technique is that it leads to more robustness against the error resultant from frequency shifts since the utilized NWM coding method not only depends on the notch bandwidth but also on the notch resonance frequency. So, the error of detection may result either from the bandwidth or the frequency shift. The proposed SSVD provides greater robustness against errors due to the bandwidth but only very small values of frequency shift are allowed. However, the DTW provides much better robustness against errors due to bandwidth and frequency shifts. The disadvantage of the DTW method is that its complexity is greater than that of the SSVD algorithm.

List of Publications and Awards

Journal Papers

[1] A. El-Awamry, M. Khaliel, A. Fawky and T. Kaiser, "Adaptive Spectrum Scanning Techniques for Reducing the Identification Time of the Frequency Coded Chipless RFID System," Transactions on Emerging Telecommunications Technologies (2017).

[2] M. Khaliel, A. El-Awamry, A. Fawky and T. Kaiser, "A Novel Design Approach for Co/Cross-Polarizing Chipless RFID Tags of High Coding Capacity," IEEE Journal of Radio Frequency Identification, 2017.

[3] M. El-Hadidy, A. El-Awamry, A. Fawky, M. Khaliel and T. Kaiser, "Real-World Testbed for Multi-Tag UWB Chipless RFID System based on a Novel Collision Avoidance MAC Protocol," Transactions on Emerging Telecommunications Technologies (Wiley), 2016, pp. 1-8.

Conference Papers

[1] A. El-Awamry, M. Khaliel, A. Fawky and T. Kaiser, "A Novel Multi-Tag Identification Technique for Frequency Coded Chipless RFID Systems based on Look-Up-Table Approach," 2017 11th European Conference on Antennas and Propagation (EuCAP), Paris, 2017, pp. 1-5.

[2] A. El-Awamry, A. Fawky, M. Khaliel and T. Kaiser, "A Novel Adaptive Spectrum Scanning Technique for Reducing the Identification Time of the UWB Chipless RFID System," 14th IEEE International Conference on Networking, Sensing and Control, Calabria, Italy, 2017, pp. 1-6.

[3] M. Khaliel, A. El-Awamry, A. Fawky and T. Kaiser, "Long Reading Range Chipless RFID

System Based on Rflectarray Antennas," 2017 11th European Conference on Antennas and Propagation (EuCAP), Paris, 2017, pp. 1-5.

[4] A. Fawky, M. Khaliel, A. El-Awamry and T. Kaiser, "Frequency Coded Chipless RFID Tag Localization using Multiple Antennas," 2017 11th European Conference on Antennas and Propagation (EuCAP), Paris, 2017, pp. 1-5.

[5] M. Khaliel, A. Fawky, A. El-Awamry, A. Mahmoud and T. Kaiser, "Printable, High Coding Capacity Chipless RFID Tags for Low Cost Item Tagging," 14th IEEE International Conference on Networking, Sensing and Control, Calabria, Italy, 2017, pp. 1-6.

[6] A. Fawky, A. El-Awamry, M. Khaliel and T. Kaiser, "Novel Notch Detection Techniques for Frequency Coded Chipless RFID," 14th IEEE International Conference on Networking, Sensing and Control, Calabria, Italy, 2017, pp. 1-6.

[7] M. El-Hadidy, A. El-Awamry, A. Fawky, M. Khaliel and T. Kaiser, "A Novel Collision Avoidance MAC Protocol for Multi-Tag UWB Chipless RFID Systems based on Notch Position Modulation," 2015 9th European Conference on Antennas and Propagation (EuCAP), Lisbon, 2015, pp. 1-5.

[8] A. El-Awamry, M. Khaliel, A. Fawky, M. El-Hadidy and T. Kaiser, "Novel Adaptive Sliding Window Algorithm Reducing Latency for Multi-Tag Chipless RFID Systems," Radio Science Meeting (Joint with AP-S Symposium), 2015 USNC-URSI, Vancouver, BC, Canada, 2015, pp. 206-206.

[9] A. El-Awamry, A. Fawky, M. El-Hadidy and T. Kaiser, "Smart Notch Detection Techniques for Robust Frequency Coded Chipless RFID Systems," 2015 9th European Conference on Antennas and Propagation (EuCAP), Lisbon, 2015, pp. 1-5.

[10] A. Fawky, M. Khaliel, A. El-Awamry, M. El-Hadidy and T. Kaiser, "Novel Pseudo-Noise Coded Chipless RFID System for Clutter Removal and Tag Detection," 2015 IEEE International Conference on RFID (RFID), San Diego, CA, 2015, pp. 100-104.

[11] A. El-Awamry, M. Khaliel, A. Fawky, M. El-Hadidy and T. Kaiser, "Novel Notch Modulation Algorithm for Enhancing the Chipless RFID Tags Coding Capacity," 2015 IEEE International Conference on RFID (RFID), San Diego, CA, 2015, pp. 25-31.

[12] M. Khaliel, A. El-Awamry, A. Fawky, M. El-Hadidy and T. Kaiser, "A Novel Co/Cross-polarizing Chipless RFID Tags for High Coding Capacity and Robust Detection," 2015 IEEE International Symposium on Antennas and Propagation and USNC/URSI National Radio Science Meeting, Vancouver, BC, 2015, pp. 159-160.

Organized IEEE Workshops

[1] "Chipless RFID Future and Challenges," 2015 9th European Conference on Antennas and Propagation (EuCAP), Lisbon, 2015.

[2] "Chipless RFID System and Testbed: Reader and Tag Antennas, Reader and Tag Design, Multi-Tag Scenarios, Modulation, Clutter Effects and Channel Estimation, Signaling and Real-world Testbed," Radio Science Meeting (Joint with AP-S Symposium), 2015 USNC-URSI, Vancouver, BC, Canada, 2015.

Awards

1. Awarded a three year Deutscher Akademischer Austauschdienst (DAAD) PhD. student scholarship under the Deutsch-Arabische Forschungspartnerschaft program grants in ID4EGYPT Project.

2. The paper "A Novel Collision Avoidance MAC Protocol for Multi-Tag UWB Chipless RFID Systems based on Notch Position Modulation," is nominated for the **best student paper award** at 2015 9th European Conference on Antennas and Propagation (EuCAP) conference.

3. The paper "Long Reading Range Chipless RFID System Based on Rflectarray Antennas," is nominated for the **best student paper award** at 2017 11th European Conference on Antennas and Propagation (EuCAP) conference.

Bibliography

[1] F. Xia, L. T. Yang, L. Wang, and A. Vinel, "Internet of things," *International Journal of Communication Systems*, vol. 25, no. 9, p. 1101, 2012.

[2] Y. W. X. Zhang, *Internet of Things*. Springer, 2011.

[3] L. Atzori, A. Iera, and G. Morabito, "The internet of things: A survey," *Computer networks*, vol. 54, no. 15, pp. 2787–2805, 2010.

[4] E. Welbourne, L. Battle, G. Cole, K. Gould, K. Rector, S. Raymer, M. Balazinska, and G. Borriello, "Building the internet of things using RFID: the RFID ecosystem experience," *Internet Computing, IEEE*, vol. 13, no. 3, pp. 48–55, 2009.

[5] S. A. Weis, "Rfid (radio frequency identification): Principles and applications," *System*, vol. 2, p. 3Principles, 2007.

[6] S. Preradovic, "Chipless RFID system for barcode replacement," Ph.D. dissertation, Monash University. Faculty of Engineering. Department of Electrical and Computer Systems Engineering, 2010.

[7] P. J. Sweeney *et al.*, *RFID for Dummies*. John Wiley & Sons, 2010.

[8] K. Finkenzeller, "Rfid handbook, 2010," *John Willey, Chichester, UK*, 2010.

[9] R. Want, "An introduction to rfid technology," *IEEE Pervasive Computing*, vol. 5, no. 1, pp. 25–33, Jan 2006.

[10] Z. Tang, Y. He, Z. Hou, and B. Li, "The effects of antenna properties on read distance in passive backscatter rfid systems," in *Networks Security, Wireless Communications and Trusted Computing, 2009. NSWCTC '09. International Conference on*, vol. 1, April 2009, pp. 120–123.

[11] C. C. Yen, A. E. Gutierrez, D. Veeramani, and D. van der Weide, "Radar cross-section analysis of backscattering rfid tags," *IEEE Antennas and Wireless Propagation Letters*, vol. 6, pp. 279–281, 2007.

[12] E. W. Schuster, "Auto-id technology: creating an intelligent infrastructure for business," *The Data Center Massachusetts Institute of Technology Cambridge*, 2005.

[13] K. Domdouzis, B. Kumar, and C. Anumba, "Radio-frequency identification (rfid) applications: A brief introduction," *Advanced Engineering Informatics*, vol. 21, no. 4, pp. 350–355, 2007.

[14] M. Bolic, D. Simplot-Ryl, and I. Stojmenovic, *RFID systems: research trends and challenges*. John Wiley & Sons, 2010.

[15] P. V. Nikitin and K. Rao, "Performance limitations of passive uhf rfid systems," in *IEEE Antennas and Propagation Society International Symposium*, vol. 1011, 2006.

[16] R. R. Fletcher, "Low-cost electromagnetic tagging: design and implementation," Ph.D. dissertation, Citeseer, 2002.

[17] S. Natarajan, M. Armstrong, M. Bost, R. Brain, M. Brazier, C. H. Chang, V. Chikarmane, M. Childs, H. Deshpande, K. Dev, G. Ding, T. Ghani, O. Golonzka, W. Han, J. He, R. Heussner, R. James, I. Jin, C. Kenyon, S. Klopcic, S. H. Lee, M. Liu, S. Lodha, B. McFadden, A. Murthy, L. Neiberg, J. Neirynck, P. Packan, S. Pae, C. Parker, C. Pelto, L. Pipes, J. Sebastian, J. Seiple, B. Sell, S. Sivakumar, B. Song, K. Tone, T. Troeger, C. Weber, M. Yang, A. Yeoh, and K. Zhang, "A 32nm logic technology featuring 2nd-generation high-k + metal-gate transistors, enhanced channel strain and 0.171 x03bc;m2 sram cell size in a 291mb array," in *2008 IEEE International Electron Devices Meeting*, Dec 2008, pp. 1–3.

[18] S. Preradovic and N. C. Karmakar, "Chipless rfid: Bar code of the future," *IEEE Microwave Magazine*, vol. 11, no. 7, pp. 87–97, Dec 2010.

[19] S. Tedjini, N. Karmakar, E. Perret, A. Vena, R. Koswatta, and R. E-Azim, "Hold the chips: Chipless technology, an alternative technique for rfid," *Microwave Magazine, IEEE*, vol. 14, no. 5, pp. 56–65, July 2013.

[20] Á. R. Félix, "Application of ultra-wideband technology to rfid and wireless sensors," Ph.D. dissertation, Universitat Rovira i Virgili. Departament d'Enginyeria Electrònica, Elèctrica i Automàtica, 2015.

[21] S. Preradovic and N. C. Karmakar, "Low cost chipless rfid systems," in *Multiresonator-Based Chipless RFID*. Springer, 2012, pp. 9–24.

[22] N. C. Karmakar, R. Koswatta, P. Kalansuriya, E. Rubayet *et al.*, *Chipless RFID Reader Architecture*. Artech House, 2013.

[23] L. Margulis, *Preradovic, Stevan and Karmakar, Nemai*. Croatia: INTECH Open Access Publisher, 2011.

[24] A. El-Awamry, M. Khaliel, A. Fawky, M. El-Hadidy, and T. Kaiser, "Novel notch modulation algorithm for enhancing the chipless rfid tags coding capacity," in *RFID (RFID), 2015 IEEE International Conference on*, April 2015, pp. 25–31.

[25] C. Hartmann, "A global saw id tag with large data capacity," in *Ultrasonics Symposium, 2002. Proceedings. 2002 IEEE*, vol. 1, Oct 2002, pp. 65–69 vol.1.

[26] L. Reindl, G. Scholl, T. Ostertag, H. Scherr, U. Wolff, and F. Schmidt, "Theory and application of passive saw radio transponders as sensors," *IEEE Transactions on Ultrasonics, Ferroelectrics, and Frequency Control*, vol. 45, no. 5, pp. 1281–1292, Sept 1998.

[27] P. Harrop and R. Das, "Chipless rfid forecasts, technologies & players 2006-2016," 2006.

[28] H. Klauk, D. J. Gundlach, and T. N. Jackson, "Fast organic thin-film transistor circuits," *Electron Device Letters, IEEE*, vol. 20, no. 6, pp. 289–291, 1999.

[29] K. Myny, A. K. Tripathi, J. L. van der Steen, and B. Cobb, "Flexible thin-film nfc tags," *IEEE Communications Magazine*, vol. 53, no. 10, pp. 182–189, October 2015.

[30] A. Chamarti and K. Varahramyan, "Transmission delay line based id generation circuit for rfid applications," *IEEE Microwave and Wireless Components Letters*, vol. 16, no. 11, pp. 588–590, Nov 2006.

[31] J. Vemagiri, A. Chamarti, M. Agarwal, and K. Varahramyan, "Transmission line delay-based radio frequency identification (rfid) tag," *Microwave and optical technology letters*, vol. 49, no. 8, pp. 1900–1904, 2007.

[32] S. Shrestha, J. Vemagiri, M. Agarwal, and K. Varahramyan, "Transmission line reflection and delay-based id generation scheme for rfid and other applications," *International Journal of Radio Frequency Identification Technology and Applications*, vol. 1, no. 4, pp. 401–416, 2007.

[33] I. Jalaly and I. D. Robertson, "Rf barcodes using multiple frequency bands," in *Microwave Symposium Digest, 2005 IEEE MTT-S International*, June 2005, pp. 139–142.

[34] J. McVay, A. Hoorfar, and N. Engheta, "Space-filling curve rfid tags," in *Radio and Wireless Symposium, 2006 IEEE*, Jan 2006, pp. 199–202.

[35] M. Khaliel, M. El-Hadidy, and T. Kaiser, "Printable depolarizing chipless rfid tag based on dgs resonators for suppressing the clutter effects," in *2015 9th European Conference on Antennas and Propagation (EuCAP)*, May 2015, pp. 1–5.

[36] A. El-Awamry, A. Fawky, M. El-Hadidy, and T. Kaiser, "Smart notch detection techniques for robust frequency coded chipless rfid systems," in *Antennas and Propagation (EuCAP), 2015 9th European Conference on*, April 2015.

[37] A. Vena, E. Perret, and S. Tedjni, "A depolarizing chipless rfid tag for robust detection and its fcc compliant uwb reading system," *IEEE Transactions on Microwave Theory and Techniques*, vol. 61, no. 8, pp. 2982–2994, Aug 2013.

[38] F. Costa, S. Genovesi, A. Monorchio, and G. Manara, "A robust differential-amplitude codification for chipless rfid," *IEEE Microwave and Wireless Components Letters*, vol. 25, no. 12, pp. 832–834, Dec 2015.

[39] K. V. S. Rao, P. V. Nikitin, and S. F. Lam, "Antenna design for uhf rfid tags: a review and a practical application," *IEEE Transactions on Antennas and Propagation*, vol. 53, no. 12, pp. 3870–3876, Dec 2005.

[40] M. Schüßler, C. Mandel, M. Maasch, A. Giere, and R. Jakoby, "Phase modulation scheme for chipless rfid- and wireless sensor tags," in *Microwave Conference, 2009. APMC 2009. Asia Pacific*, Dec 2009, pp. 229–232.

[41] S. Mukherjee, "Chipless radio frequency identification by remote measurement of complex impedance," in *Wireless Technologies, 2007 European Conference on*, Oct 2007, pp. 249–252.

[42] I. Balbin and N. C. Karmakar, "Phase-encoded chipless rfid transponder for large-scale low-cost applications," *IEEE Microwave and Wireless Components Letters*, vol. 19, no. 8, pp. 509–511, Aug 2009.

[43] L. Yang, R. Zhang, D. Staiculescu, C. P. Wong, and M. M. Tentzeris, "A Novel Conformal RFID-Enabled Module Utilizing Inkjet-Printed Antennas and Carbon Nanotubes for Gas-Detection Applications," *IEEE Antennas and Wireless Propagation Letters*, vol. 8, pp. 653–656, 2009.

[44] J. Mitola, "The software radio architecture," *IEEE Communications Magazine*, vol. 33, no. 5, pp. 26–38, May 1995.

[45] E. Blossom, "Gnu radio: tools for exploring the radio frequency spectrum," *Linux journal*, vol. 2004, no. 122, p. 4, 2004.

[46] B. Razavi, "Design considerations for direct-conversion receivers," *IEEE Transactions on Circuits and Systems II: Analog and Digital Signal Processing*, vol. 44, no. 6, pp. 428–435, Jun 1997.

[47] F. Zheng and T. Kaiser, "A space-time coding approach for rfid mimo systems," *EURASIP Journal on Embedded Systems*, vol. 2012, no. 1, p. 9, 2012.

[48] R. Anee and N. Karmakar, "Chipless rfid tag localization," *Microwave Theory and Techniques, IEEE Transactions on*, vol. 61, no. 11, pp. 4008–4017, Nov 2013.

[49] S. Hu, Y. Zhou, C. Law, and W. Dou, "Study of a uniplanar monopole antenna for passive chipless uwb-rfid localization system," *Antennas and Propagation, IEEE Transactions on*, vol. 58, no. 2, pp. 271–278, Feb 2010.

[50] R. Rezaiesarlak and M. Manteghi, "A space-frequency technique for chipless rfid tag localization," *Antennas and Propagation, IEEE Transactions on*, vol. 62, no. 11, pp. 5790–5797, Nov 2014.

[51] D. Dardari, F. Guidi, C. Roblin, and A. Sibille, "Ultra-wide bandwidth backscatter modulation: Processing schemes and performance," *EURASIP Journal on Wireless Communications and Networking*, vol. 2011, no. 1, pp. 1–15, 2011.

[52] D. Dardari, R. D'Errico, C. Roblin, A. Sibille, and M. Win, "Ultrawide bandwidth rfid: The next generation?" *Proceedings of the IEEE*, vol. 98, no. 9, pp. 1570–1582, Sept 2010.

[53] A. Vena, E. Perret, and S. Tedjini, "A compact chipless rfid tag using polarization diversity for encoding and sensing," in *RFID (RFID), 2012 IEEE International Conference on*, April 2012, pp. 191–197.

[54] M. El-Hadidy, A. El-Awamry, A. Fawky, M. Khaliel, and T. Kaiser, "A novel collision avoidance mac protocol for multi-tag uwb chipless rfid systems based on notch position modulation," in *2015 9th European Conference on Antennas and Propagation (EuCAP)*, May 2015, pp. 1–5.

[55] Nordic Identification, "Nordic id ar55," *RFID reader datasheet*, 2016.

[56] M. El-Hadidy, A. El-Awamry, A. Fawky, M. Khaliel, and T. Kaiser, "Real-world testbed for multi-tag uwb chipless rfid system based on a novel collision avoidance mac protocol," *Transactions on Emerging Telecommunications Technologies*, 2016.

[57] C. Meguerditchian, H. Safa, and W. El-Hajj, "New reader anti-collision algorithm for dense rfid environments," in *Electronics, Circuits and Systems (ICECS), 2011 18th IEEE International Conference on*, Dec 2011, pp. 85–88.

[58] D. Klair, K.-W. Chin, and R. Raad, "A survey and tutorial of rfid anti-collision protocols," *Communications Surveys Tutorials, IEEE*, vol. 12, no. 3, pp. 400–421, Third 2010.

[59] S. E. Sarma, S. A. Weis, and D. W. Engels, "Rfid systems and security and privacy implications," in *Cryptographic Hardware and Embedded Systems-CHES 2002*. Springer, 2002, pp. 454–469.

[60] S. Jain and S. R. Das, "Collision avoidance in a dense rfid network," in *Proceedings of the 1st international workshop on Wireless network testbeds, experimental evaluation & characterization*. ACM, 2006, pp. 49–56.

[61] E. EPCglobal, "Radio-frequency identity protocols class-1 generation-2 uhf rfid protocol for communications at 860 mhz–960 mhz version 1.0. 9," *K. Chiew et al./On False Authenticationsfor C1G2 Passive RFID Tags*, vol. 65, 2004.

[62] M. Azambuja, C. A. Marcon, and F. P. Hessel, "Survey of standardized iso 18000-6 rfid anti-collision protocols," in *Sensor Technologies and Applications, 2008. SENSORCOMM'08. Second International Conference on*. IEEE, 2008, pp. 468–473.

[63] R.-E. Azim and N. Karmakar, "A collision avoidance methodology for chipless rfid tags," in *Microwave Conference Proceedings (APMC), 2011 Asia-Pacific*, Dec 2011, pp. 1514–1517.

[64] R. Anee and N. Karmakar, "Efficient collision detection method in chipless rfid systems," in *Electrical Computer Engineering (ICECE), 2012 7th International Conference on*, Dec 2012, pp. 830–833.

[65] R. Rezaiesarlak and M. Manteghi, "A new anti-collision algorithm for identifying chipless rfid tags," in *Antennas and Propagation Society International Symposium (APSURSI), 2013 IEEE*, July 2013, pp. 1722–1723.

[66] R. Measel, C. Lester, Y. Xu, R. Primerano, and M. Kam, "Detection performance of spread spectrum signatures for passive, chipless rfid," in *RFID (IEEE RFID), 2014 IEEE International Conference on*, April 2014, pp. 55–59.

[67] R. Rezaiesarlak and M. Manteghi, "A new anti-collision algorithm for identifying chipless rfid tags," in *Antennas and Propagation Society International Symposium (APSURSI), 2013 IEEE*, July 2013, pp. 1722–1723.

[68] ——, "A space time frequency anticollision algorithm for identifying chipless rfid tags," *Antennas and Propagation, IEEE Transactions on*, vol. 62, no. 3, pp. 1425–1432, March 2014.

[69] R. E. A. Anee and N. C. Karmakar, "Anti-collision methods for chipless rfid systems," in *2015 Asia-Pacific Microwave Conference (APMC)*, vol. 2, Dec 2015, pp. 1–3.

[70] A. Fawky, M. Mohammed, M. El-Hadidy, and T. Kaiser, "Uwb chipless rfid system performance based on real world 3d-deterministic channel model and zf equalization," in *Antennas and Propagation (EuCAP), 2014 8th European Conference on*, April 2014, pp. 1765–1768.

[71] M. Khaliel, A. Fawky, M. El-Hadidy, and T. Kaiser, "Uwb reflectarray antenna for chipless rfid applications," in *Radio Science Conference (NRSC), 2014 31st National*, April 2014, pp. 17–20.

[72] S. Jain, *Efficient medium access protocols for wireless and rfid networks*. ProQuest, 2007.

[73] M. El-Hadidy, B. Nagy, M. Khaliel, A. Fawky, E. Abdallah, H. Elhennawy, and T. Kaiser, "Novel methodology for increasing the reading range of the uwb passive rfid chipless tags considering power regulations," *Session 2A10 SC4: Antenna-channel Interactions and Multipath Wireless Channels*, p. 576, 2013.

[74] M. El-Hadidy, A. Fawky, B. Nagy, M. Khaliel, E. Abdallah, H. Elhennawy, and T. Kaiser, "Evaluation of uwb chipless rfid system performance considering indoor multipath propagation channel and real world aspects," *Session 2A10 SC4: Antenna-channel Interactions and Multipath Wireless Channels*, p. 571, 2013.

[75] Federal communications commission, da 07-198, washington, d.c. 20554, adopted: January 25, 2007, released: January 26, 2007.

[76] M. El-Hadidy, B. Nagy, M. Khaliel, A. Fawky, E. Abdallah, H. Elhennawy, and T. Kaiser, "Novel methodology for increasing the reading range of the uwb passive rfid chipless tags considering power regulations," *Session 2A10 SC4: Antenna-channel Interactions and Multipath Wireless Channels*, p. 576, 2013.

[77] M. El-Hadidy, A. Fawky, B. Nagy, M. Khaliel, E. Abdallah, H. Elhennawy, and T. Kaiser, "Evaluation of uwb chipless rfid system performance considering indoor multipath propagation channel and real world aspects," *Session 2A10 SC4: Antenna-channel Interactions and Multipath Wireless Channels*, p. 571, 2013.

[78] M. Islam and N. Karmakar, "A novel compact printable dual-polarized chipless rfid system," *Microwave Theory and Techniques, IEEE Transactions on*, vol. 60, no. 7, pp. 2142–2151, July 2012.

[79] Microwave Studio, "Cst-computer simulation technology," *Bad Nuheimer Str*, vol. 19, p. 64289, 2008.

[80] "USRP N210," (Date last accessed 28.03.2016). [Online]. Available: http://www.ettus.com/product/details/UN210-KIT

[81] "CBX 1200-6000 MHz Rx/Tx (40 MHz)," (Date last accessed 04.04.2016). [Online]. Available: http://www.ettus.com/product/details/CBX

[82] A. El-Awamry, M. Khaliel, A. Fawky, M. El-Hadidy, and T. Kaiser, "Novel adaptive sliding window algorithm reducing latency for multi-tag chipless rfid systems," in *Antennas and Propagation Society International Symposium (APSURSI), 2015 IEEE*, July 2015.

[83] T. La Porta, G. Maselli, and C. Petrioli, "Anticollision protocols for single-reader rfid systems: Temporal analysis and optimization," *Mobile Computing, IEEE Transactions on*, vol. 10, no. 2, pp. 267–279, Feb 2011.

[84] I. Amadou and N. Mitton, "Revisiting backoff algorithms in csma/ca based mac for channel reservation in rfid reader networks through broadcasting," pp. 452–457, Oct 2013.

[85] X.-Q. Yan, Y.-S. Wang, Y. Liu, and X.-M. Liu, "A progressive population estimation based binary query tree protocol for efficient rfid tag collision resolution," pp. 564–571, Aug 2013.

[86] F. Hessar and S. Roy, "Energy based performance evaluation of passive epc gen 2 class 1 rfid systems," *Communications, IEEE Transactions on*, vol. 61, no. 4, pp. 1337–1348, April 2013.

[87] Y.-C. Ko, S. Roy, J. Smith, H.-W. Lee, and C.-H. Cho, "Rfid mac performance evaluation based on iso/iec 18000-6 type c," *Communications Letters, IEEE*, vol. 12, no. 6, pp. 426–428, June 2008.

[88] H. Landaluce, A. Perallos, and I. Zuazola, "A fast rfid identification protocol with low tag complexity," *Communications Letters, IEEE*, vol. 17, no. 9, pp. 1704–1706, September 2013.

[89] R. Tanbourgi, J. Elsner, H. Jakel, and F. Jondral, "Adaptive frequency hopping in ad hoc networks with rayleigh fading and imperfect sensing," *Wireless Communications Letters, IEEE*, vol. 1, no. 3, pp. 185–188, June 2012.

[90] C. E. Perkins, *Ad hoc networking*. Addison-Wesley Professional, 2008.

[91] M. Frodigh, P. Johansson, and P. Larsson, "Wireless ad hoc networking: the art of networking without a network," *Ericsson Review*, vol. 4, no. 4, p. 249, 2000.

[92] C. S. R. Murthy and B. Manoj, *Ad Hoc Wireless Networks: Architectures and Protocols, Portable Documents*. Pearson education, 2004.

[93] J. Zander and G. Malmgren, "Adaptive frequency hopping in hf communications," *Communications, IEE Proceedings-*, vol. 142, no. 2, pp. 99–105, Apr 1995.

[94] P. Popovski, H. Yomo, and R. Prasad, "Strategies for adaptive frequency hopping in the unlicensed bands," *Wireless Communications, IEEE*, vol. 13, no. 6, pp. 60–67, Dec 2006.

[95] S.-H. Lee and Y.-H. Lee, "Adaptive frequency hopping for bluetooth robust to wlan interference," *Communications Letters, IEEE*, vol. 13, no. 9, pp. 628–630, Sept 2009.

[96] H. Kwon and B. Kang, "Linear frequency modulation of voltage-controlled oscillator using delay-line feedback," *Microwave and Wireless Components Letters, IEEE*, vol. 15, no. 6, pp. 431–433, 2005.

[97] M.-A. Govoni, *Linear frequency modulation of stochastic radar waveform*. STEVENS INSTITUTE OF TECHNOLOGY, 2011.

[98] J. Blanton, "Generation of wideband linear frequency modulation signals," Dec. 20 1994, uS Patent 5,374,903. [Online]. Available: https://www.google.com/patents/US5374903

[99] P. C. Suo, S. Tao, R. Tao, and Z. Nan, "Detection of high-speed and accelerated target based on the linear frequency modulation radar," *Radar, Sonar Navigation, IET*, vol. 8, no. 1, pp. 37–47, January 2014.

[100] N. Grein and H. Winner, "Fmcw radar system with linear frequency modulation," Oct. 12 1993, uS Patent 5,252,981. [Online]. Available: https://www.google.com/patents/US5252981

[101] S. Scheiblhofer, S. Schuster, and A. Stelzer, "High-speed fmcw radar frequency synthesizer with dds based linearization," *Microwave and Wireless Components Letters, IEEE*, vol. 17, no. 5, pp. 397–399, May 2007.

[102] L. Hua, D. Cooper, and E. Shearman, "A prototype fmcw radar using an analogue linear frequency sweep," in *High Time-Bandwidth Product Waveforms in Radar and Sonar, IEE Colloquium on*, May 1991, pp. 11/1–11/4.

[103] A. Stove, "Linear fmcw radar techniques," *Radar and Signal Processing, IEE Proceedings F*, vol. 139, no. 5, pp. 343–350, Oct 1992.

[104] A. Webster, "Useful mathematical formulas for transform limited pulses."

[105] M. Islam, Y. Yap, N. Karmakar, and A. Azad, "Orientation independent compact chipless rfid tag," in *RFID-Technologies and Applications (RFID-TA), 2012 IEEE International Conference on*, Nov 2012, pp. 137–141.

[106] A. Fawky, M. Khaliel, A. El-Awamry, M. El-Hadidy, and T. Kaiser, "Novel pseudo-noise coded chipless rfid system for clutter removal and tag detection," in *RFID (RFID), 2015 IEEE International Conference on*, April 2015, pp. 100–104.

[107] F. C. Commission *et al.*, "Revision of part 15 of the commission's rules regarding ultra-wideband transmission systems,"first report and order," fcc 02," *V48, April*, 2002.

[108] F. Costa, S. Genovesi, and A. Monorchio, "Chipless rfids by using metasurfaces," in *Antennas and Propagation (EuCAP), 2014 8th European Conference on*, April 2014, pp. 2384–2388.

[109] W. Zhao, X. Liu, S. Ma, C. Yuan, and L. Wang, "Formal specification of hierarchical region rfid code resolution service," in *Intelligent Systems and Applications (ISA), 2011 3rd International Workshop on*, May 2011, pp. 1–10.

[110] J. S. Lee and H. J. Kim, "Rfid code structure and tag data structure for mobile rfid services in korea," in *Advanced Communication Technology, 2006. ICACT 2006. The 8th International Conference*, vol. 2, Feb 2006, pp. 3 pp.–1055.

[111] Y. Sato, J. Mitsugi, O. Nakamura, and J. Murai, "Theory and performance evaluation of group coding of rfid tags," *IEEE Transactions on Automation Science and Engineering*, vol. 9, no. 3, pp. 458–466, July 2012.

[112] D. Girbau, A. Lazaro, and A. Ramos, "Time-coded chipless rfid tags: Design, characterization and application," in *RFID-Technologies and Applications (RFID-TA), 2012 IEEE International Conference on*, Nov 2012, pp. 12–17.

[113] M. Zomorrodi, N. Karmakar, and S. Bansal, "Introduction of electromagnetic image-based chipless rfid system," in *Intelligent Sensors, Sensor Networks and Information Processing, 2013 IEEE Eighth International Conference on*, April 2013, pp. 443–448.

[114] A. Vena, E. Perret, and S. Tedjini, "Rfid chipless tag based on multiple phase shifters," in *Microwave Symposium Digest (MTT), 2011 IEEE MTT-S International*, June 2011, pp. 1–4.

[115] R. Nair, E. Perret, and S. Tedjini, "Temporal multi-frequency encoding technique for chipless rfid applications," in *Microwave Symposium Digest (MTT), 2012 IEEE MTT-S International*, June 2012, pp. 1–3.

[116] "Gs1 barcodes," (Date last accessed 04.04.2016). [Online]. Available: http://www.gs1.org/gsmp/kc/barcodes

[117] EPCglobal Gen, "EPC Radio-Frequency Identity Protocols Class-1 Generation-2 UHF RFID Protocol for Communications at 860 MHz-960 MHz," 2008.

[118] S. Preradovic, I. Balbin, N. Karmakar, and G. Swiegers, "Multiresonator-based chipless rfid system for low-cost item tracking," *Microwave Theory and Techniques, IEEE Transactions on*, vol. 57, no. 5, pp. 1411–1419, May 2009.

[119] C. M. Nijas, R. Dinesh, U. Deepak, A. Rasheed, S. Mridula, K. Vasudevan, and P. Mohanan, "Chipless rfid tag using multiple microstrip open stub resonators," *IEEE Transactions on Antennas and Propagation*, vol. 60, no. 9, pp. 4429–4432, Sept 2012.

[120] D. Girbau, J. Lorenzo, A. Lazaro, C. Ferrater, and R. Villarino, "Frequency-coded chipless rfid tag based on dual-band resonators," *IEEE Antennas and Wireless Propagation Letters*, vol. 11, pp. 126–128, 2012.

[121] A. Vena, E. Perret, and S. Tedjini, "Chipless rfid tag using hybrid coding technique," *IEEE Transactions on Microwave Theory and Techniques*, vol. 59, no. 12, pp. 3356–3364, Dec 2011.

[122] C. M. Nijas, U. Deepak, P. V. Vinesh, R. Sujith, S. Mridula, K. Vasudevan, and P. Mohanan, "Low-cost multiple-bit encoded chipless rfid tag using stepped impedance resonator," *IEEE Transactions on Antennas and Propagation*, vol. 62, no. 9, pp. 4762–4770, Sept 2014.

[123] O. Rance, R. Siragusa, P. Lemaître-Auger, and E. Perret, "Toward rcs magnitude level coding for chipless rfid," *IEEE Transactions on Microwave Theory and Techniques*, vol. PP, no. 99, pp. 1–11, 2016.

[124] B. Shao, Q. Chen, Y. Amin, S. M. David, R. Liu, and L. R. Zheng, "An ultra-low-cost rfid tag with 1.67 gbps data rate by ink-jet printing on paper substrate," in *Solid State Circuits Conference (A-SSCC), 2010 IEEE Asian*, Nov 2010, pp. 1–4.

[125] H. Zumbahlen, *Basic linear design*. Analog Devices, 2007.

[126] P. Kalansuriya, N. Karmakar, and E. Viterbo, "Signal space representation of chipless rfid tag frequency signatures," in *Global Telecommunications Conference (GLOBECOM 2011), 2011 IEEE*, Dec 2011, pp. 1–5.

[127] S. Haykin, *Communication systems*. John Wiley & Sons, 2008.

[128] B. P. Lathi, *Modern Digital and Analog Communication Systems 3e Osece*. Oxford university press, 1998.

[129] J. G. Proakis, "Digital communications. 1995," *McGraw-Hill, New York*.

[130] F. J. MacWilliams and N. J. A. Sloane, *The theory of error correcting codes*. Elsevier, 1977.

[131] B. Sklar, *Digital communications*. Prentice Hall NJ, 2001, vol. 2.

[132] M. Bossert, *Channel coding for telecommunications*. John Wiley & Sons, Inc., 1999.

[133] A. H. Vinck, "Coding concepts and reed-solomon codes," *Institute for Experimental Mathematics, Essen, Germany*, 2013.

[134] A. J. H. Vinck and Y. Luo, "Optimum distance profiles of linear block codes," in *2008 IEEE International Symposium on Information Theory*, July 2008, pp. 1958–1962.

[135] Y. Luo, A. J. H. Vinck, and Y. Chen, "On the optimum distance profiles about linear block codes," *IEEE Transactions on Information Theory*, vol. 56, no. 3, pp. 1007–1014, March 2010.

[136] K. Rasilainen, J. Ilvonen, A. Lehtovuori, J. M. Hannula, and V. Viikari, "On Design and Evaluation of Harmonic Transponders," *IEEE Transactions on Antennas and Propagation*, vol. 63, no. 1, pp. 15–23, Jan 2015.

[137] V. Palazzi, F. Alimenti, P. Mezzanotte, M. Virili, C. Mariotti, G. Orecchini, and L. Roselli, "Low-Power Frequency Doubler in Cellulose-Based Materials for Harmonic RFID Applications," *IEEE Microwave and Wireless Components Letters*, vol. 24, no. 12, pp. 896–898, Dec 2014.

[138] C. Mandel, C. Schuster, B. Kubina, M. Schüßler, and R. Jakoby, "Dual Frequency Selective Multiple Access With Quasi-Chipless/Powerless RFID Mixer Tags," *IEEE Microwave and Wireless Components Letters*, vol. 24, no. 8, pp. 572–574, Aug 2014.

[139] J. Romeu Gómez, "Design of a Chipless Harmonic Radar Temperature Sensor," 2013.

[140] R. N. Simons and P. G. Neudeck, "Intermodulation-distortion performance of silicon-carbide Schottky-barrier RF mixer diodes," *IEEE Transactions on Microwave Theory and Techniques*, vol. 51, no. 2, pp. 669–672, Feb 2003.

[141] B. Kubina, J. Romeu, C. Mandel, M. Schüßler, and R. Jakoby, "Quasi-chipless wireless temperature sensor based on harmonic radar," *Electronics Letters*, vol. 50, no. 2, pp. 86–88, January 2014.

[142] C. Boyer and S. Roy, "Space Time Coding for Backscatter RFID," *IEEE Transactions on Wireless Communications*, vol. 12, no. 5, pp. 2272–2280, May 2013.

[143] D. J. Berndt and J. Clifford, "Using Dynamic Time Warping to Find Patterns in Time Series." in *KDD workshop*, vol. 10, no. 16. Seattle, WA, 1994, pp. 359–370.